ABSTRACT

Jefferson C. Davis

CHARACTERIZING PARTICLES DEPOSITED ONTO A SURFACE
USING THE ATOMIC FORCE MICROSCOPE

(Thesis Advisor; Dr. Parker Reist,)

Sub-micron sized particles by count make up a significant portion of the air-borne particles we are exposed to. Detection and characterization of these particles, particularly after they have deposited onto a surface, can be difficult. The Atomic Force Microscope (AFM) produces a high resolution topographic image of a sample surface that can resolve differences in surface features less than 5 nanometers (nm). Selection of a suitable substrate material is critical as the scale of interest decreases. Variation in the substrates surface structure adversely impacts the ability of the AFM to identify and measure particles. Analysis of deposited sub-micron particles of known size on various materials allows selection of suitable substrate.

Table of Contents

Page numbers

LIST OF ABBREVATIONS

afm	atomic force microscope
C_c	Cunningham slip correction
cm	centimeter
ρ	density
d_p	diameter of particle
D_B	diffusion coefficient
g/cm^3	gram per cubic centimeter
k_B	Boltzmann's constant
lpm	liter per minute
ml	milliliter
N	number of data points
nm	nanometers
p_f	density of fluid medium
psl	polystyrene latex
τ	relaxation time
ra	mean roughness
rms	root mean square
stp	standard temperature and pressure
um	micrometers
t	temperature (K)
U	velocity
U_t	terminal velocity
μ	viscosity
λ	gas free mean path
Z_{cp}	center plane Z value
Z_i	current Z value

LIST OF TABLES

I. INTRODUCTION/PURPOSE

Sub-micron sized particles by count make up a significant portion of the air-borne particles we are exposed to, and as such, are suspected to pose a possible health risk (Stone and Donaldson, 12-14). Yet, because of their small size, their contribution to the total mass of particulate is almost negligible. Detection and characterization of these particles, particularly after they have deposited onto a surface, can be difficult. Sub-micron sized particles are generally too small to be easily detected optically. Instruments such as the Scanning Electron Microscope (SEM) require substantial sample preparation prior to analysis and significant environmental support to operate. The sample must be collected on a special substrate and coated with a conductive material; the sample is then placed under vacuum and scanned by a high energy electron beam. Each step along the way can alter or destroy the particles. Indirect methods of analysis such as fluorescence or ion analysis, using specially prepared aerosols, can determine the total particulate mass deposited onto a surface, but they provide no indication of the particles size. In addition, the analysis process destroys the sample.

The Atomic Force Microscope (AFM) produces a high resolution topographic image of a sample surface. The AFM has the capability of resolving surface features structure where the differences are less than 5 nanometers (nm). Samples require no special preparation. They may be collected on nearly any material and are scanned under ambient atmospheric conditions (Prater et al, 1-2). The sample is unaffected by analysis, and can be preserved for additional study. Some AFM models are easily transported and can be

set up in a field laboratory. The microscope assembly can be hand carried and is easily supported by a computer system similar to a home personal computer.

The forces which effect the deposition of sub-micron particles onto a surface change in relative importance as the particles become smaller. For larger particles in a still environment, gravitational settling tends to take a prominent role. As the diameter of the particle decreases, diffusion starts to have a greater influence on the particle.

The object of this study was to evaluate the use of the AFM to identify sub-micron sized particles that have deposited onto sample collection substrates, and to evaluate its effectiveness as an analytical tool for counting and sizing sub-micron particles on a surface. A companion to this objective was to determine, using the AFM, whether the predominate force (diffusion or sedimentation) acting on a sub-micron particle can be inferred.

II. BACKGROUND

A. Aerosol Deposition Mechanisms

Aerosol particle size, shape, density, and hygroscopicity (tendency to absorb water vapor) determine to a large extent how the particles behave in air and deposit on a surface. In this section the primary deposition mechanisms of sedimentation and diffusion are described.

Sedimentation refers to movement of an aerosol particle through a gaseous medium under the influence of gravity. The rate of settling will depend on the particle's size, shape, mass, and on the air density and viscosity. An airborne particle is subjected to a gravitational force and will accelerate according to Newton's Second Law. The acceleration force is given by the product of the particle mass and the gravitational constant g, and for a sphere of diameter d_p and density ρ is (Willike and Baron 32)

$$F_s = \frac{\pi d_p^3}{6} \rho g$$

Opposing this force is the drag force on the particle due to gas viscosity. For laminar flow, the drag force on a spherical particle moving with velocity U through a medium having a viscosity μ is given by Stokes' Law (Reist 59)

$$F_D = 3 \pi \mu d_p U$$

where $\mu = 1.84 \times 10^{-4}$ g/cm-sec at STP (1 atm, 20°C). Since the particle displaces its own volume of air even at rest, there is also a small buoyant force acting opposite the gravity

force, namely (Hinds 46)

$$F_b = \frac{\pi\, d_p^3}{6} \rho_f g$$

where ρ_f is the density of the fluid medium (for air, $\rho_f = 1.29 \times 10^{-3}$ g/cm^3 at STP). The gravitational and buoyant forces are constant, but the drag force increases linearly with particle velocity, so that at some point the sum of the buoyant and fluid drag forces exactly equals the gravitational force, the acceleration becomes zero, and the particle attains a constant velocity. This terminal settling velocity is obtained by setting the sum of the forces equal to zero. Normally the buoyant force is negligible compared with the gravitational force. Making this assumption the terminal settling velocity expression becomes (Willike and Baron 32):

$$U_T = \frac{d_p^2 \rho}{18 \mu} g = \tau\, g$$

where τ is the particle's "relaxation time" and has units of seconds. As the particle diameter becomes smaller, an additional factor must be included in Stokes' Law to take account of the "slip" of the particle. This factor is known as the Cunningham slip correction, C_c, and is given by the expression (Hinds 49)

$$C_c = 1 + \frac{\lambda}{d}\left[2.34 + 1.05 \exp\left(-0.39 \frac{d}{\lambda}\right)\right]$$

where d_p is the particle diameter in micrometers and λ is the gas free mean path. This expression is appropriate for all particles in laminar flow. The time required for a particle initially at rest to reach U_T is approximately 7τ (Reist 82), which ranges from 10^{-6} to 10^{-3} sec for particles in the range of 0.1 to 10 um, respectively.

The terminal velocity becomes (Hinds 49)

$$U_T = \frac{d_p^2 \rho}{18 \mu} g \; C_c$$

Diffusion of aerosol particles in a gas medium results from the bombarded collisions with individual gas molecules that are in Brownian motion. This causes the particles to undergo random displacements. The particle parameter that describes this process is the particle diffusivity or diffusion coefficient, D_B. An expression for particle diffusivity is given by the Stokes-Einstein equation: (Hinds 152)

$$D_B = \frac{k_B \; C_C \; T}{3 \; \pi \; \mu \; d_p}$$

where k_B is Boltzmann's constant (1.38×10^{-16} dyn cm/K) and T is absolute temperature (K). The diffusion coefficient is inversely proportional to the particle's geometric size and is independent of particle density. The units of D_B. are cm^2/sec. Net motion by diffusion occurs when a particle concentration gradient exists. Fick's Law of Diffusion states that the flux of particles, J (particles per unit cross sectional area per unit time), is the product of the diffusivity, D, and the concentration gradient, dc/dx. Diffusive transport is favored by small particle diameter, large concentration differences, and short distances over which diffusion occurs. (Hinds 151 – 153)

Table 1 summarizes the properties of airborne particles that were used for this experiment. The values are for standard density particles (1.0 g/cm^3) at standard atmospheric conditions (1 atm and 20°C). The actual particle density and conditions experienced were not significantly different as to adversely impact these values.

TABLE 1 Particle Properties for Unit-Density Particles under Standard Conditions

Particle Diameter (um)	Slip Correction Factor C_c	Settling Velocity (cm/s)	Diffusion Coefficient (cm^2/s)
1.0	1.155	3.48×10^{-3}	2.74×10^{-7}
0.48	1.316	9.91×10^{-4}	6.24×10^{-7}
0.31	1.554	4.21×10^{-4}	1.23×10^{-6}
0.20	1.878	2.26×10^{-4}	2.23×10^{-6}
0.10	2.928	8.82×10^{-5}	6.94×10^{-6}
0.049	5.120	3.85×10^{-5}	2.43×10^{-5}

Using the diffusion coefficient, the root mean square displacement (X_{rms}) of a particle by Brownian motion along a given axis over a given period of time is (Hinds 157)

$$x_{rms} = \sqrt{2Dt}$$

The net displacement of the various particle diameters that were used for this experiment due to Brownian Motion and gravitational forces (terminal settling velocity x time) for one second are compared in Table 2.

TABLE 2 Displacement of Standard Density Spheres at STP due to Brownian Motion and Gravity (in one second)

Particle Diameter (um)	rms Brownian Displacement (x_{BM}) (cm)	Gravitational Settling (X_{grav}) (cm)	X_{BM}/X_{grav}
1.0	7.35×10^{-4}	3.48×10^{-3}	0.21
0.48	1.12×10^{-3}	9.91×10^{-4}	1.1
0.31	1.57×10^{-3}	4.21×10^{-4}	3.7
0.20	2.11×10^{-3}	2.26×10^{-4}	9.3
0.10	3.73×10^{-3}	8.82×10^{-5}	42.3
0.049	6.97×10^{-3}	3.85×10^{-5}	181.0

The ratio of Brownian to gravitational displacement (X_{BM}/X_{grav}) gives an indication of the of the forces effecting displacement. As the diameter of a particle decreases, especially below 0.10 um, the importance of diffusion and Brownian Motion to the displacement of a particle becomes more significant.

B. AFM Operation

The Dimension 3100 Atomic Force Microscope (AFM) produces high-resolution, three-dimensional images by scanning a sharp probe over the sample surface. The probe is part of a flexible cantilever which is mounted on one end of a cylindrical piezoelectric tube. The piezo tube is rigidly mounted near the top of the microscope. Voltages applied to the X and Y electrodes on the piezoelectric tube deflect the tube horizontally to produce a precise raster scan over the sample surface. The vertical height of the probe is controlled by a voltage applied to the Z electrode on the piezo tube. A stepper motor coupled to a

lead screw translates a slide to which the sample is attached. A separate motor drive allows the height of the microscope and probe to be adjusted relative to the sample surface .

1. Modes of Operation: Tapping or Contact

Surface topography of a sample may be evaluated by the AFM using either contact or TappingModes (TappingMode is a trademark of Digital Instruments) of operation. In contact mode AFM, the probe tip is pulled across the surface and the resulting image is a topographical map of the surface of the sample. The drawback with this method is that the dragging motion of the probe tip, combined with adhesive forces between the tip and the surface, can cause substantial damage to both sample and probe and create artifacts in image data.

Under ambient air conditions, surfaces are covered by a layer of adsorbed gases (condensed water vapor and other contaminants) which is typically several nanometers thick. When the scanning tip touches this layer, capillary action causes a meniscus to form and surface tension pulls the cantilever down into the layer. Trapped electrostatic charges on the tip and sample can contribute additional adhesive forces. These downward forces increase the overall force on the sample and, when combined with lateral shear forces caused by the scanning motion, can distort measurement data and cause severe damage to the sample, including movement or tearing of surface features.

Tapping Mode allows high-resolution topographic imaging of sample surfaces that are easily damaged, loosely held to their substrate, or otherwise difficult to image. Specifically, TappingMode overcomes problems associated with friction, adhesion, and electrostatic forces.

TappingMode imaging alternately places the probe tip in contact with the surface to provide high resolution and then lifting the tip off the surface to avoid dragging the tip across the surface. TappingMode imaging is implemented in ambient air by oscillating the cantilever assembly at or near the cantilever's resonant frequency using a piezoelectric crystal. The piezo motion causes the cantilever to oscillate at a high amplitude (the "free air" amplitude, typically greater than 20nm) when the tip is not in contact with the surface. The oscillating tip is then moved toward the surface until it begins to lightly touch, or "tap," the surface. During scanning, the vertically oscillating tip alternately contacts the surface and lifts off, generally at a frequency of 50,000 to 500,000 cycles per second. As the oscillating cantilever begins to intermittently contact the surface, the cantilever oscillation is necessarily reduced due to energy loss caused by the tip contacting the surface. The reduction in oscillation amplitude is used to identify and measure surface features. (Prater et al, 1-4)

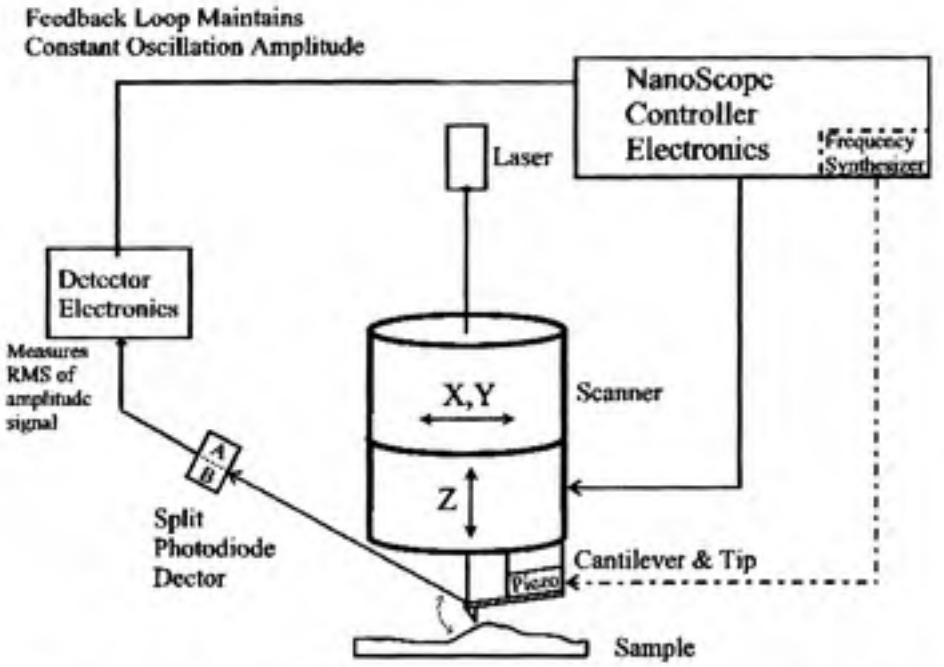

FIGURE 1. Schematic of major components of the AFM showing feedback loop for TappingMode operation.

During TappingMode operation, Figure 1, the cantilever oscillation amplitude is maintained constant by a feedback loop. Selection of the optimal oscillation frequency is software-assisted, and the force on the sample is automatically set and maintained at the lowest possible level. When the tip passes over a bump in the surface, the cantilever has less room to oscillate and the amplitude of oscillation decreases. Conversely, when the tip passes over a depression, the cantilever has more room to oscillate and the amplitude increases (approaching the maximum free air amplitude). The oscillation amplitude of the tip is measured by the detector and input to the controller electronics. The digital feedback loop then adjusts the tip/sample separation to maintain a constant amplitude and force on the sample. TappingMode prevents the tip from sticking to the surface and causing damage during scanning. When the tip contacts the surface, it has sufficient oscillation amplitude to overcome the tip/sample adhesion forces.

2. Scan Results

Surface data from scans may be presented in a number of formats for evaluation. (Digital Instruments, NanoScope Command Reference Manual, 12-20),

Top View: displays the scan data from a top-down perspective. X and Y coordinate information is in the plane of the display, and height information (Z coordinate) is represented by the color at a given point. The data scale value and display colors may be altered after a scan is completed to highlight a particular surface feature of interest.

Surface Plot: scan data is displayed with color-coded height information in a three-dimensional, oblique perspective. The viewing angle and illumination angle for a modeled light source are user selectable to help differentiate between adjacent structures.

Section Analysis: a top view image of the scan data is displayed, upon which up to three reference lines may be drawn. The cross-sectional profiles of data along these lines are shown in separate windows on the output. Up to three cursors may be placed on the line section at any point to make horizontal and vertical measurements along the surface structure. These measurements are reported in the box at the lower right of the display.

Roughness: using ASME methodology, roughness provides an indication of the 'texture' of a surface (Digital Instruments, NanoScope Command Reference Manual 12-20). Useful values include;

Z Range: vertical difference between the highest and lowest data points within the image.

Ra: the mean roughness, represents the arithmetic average of the deviations of each data point from a calculated center plane.

$$R_a = \frac{\sum_{i=1}^{N} | Z_i - Z_{cp} |}{N}$$

Z_{cp} is the Z value of the center plane, Z_i is the current Z value, and N is the number of data points within the image area.

Rms (Rq): The root mean square (RMS) is the standard deviation of the Z values within the image.

$$RMS = \sqrt{\frac{\sum_{i=1}^{N} (Z_i - Z_{avg})^2}{N}}$$

Z_{avg} is the average Z value within the image area, Z_i is the current Z value, and N is the number of data points within the image area.

Pixelization, Resolution, and Scan Size

A pixel represents each data point in the X and Y direction of the scan. The available choices for the Digital Instruments 3100 AFM are 512, 256, or 128 pixels per line under the Sample/Line parameter of the scanning menu. Pixelization affects resolution in that features smaller than the image's pixel size cannot be resolved. Pixel size is determined

by dividing the scan size by the pixel per line number selected from the Sample/Line parameter menu. To illustrate, if one were acquiring a 50 um by 50 um image with the Sample/Line parameter set to 256 pixels per line, then the pixel size would be 195nm (50um / 256 = 0.195 um or 195 nm). One would not be able to resolve features smaller than 195 nm at a 50 um by 50 um scan size. To view 50 nm surface feature using 512 pixels per line value, the scan size must be less than 25.6um (0.050um x 512 = 25.6um). Selecting a larger scan size would mean that the 50 nm feature would not be seen. (Digital Instruments, Scanning Probe Microscopy Training Notebook, 19.5.1),

III. MATERIALS AND METHODS

A. Selection of Substrate:

To determine a suitable substrate for deposition of sub-micron particles for analysis using the AFM, sample targets were produced from materials available on hand in the laboratory. Sample targets, approximately 4 cm^2, were produced from polished glass, frosted glass, mica, plastic (from a compact disk case), stainless steel (cold rolled), and aluminum (cold rolled). The targets were thoroughly cleaned and rinsed with distilled water to remove any surface contaminates. For the mica target, a new surface was obtained by peeling off the outermost mica layer and exposing a fresh surface. Baseline scans were taken of the sample targets to determine their surface characteristics prior to depositing particles.

After baseline scans were completed, the sample targets were placed on an elevated tray within a small circular glass chamber measuring 30 cm diameter by 50 cm high. Nebulizing a liquid suspension containing monodispersed solid particles of a known size generated a monodispersed solid particle aerosol. A suspension of 0.480 um polystyrene latex (PSL) beads (Duke Scientific Corp.) was used for this exercise. A solid particle aerosol was generated at a flow rate of 5 lpm using a constant output atomizer (TSI, Model 9302A). A small capture flask collected liquid that deposited in the tubing on the output of the atomizer and prevented any obstruction to the aerosol. After nebulization, a diffusion dryer was used to remove the remaining liquid from the aerosol, producing a solid particle aerosol. To minimize the effects of electrostatic drift on deposition, a Boltzmann charge distribution was induced on the particles after generation and drying using a Kr-85 charge neutralizer (TSI model 3057).

The solid particle aerosol was injected into the chamber for 30 minutes. A dispersal plate mounted in the chamber, in line with the aerosol flow, provided mixing within the chamber and minimized direct impaction of the particles on the targets. After injection, the chamber was sealed, and the particles were allowed to deposit for several days (typically 48 – 72 hrs). When sufficient time had elapsed, the sample targets were removed from the glass chamber and mounted on the AFM microscope stage. The AFM was calibrated and tuned at the start of each series of measurements. The targets were scanned and results recorded. This procedure was repeated using 0.300um and 0.200um PSL beads.

B. Sedimentation vs Diffusion

Once an appropriate material was selected for use as targets, the AFM was used to try to determine the extent that either sedimentation or diffusion influenced the deposition of sub-micron particles.

Inside a large Plexiglas test chamber (151.1cm height, 127.0 cm wide, and 61.6 cm deep) metal mounting plates were placed along the floor, back wall, and top (Figure 2) . Existing exhaust ventilation connections were removed, openings sealed, and the chamber isolated from its surroundings as much as practically possible. The chamber was maintained in a controlled environment where variations in temperature or humidity were minimized. Access to the lab was limited, and the chamber remained undisturbed throughout the investigation.

Targets of polished glass slides were thoroughly cleaned and rinsed with distilled water. The slides were numbered 1-5 and mounted in the chamber on the metal mounting plates, # 1 on the center of the chamber ceiling, #2 on the center line of the back wall (30.5 cm from the top), #3 in the center of the back wall, #4 on the center line of the back wall (30.5 cm from the bottom), and # 5 in the center of the chamber floor. The chamber was sealed and the mono-dispersed solid particle aerosol generation train previously described was connected to the chamber. Particles were injected at low velocity into the center of the chamber from a spherical diffuser (7.6 cm diameter) with 12 openings (each with an area of 0.5 cm^2) distributed evenly around the sphere. A small fan set at low speed, mounted in the chamber, provided mixing and uniform distribution of the particles while they were being injected into the chamber. The mounting plates on the inside of the chamber, as well as all components used to generate the aerosol, were grounded. Conductive tubing was used throughout.

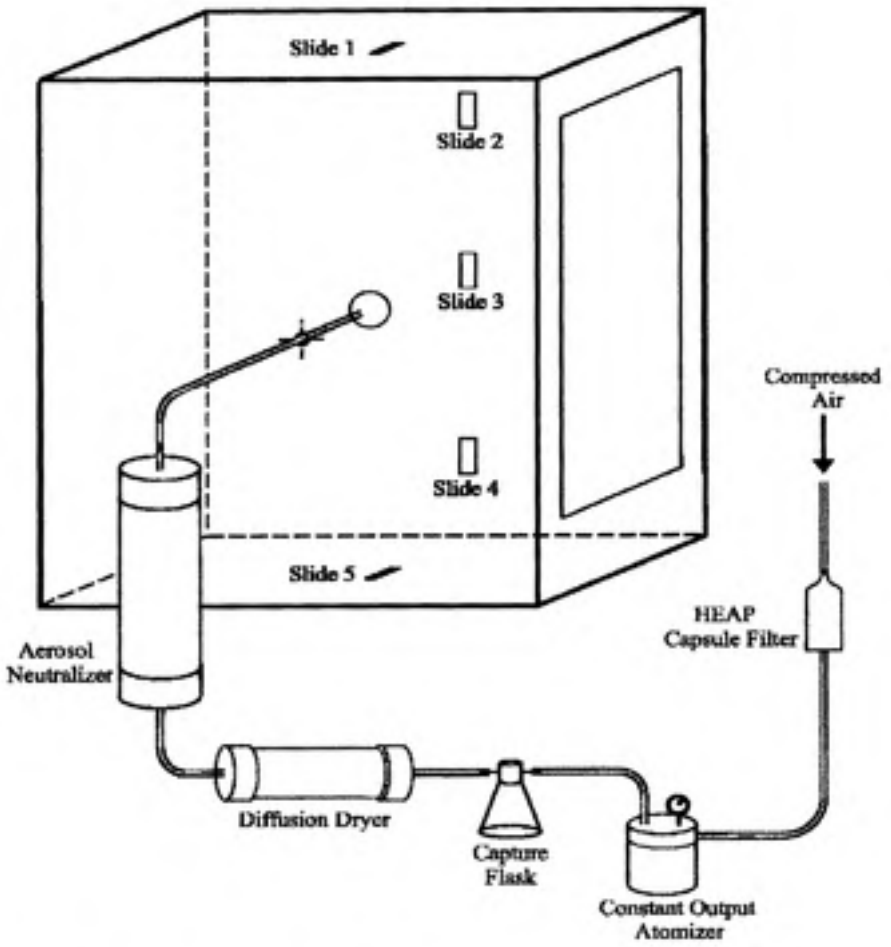

FIGURE 2 Schematic of Test Chamber, Target Slide Placement, and Aerosol Generation System

Suspensions of polystyrene latex (PSL) beads (Duke Scientific Corp.) ranging in size from 1.00 um to 0.049 um were produced for this exercise. A dilution of 0.2 ml PSL suspension was mixed with 100 ml of de-ionized water and used to fill the constant output atomizer, (a significant number of doublets/triplets formed if higher concentrations of PSL suspension were used).

A solid particle aerosol was injected into the chamber for 3 hours at a flow rate of 5 lpm. After injection, the mixing fan was turned off, the chamber sealed, and the particles

allowed to deposit. Attempts to measure the quantity of suspended particles in the chamber was attempted but unsuccessful due to equipment failure.

The particles' terminal settling velocity and chamber height determined settling times. Table 3 provides the settling velocities and the maximum time it would take for the particle to transit the height of the chamber by gravitational settling. When the settling time had elapsed, the sample targets were removed from the glass chamber and placed in a sealed container to prevent contamination. The chamber and aerosol generation equipment were cleaned and purged to remove any remaining particles. The AFM was isolated from the rest of the lab to reduce the possibility of contamination. Target slides were mounted on the AFM microscope stage. The AFM was calibrated and tuned at the start of each series of measurements. The targets were scanned and results recorded.

TABLE 3 Settling Time for Standard Density Particle to Travel from the Top of the Chamber to the Floor by Gravitational Settling

Particle Diameter (um)	Settling Velocity (m/s)	Settling Time seconds (days)
1.0	3.48×10^{-5}	4.34×10^{4} (0.50)
0.48	9.91×10^{-6}	1.52×10^{5} (1.76)
0.31	4.21×10^{-6}	3.59×10^{5} (4.15)
0.20	2.26×10^{-6}	6.68×10^{5} (7.73)
0.10	8.82×10^{-7}	1.71×10^{6} (19.81)
0.049	3.85×10^{-7}	3.92×10^{6} (45.39)

The available settling time for the 0.049 um particles was cut short (22 days) due to pending construction in the laboratory and the need to remove the test chamber.

IV. RESULTS

A. Baseline Scans

Baseline scans for each substrate are shown in Appendix A. The same scan size (50um x 50um), data scale (500 nm), and number of samples (512) were used for all scans to provide a standard reference perspective and reduce confusion.

The top view and surface plots provide a visual indication of the general surface characteristics of the materials. Scans of mica and glass appear to be nearly featureless. Surface contours start to become apparent on the plastic surface and are even more visible on the aluminum and stainless steel. The surface structure of the frosted glass slide shows the most variation and in many places exceeds the 500 nm data scale used for the scans.

Section analysis plots allow the measurement of individual features of the surfaces scanned. A reference line (vertical line shown on scan) was plotted to show a cross-sectional profile of the surface along the line. Cursors were placed on selected high and low points to give a range of the surface variation along the reference line. Mica and glass again show a very uniform surface with very little variation is surface structure. Plastic, aluminum and stainless steel plots show surface features that are increasingly complex and varied. The section analysis of the frosted glass shows that the surface profile along the reference line exceeded the 500 nm scale.

Roughness analysis plots provide a top view of the material scanned and the calculated roughness statistics. Measured roughness values for each material, Table 4, provide a relative indication of the surface texture to the material.

TABLE 4 Measured Roughness Values for Each Target Material

	Z Range (nm)	Ra (nm)	RMS (nm)
Mica	12.083	0.533	0.822
Glass Slide	40.383	0.580	0.816
Plastic	107.66	7.427	10.143
Aluminum	399.94	71.144	83.051
Stainless Steel	842.91	51.013	66.431
Frosted Glass Slide	1242.00	159.91	196.15

Z Range: vertical difference between the highest and lowest data points

Ra: the mean roughness, average deviations of each data point

RMS: root mean square, standard deviation of the Z values

B. Selection of Substrate

Scans of each substrate after a mono-dispersed solid particle aerosol was generated and allowed to deposit are shown in Appendix B, C, and D. Measuring the diameter of individual PSL beads is shown on the section analysis display. One display curser is placed on the top (highest elevation) of the bead and the other is placed on the surface. The difference is displayed as the vertical distance and represents the diameter of the PSL bead.

C. Sedimentation vs Diffusion

Scans of the particles deposited onto five target slides placed in the test chamber provide an indication as to the forces affecting deposition of aerosol particles. Scans were completed after the PSL particles were injected into the test chamber and allowed to deposit onto the target slides, a representative scan for each particle size is provided in Appendix E. Twenty scans were taken of each slide and the number of PSL beads found in each scan was recorded. Total particle count for each slide was averaged and the concentration of particles deposited determined (# / cm^2), Appendix F. Table 5 summarizes the concentration of particles deposited onto target slides for each size particle used. The final column gives the percentage of the average particle concentration on targets 1-4 relative to the concentration of particles found on target 5.

TABLE 5 Particle Concentration on Target Slides for Particle Size

Particle Diameter (um)	Target 1 (# / cm^2)	Target 2 (# / cm^2)	Target 3 (# / cm^2)	Target 4 (# / cm^2)	Target 5 (# / cm^2)	%
1.0	0	0	0	0	1.95×10^4	0
0.48	0	0	7.81×10^2	1.65×10^3	2.11×10^4	5.7
0.31	0	7.81×10^2	2.34×10^3	7.03×10^3	2.65×10^4	12.7
0.20	0	7.81×10^2	4.68×10^3	1.01×10^4	3.12×10^4	16.6
0.10	2.00×10^3	6.00×10^3	1.40×10^4	2.20×10^4	6.00×10^4	18.3
0.049	1.60×10^4	2.40×10^4	5.60×10^4	8.80×10^4	1.92×10^5	23.9

V. Discussion of Results

Key points:

- In the review of the baseline scans (Appendix A), there is a good visual correlation between the roughness values measured and the three dimensional displays of the surface plots and section analysis cross sectional profiles. Scans of materials with the largest roughness values could be seen to have the greatest variation in surface structures. This was particularly evident in the scans of the frosted glass and stainless steel targets.

- Selection of material for the sample target becomes more important as the scale of interest decreases. Measuring the larger particles was relatively easy on any of the targets. As the particle size decreases, however, the ability to accurately measure the true diameter becomes more challenging. Identifying and measuring the 0.480 um PSL beads was easily accomplished no matter what target material was used. Measuring 0.200 um particles on surfaces with the highest roughness values, such as stainless steel or frosted glass, was very difficult. The extensive variation in the surfaces' cross section profiles (shown the section analysis displays) created difficulty in selecting a point on the surface from which to measure the vertical distance to the top of the deposited particle. The low roughness values and smoother cross section profiles for the glass and mica made them better suited for use as targets for the remainder of the study.

- Using the AFM to infer the predominate forces (diffusion or sedimentation) acting on a particle as it deposited onto a surface was partly successful. The AFM was able to accurately identify and measure the smallest PSL beads deposited onto the glass slides used as targets. The results obtained from the measurement of particles deposited onto the target slides tended to confirm that as the particle size decreases diffusion starts to exert more influence over the particles behavior.

If sedimentation were the only force influencing the deposition of particles, then no matter what the size, particles would collect only on the target slide on the floor of the chamber. If diffusion controlled particle deposition, then the particles would collect uniformly on all the target slides. The scans show that for the largest particles (1.0 um diameter) no particles were found on the top or side targets (slides 1-4), Appendix E. Particles were found on slide 5 located on the chamber floor. This indicates that sedimentation had the greatest effect on particle deposition. But as the particle size decreased, particles were found on the target slides attached to the wall of the test chamber. Table 5 shows that the concentration of particles deposited on the side target slides increases as the particle diameter decreases. The table also shows that the relative percentage of the particles deposited on slides 1-4 increases (when compared to slide 5) as the particle diameter decreases. This indicates that diffusion began to have an influence on the particles as their size decreased, and they deposited onto the chamber's sides before settling to the chamber's floor.

The inability to obtain or generate smaller sized particles limited the extent to which this relationship could be explored.

- Not being able to determine the concentration of suspended particles in the chamber hindered this exercise. Knowing the quantity of material injected and the concentration deposited would have allowed the development of a mass balance relationship that could have indicated how effective the design and procedures of the experiment were.

- It was possible to successfully use glass slides as targets for 0.049 um PSL beads. Using them on smaller particles could be a problem. Even though the glass slides have a very low roughness value, compared to the other materials, the variation in its cross sectional profile could make the identification and measurement of particles difficult.

  Also, it was observed that the target slides could easily become contaminated with sub-micron particles from the ambient air or lab equipment. A great deal of effort went into purging and cleaning the test chamber and aerosol generating equipment to reduce cross-contamination. Slides with particles deposited on them but not yet scanned were stored in small, sealed containers.

- As the particle size continues to decrease, the impact of pixelization on the resolution of the microscope and the scan size become more dramatic. Each data point in the X and Y direction of the scan is represented by a pixel, and the size of the pixel is determined by dividing scan size by the number of pixels per line. As the diameter of particle deposited onto the target slides becomes smaller the size of the scan must

also become smaller. Additional scans or higher concentrations of particulates would be necessary to obtain useful data as the particles become smaller.

- The time required to complete a single scan of one of the target slides ranged from 45 minutes to over 90 minutes. Large scan sizes, rough surfaces, high resolution, and target surfaces contaminated with various sized particles increased the length of time necessary to obtain a useful scan. Initially, over half the scans attempted were unreadable and discarded. As familiarity and proficiency with the equipment increased, the numbers of unreadable scans and scan times decreased. However, the number of unreadable scans and overall scans times remained high.

- One of the underlying assumptions of this experiment was that the chamber was at a steady state and not subject to temperature variations while particles were settling. Changes in temperature would have caused convection flow along the surfaces of the chamber and stirring of the suspended particulate. This would result in a more uniform deposition of particles in the chamber, giving the impression that diffusion had a stronger influence than it really did. To prevent this the chamber was maintained in a controlled environment where variations in temperature or humidity were minimized. Access to the lab was limited, and the chamber remained undisturbed throughout the investigation

VI. Conclusions:

- The AFM is a highly sophisticated, robust tool that is capable of sizing and counting sub-micron particles deposited onto the surface of materials. It is relatively simple to operate, requires no intermediary steps between collection and evaluation, and provides results in an easily understood format. Its sophistication however, limits its practical usefulness outside the laboratory. Lengthy scan times, contamination of sample surfaces from particles suspended in the ambient air, and decreasing scan size to detect smaller particles make the AFM more suitable for research than field work.

  Using a monodispersed solid particle aerosol of a known size greatly simplified the experiment design and analysis. Attempting to do the same experiment with an aerosol of mixed or unknown size particles would be extremely difficult. The particles deposited onto a surface could, with great difficulty, be sized and counted. However, it would be impossible to determine if the particles were part of the aerosol generated for the experiment or contamination from the ambient air.

  For the analysis of sub-micron sized particles deposited onto a surface, the AFM operates best in the controlled environment of the laboratory.

- The AFM was helpful in developing some insight into the forces affecting the deposition of sub-micron particles in a still environment. As particle size decreased, the AFM was able to detect and measure particles that collected on target slides located on the top and sides of the test chamber. The total number of particles counted, as well as the percentage of particles deposited on the side target slides

increased as the particle size decreased. As the particle size decreases, particularly to 0.200 um and below, diffusion begins to exert a significant influence on the deposition of particles onto a surface in a still environment.

Mica

Top View

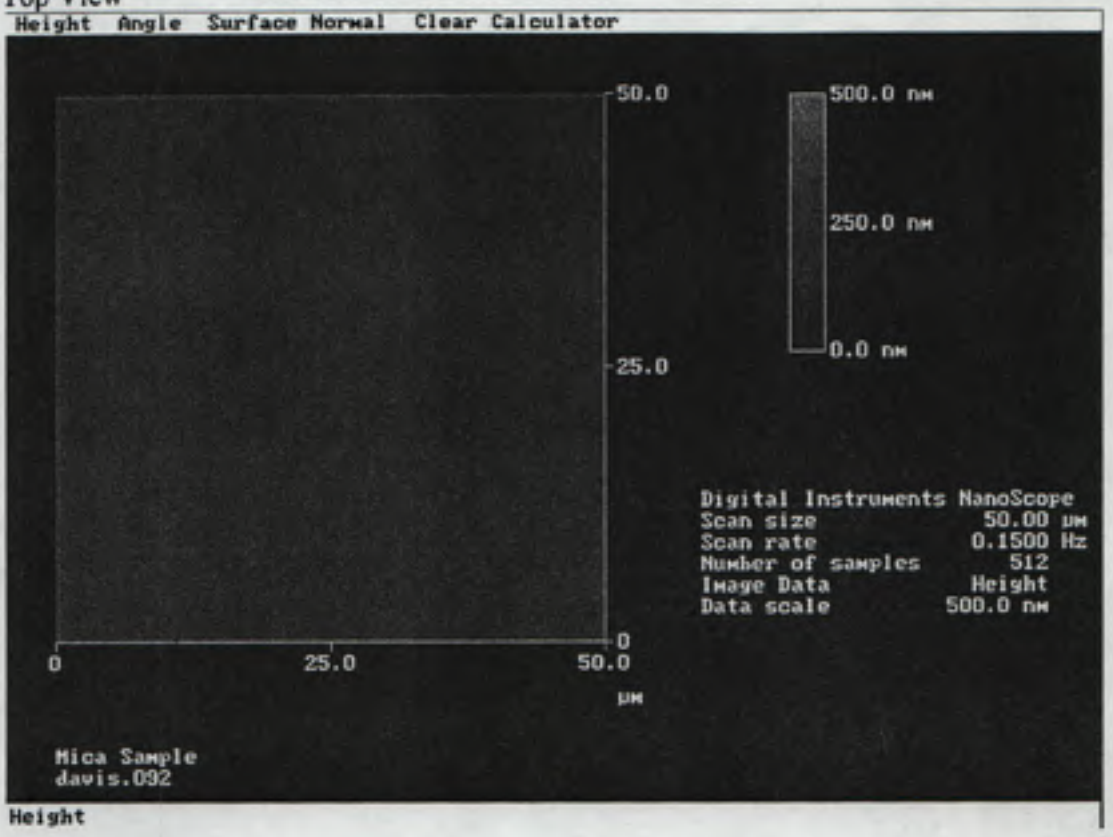

Surface Plot

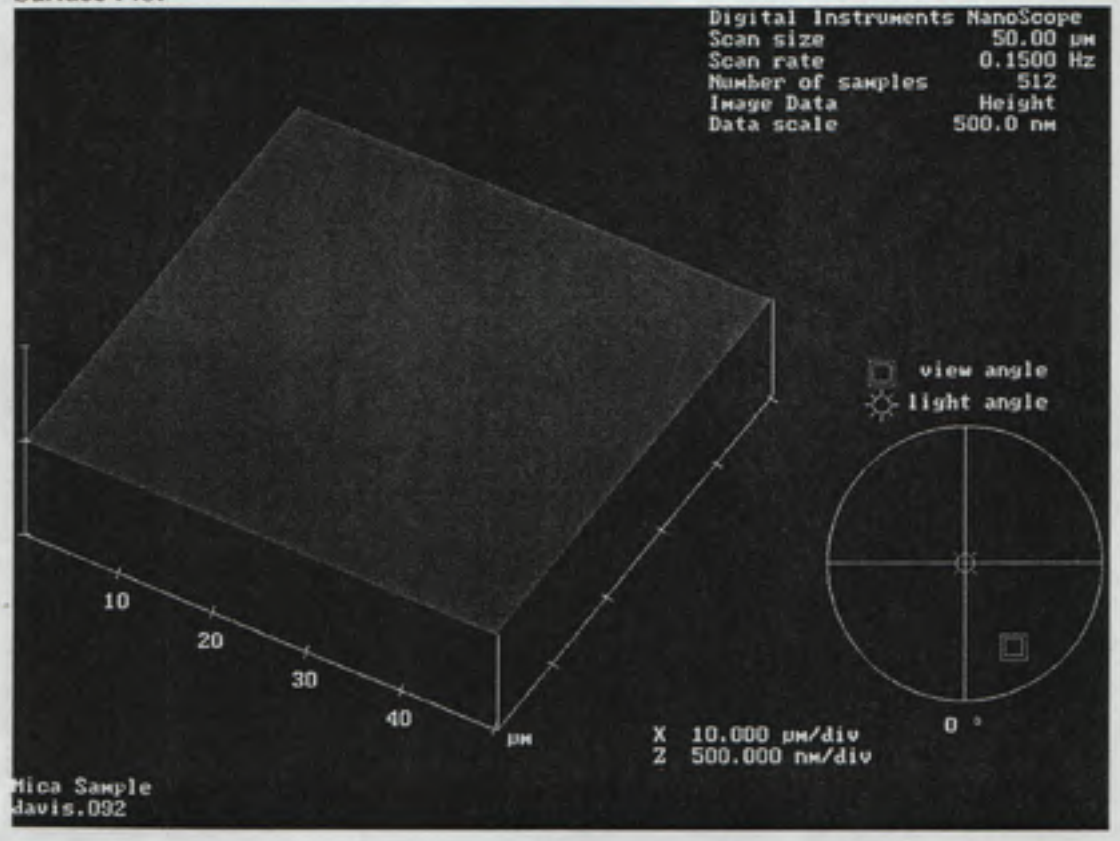

Mica

Section Analysis

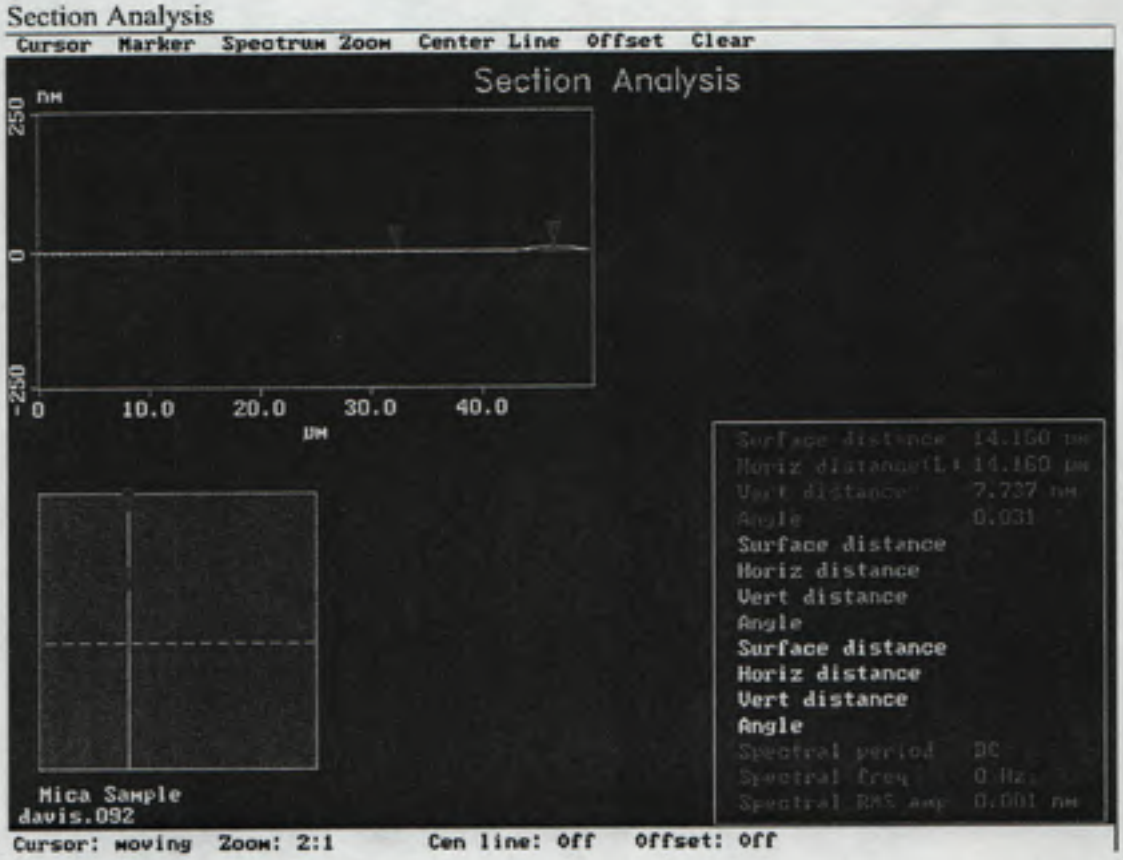

Roughness

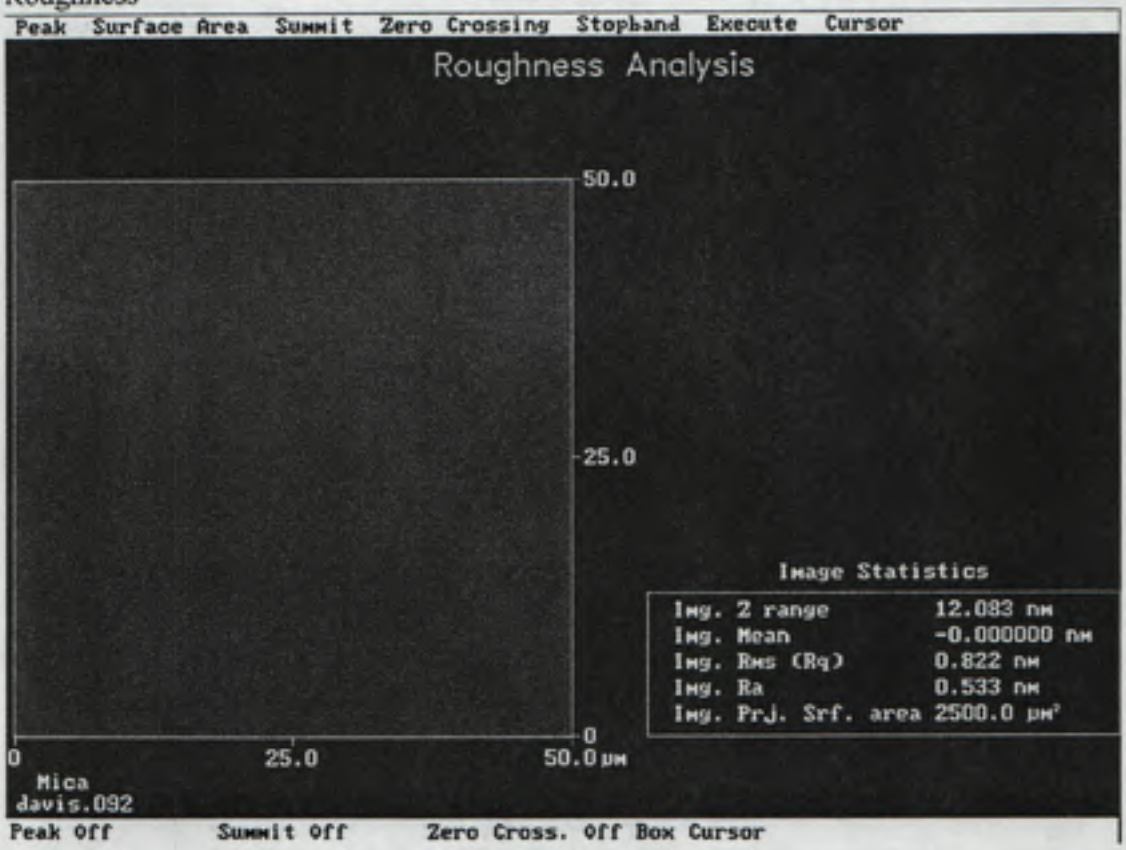

Aluminum Disk

Section Analysis

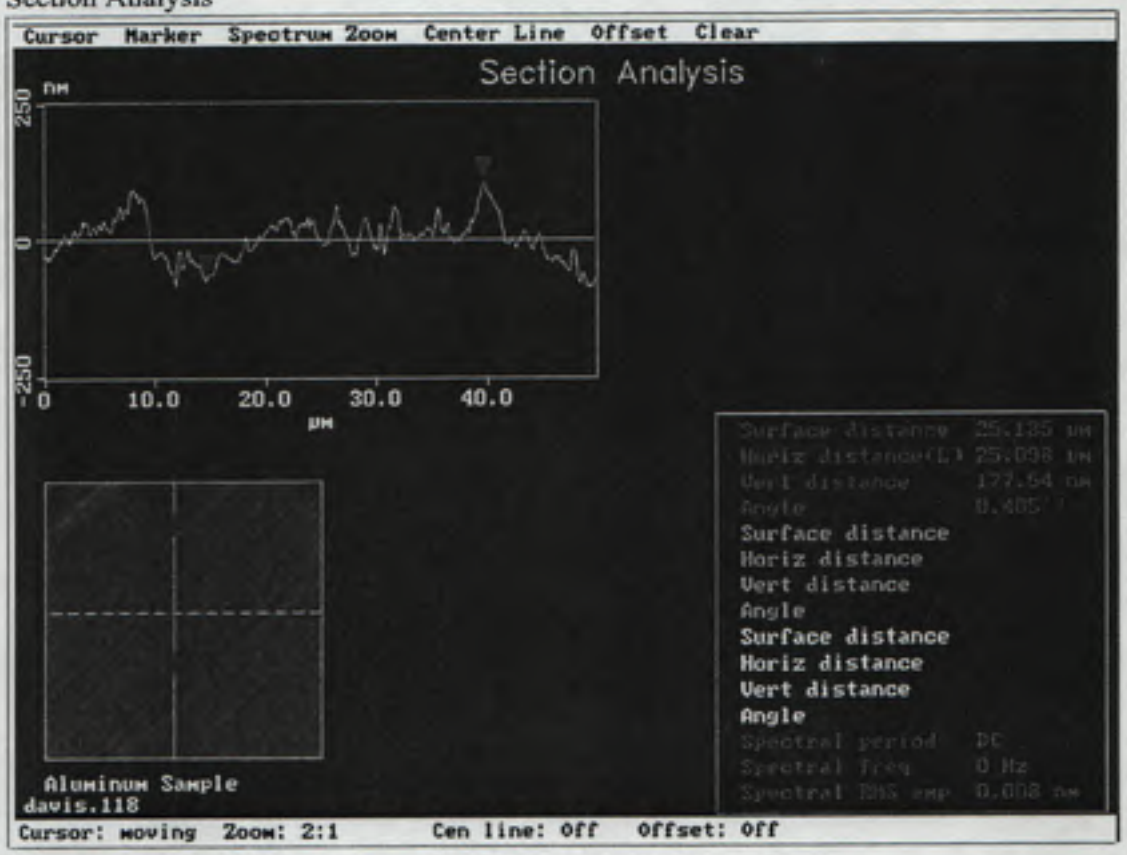

Roughness

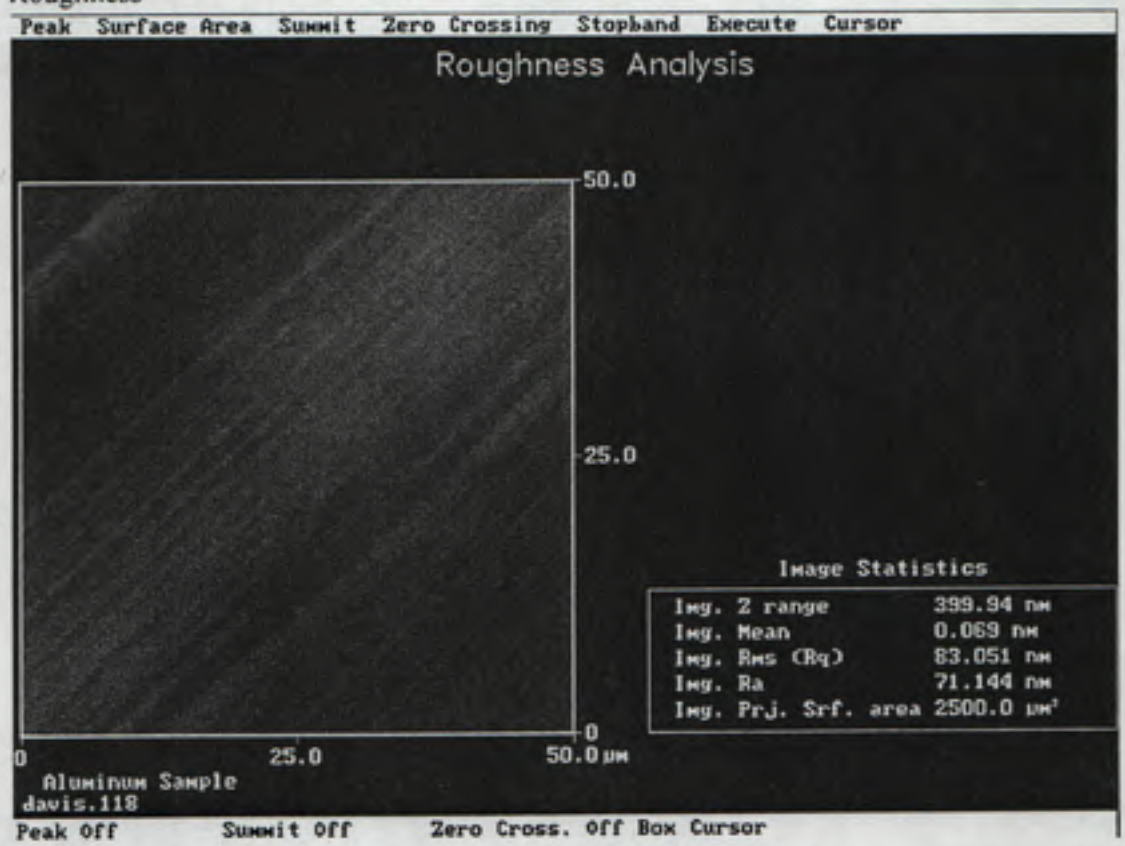

Aluminum Disk

Top View

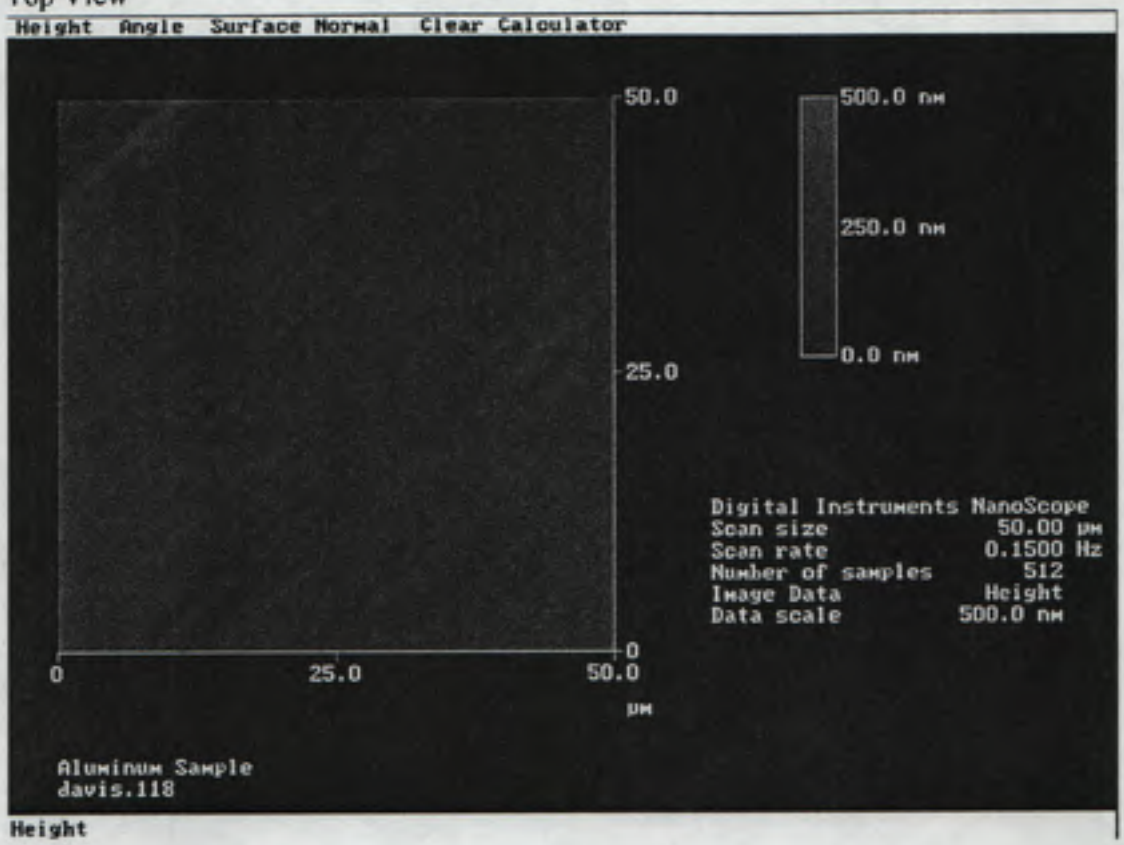

Surface Plot

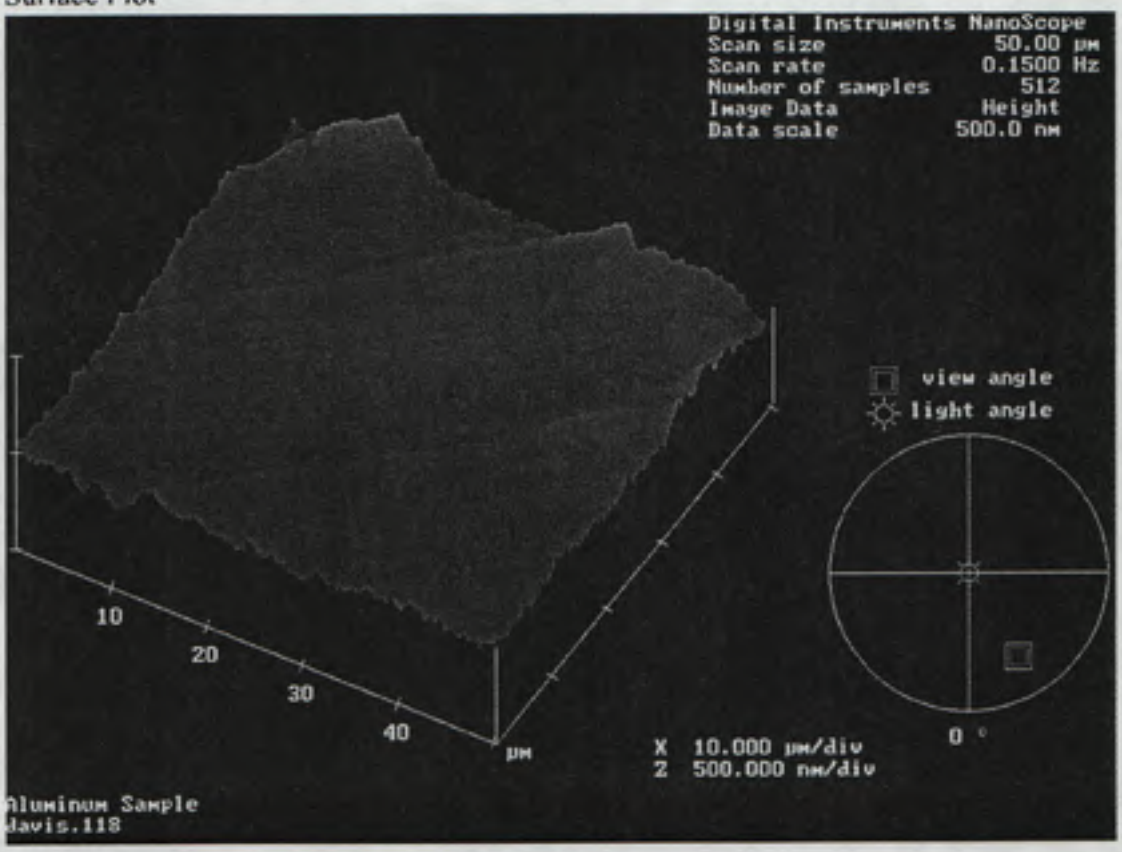

Plastic

Section Analysis

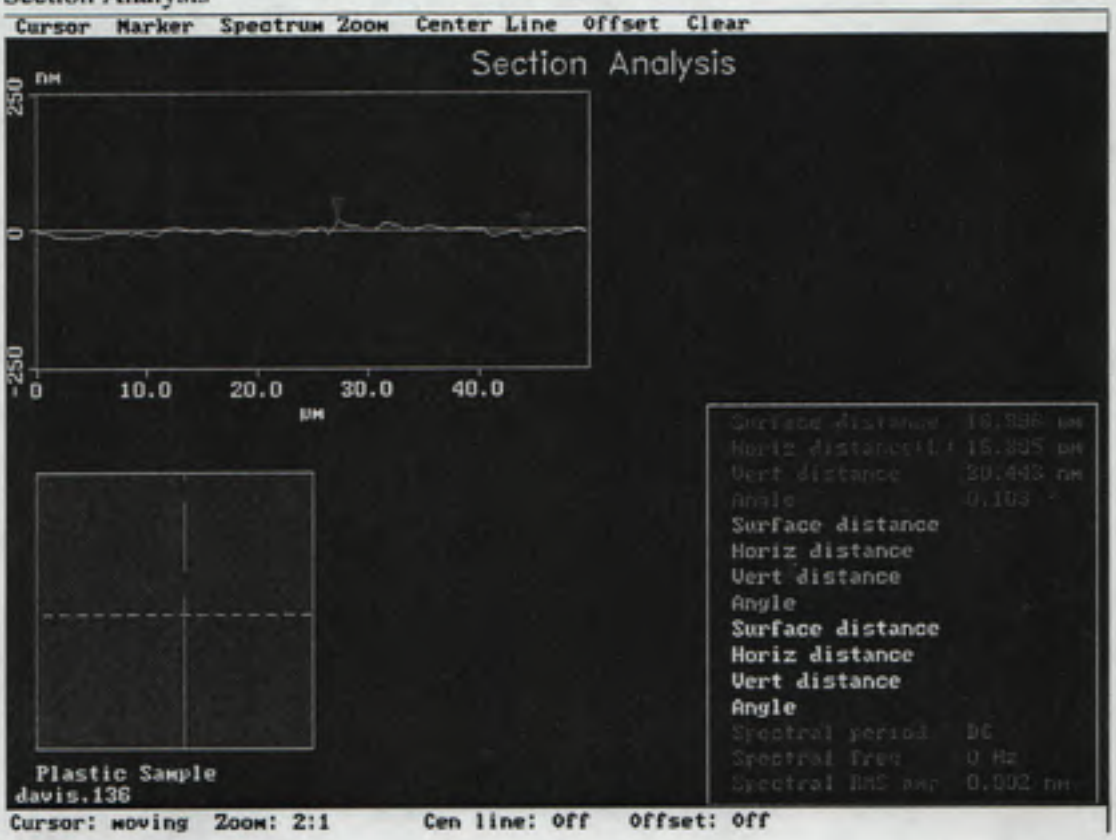

Roughness

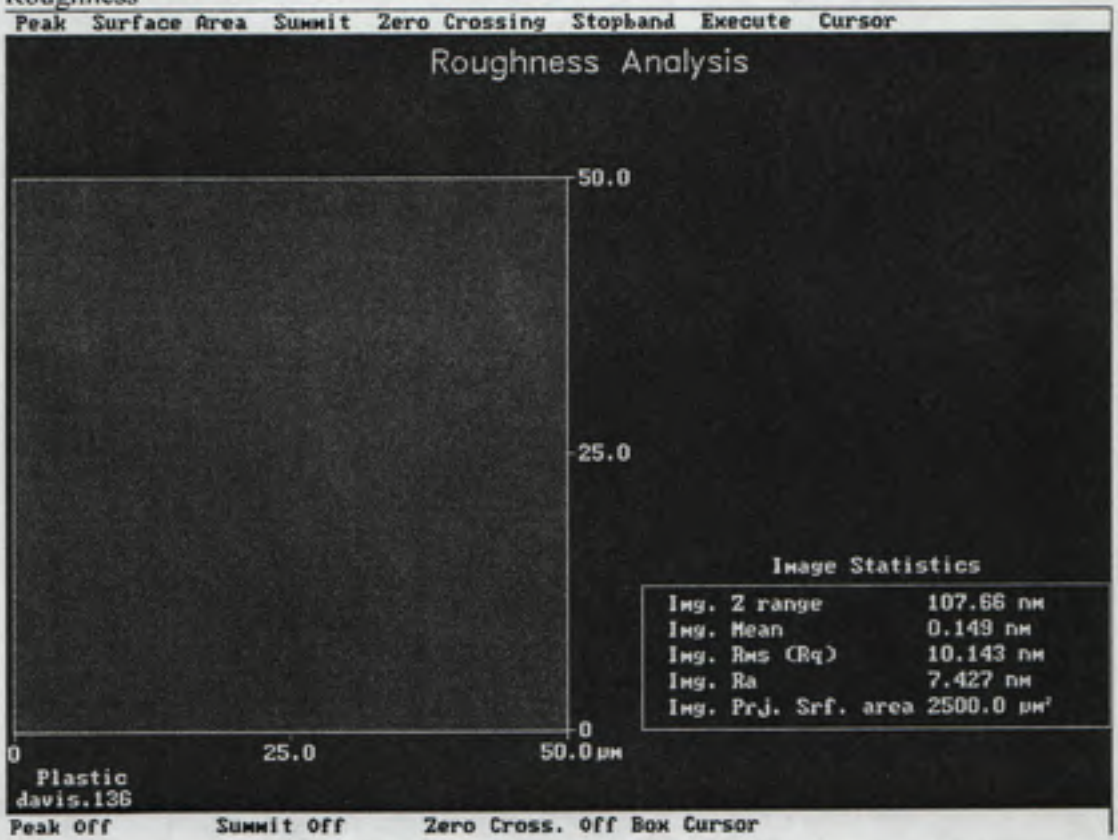

Plastic

Top View

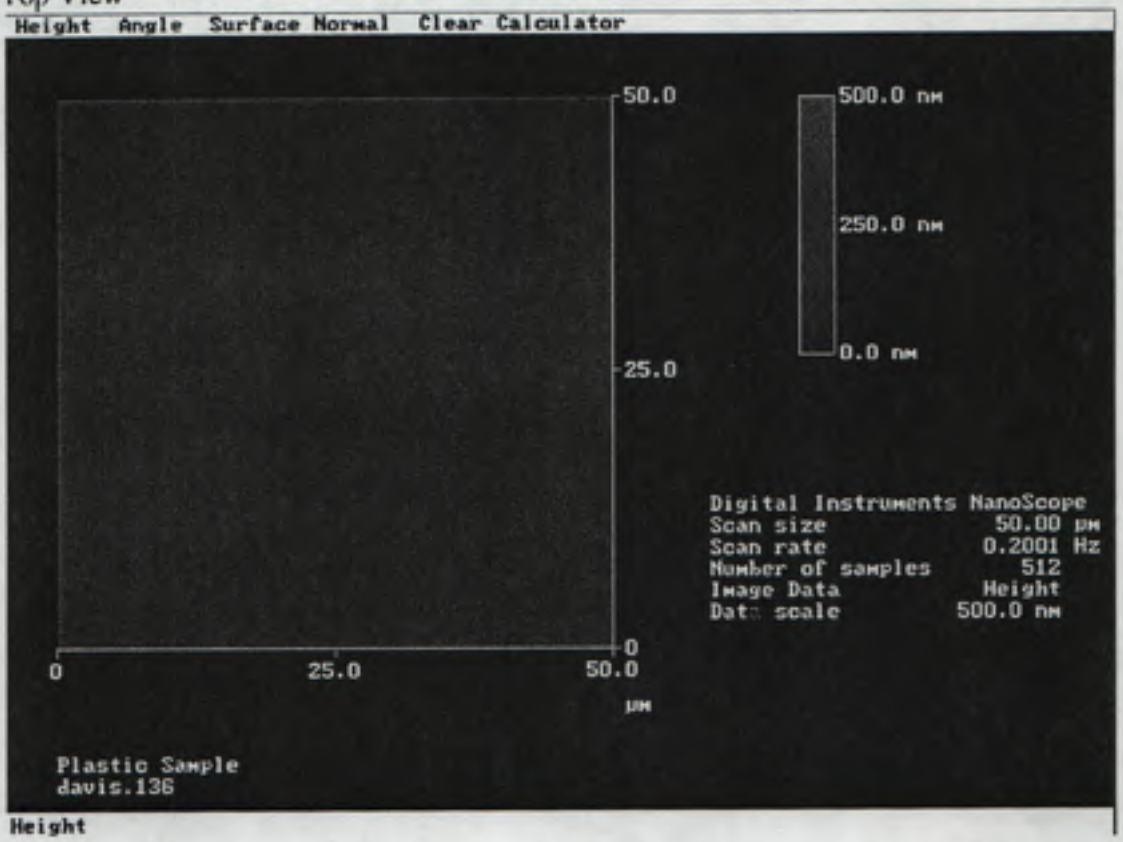

Surface Plot

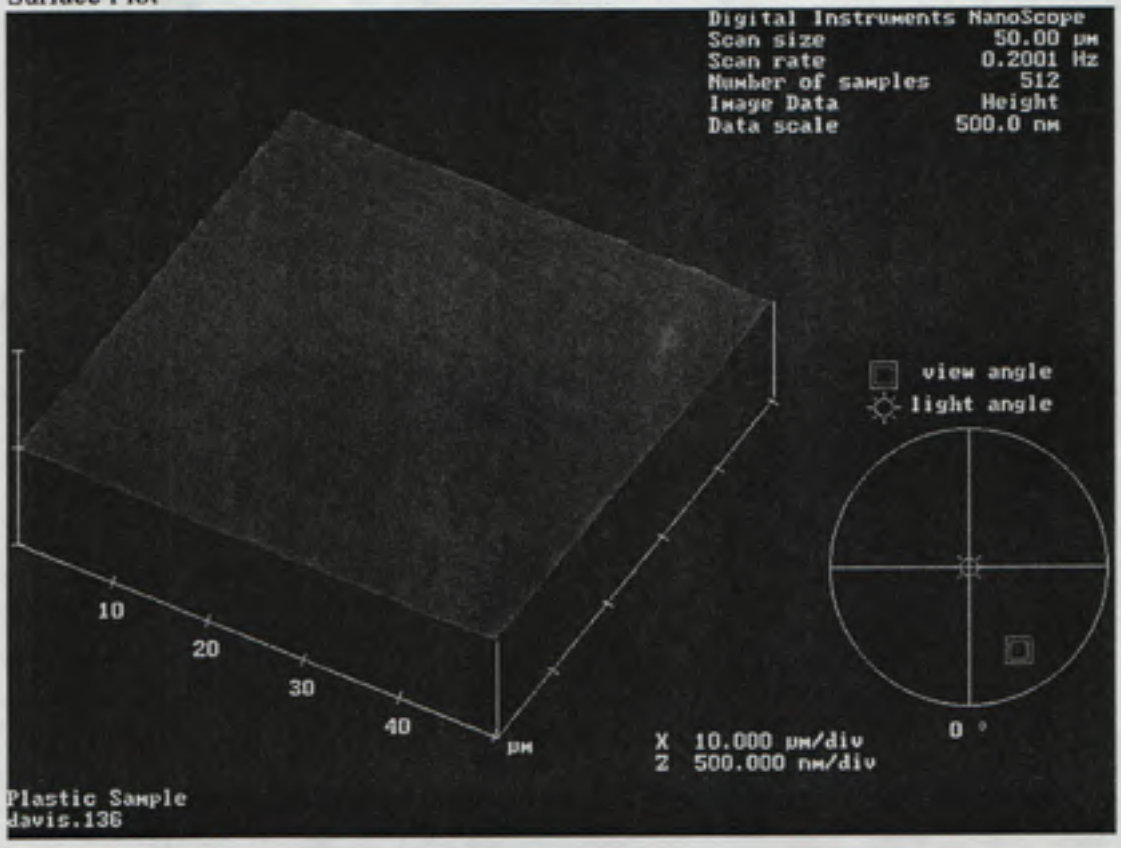

Stainless Steel

Top View

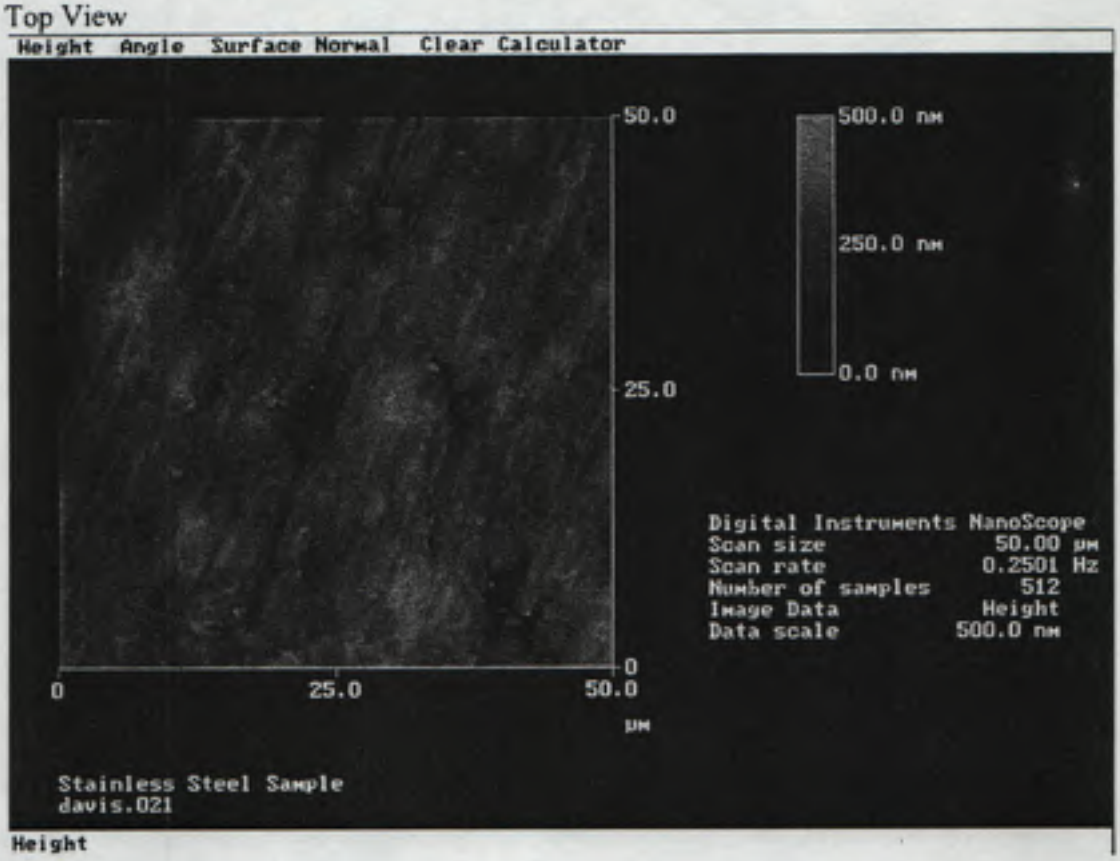

Surface Plot

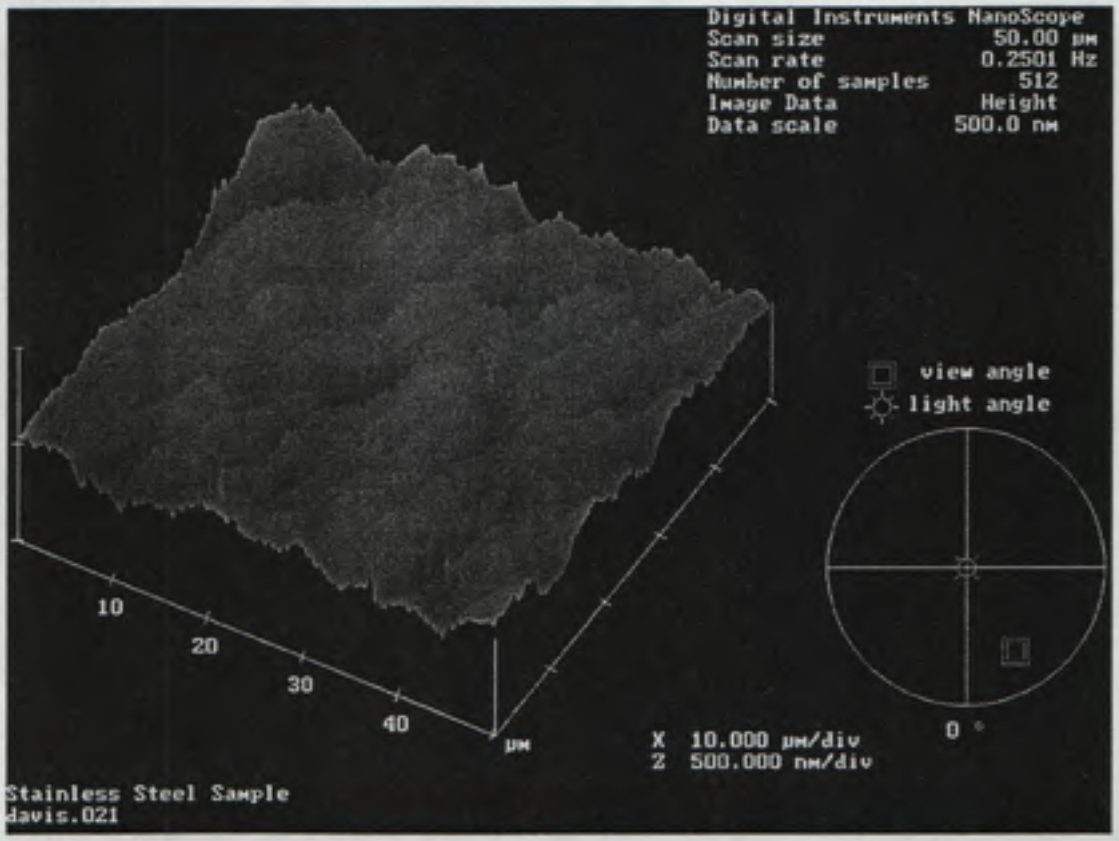

Stainless Steel

Section Analysis

Roughness

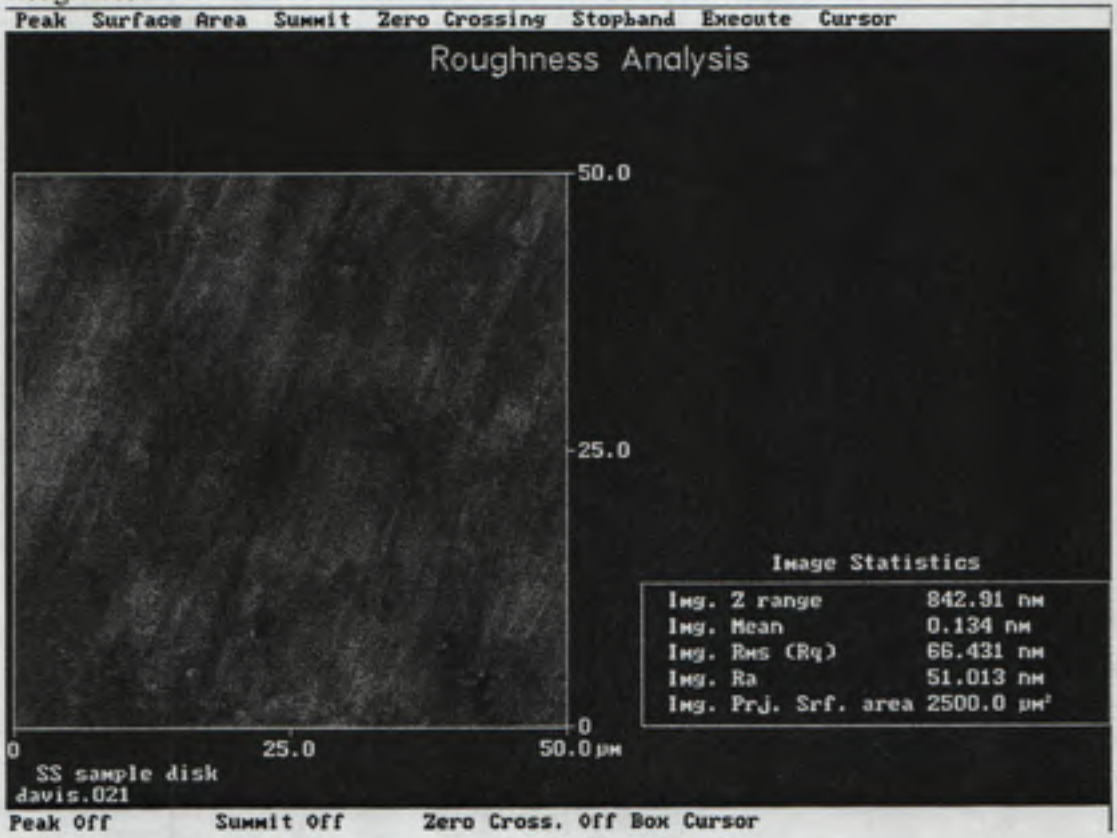

Glass Slide

Top View

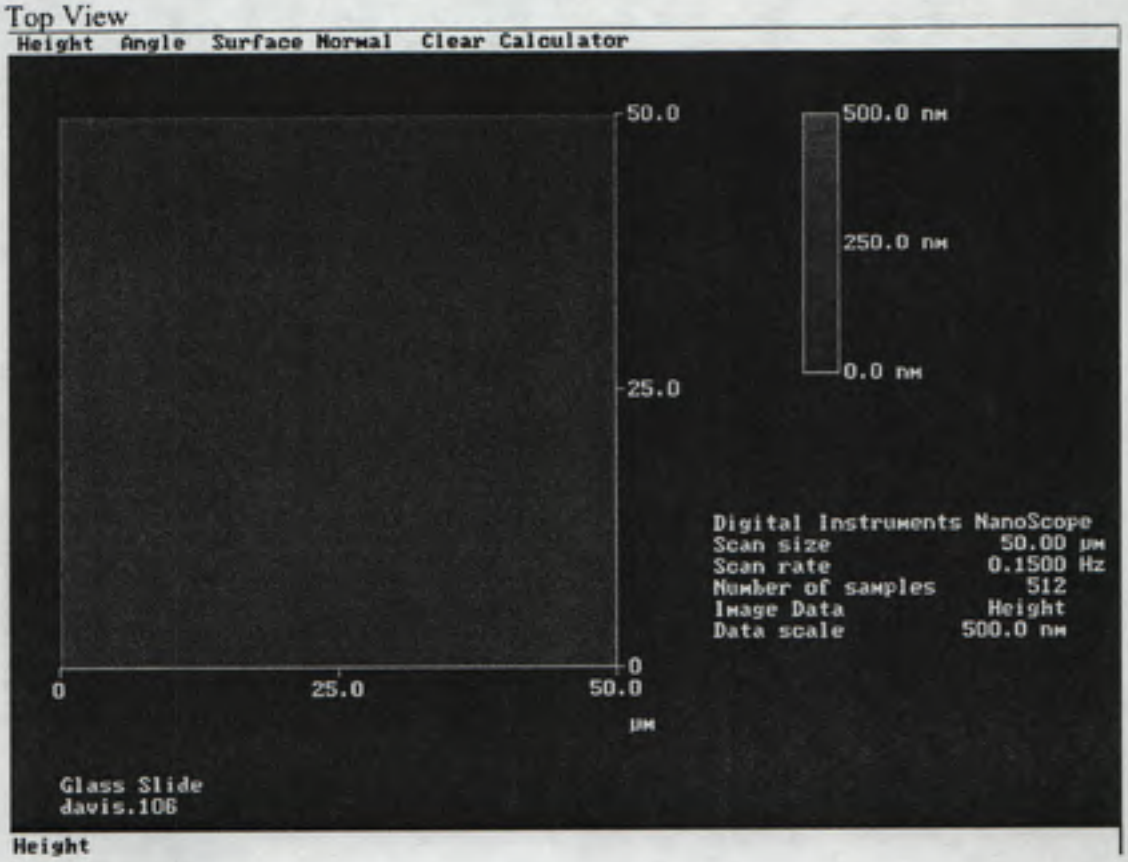

Surface Plot

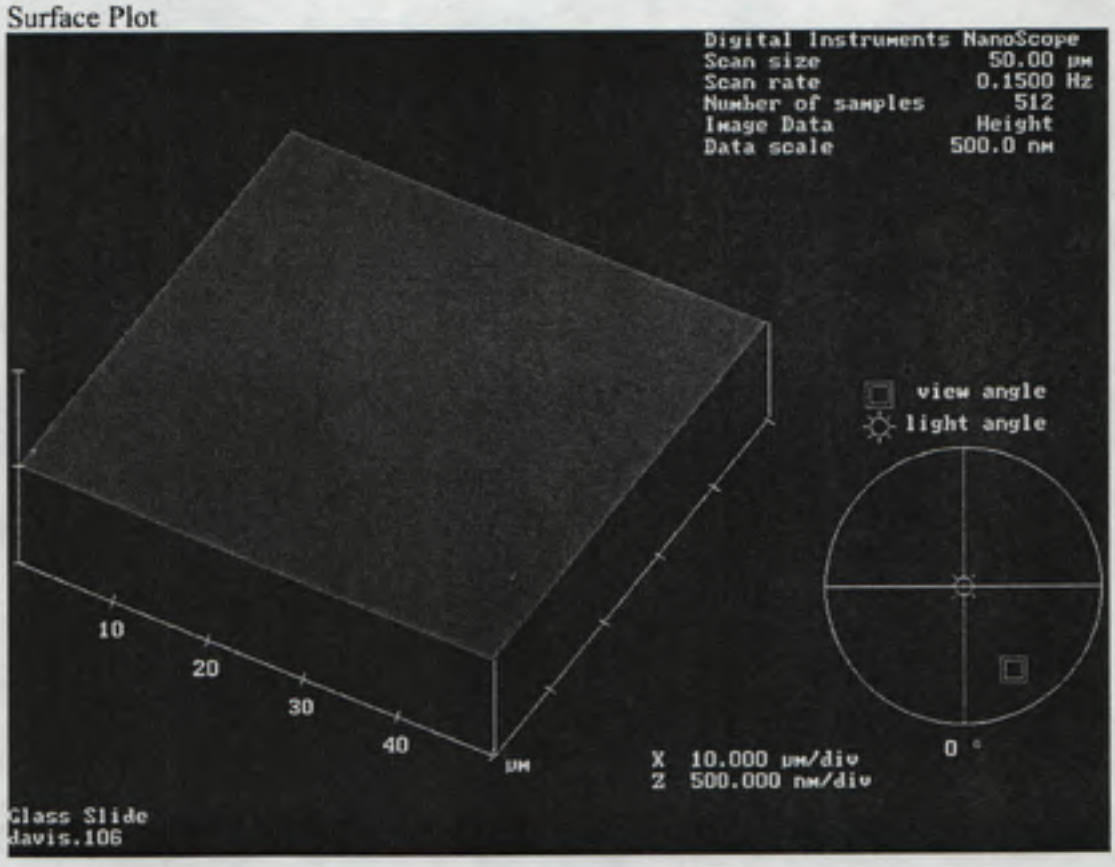

Glass Slide

Sectional Analysis

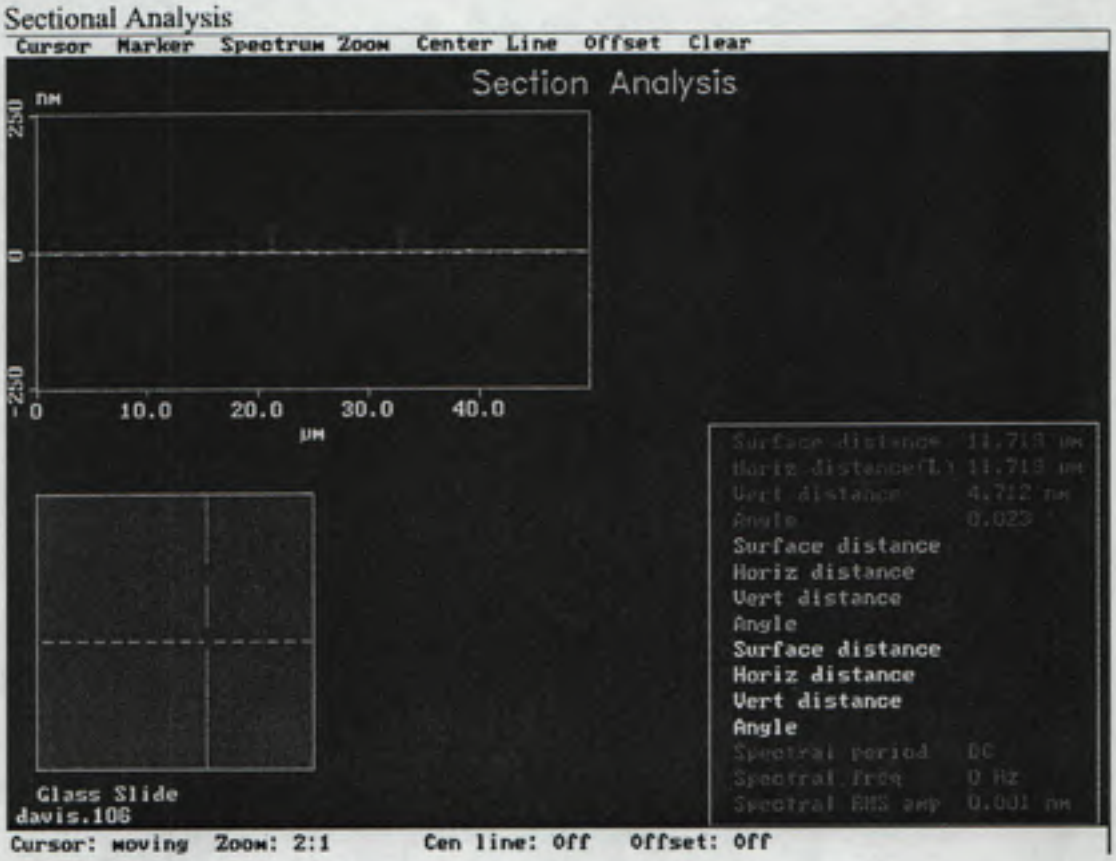

Roughness

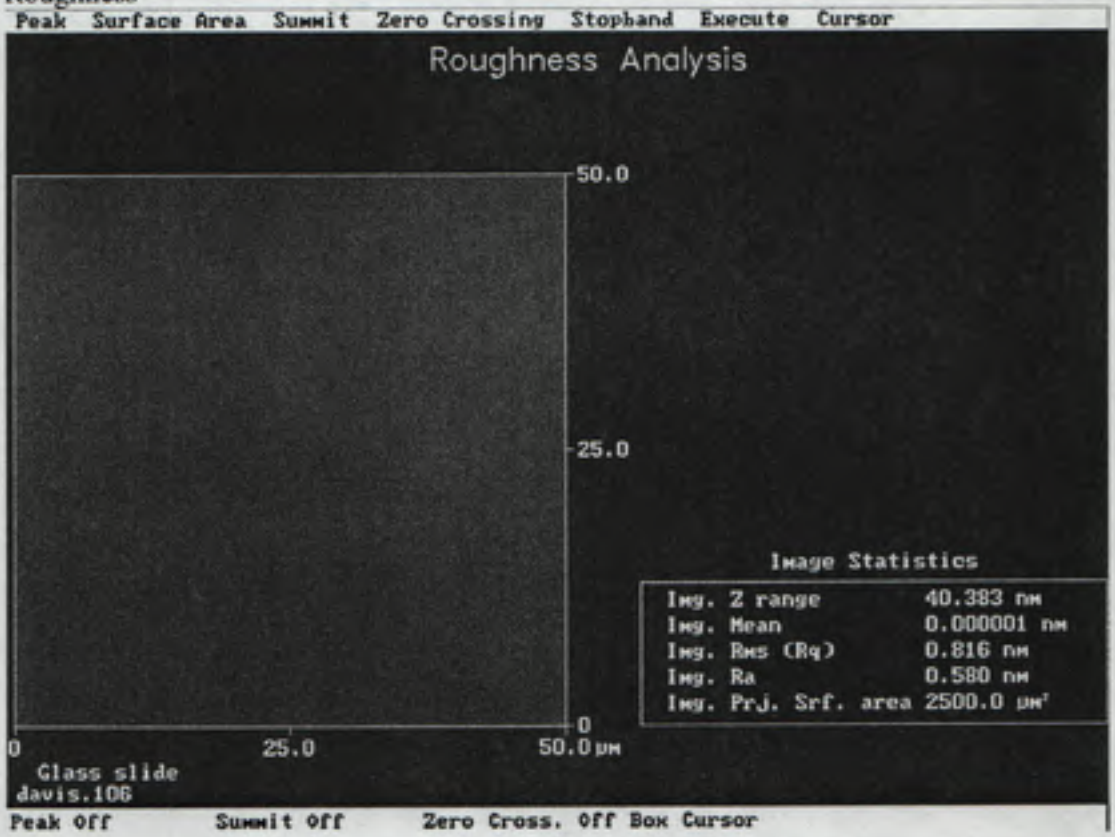

Frosted Glass Slide

Top View

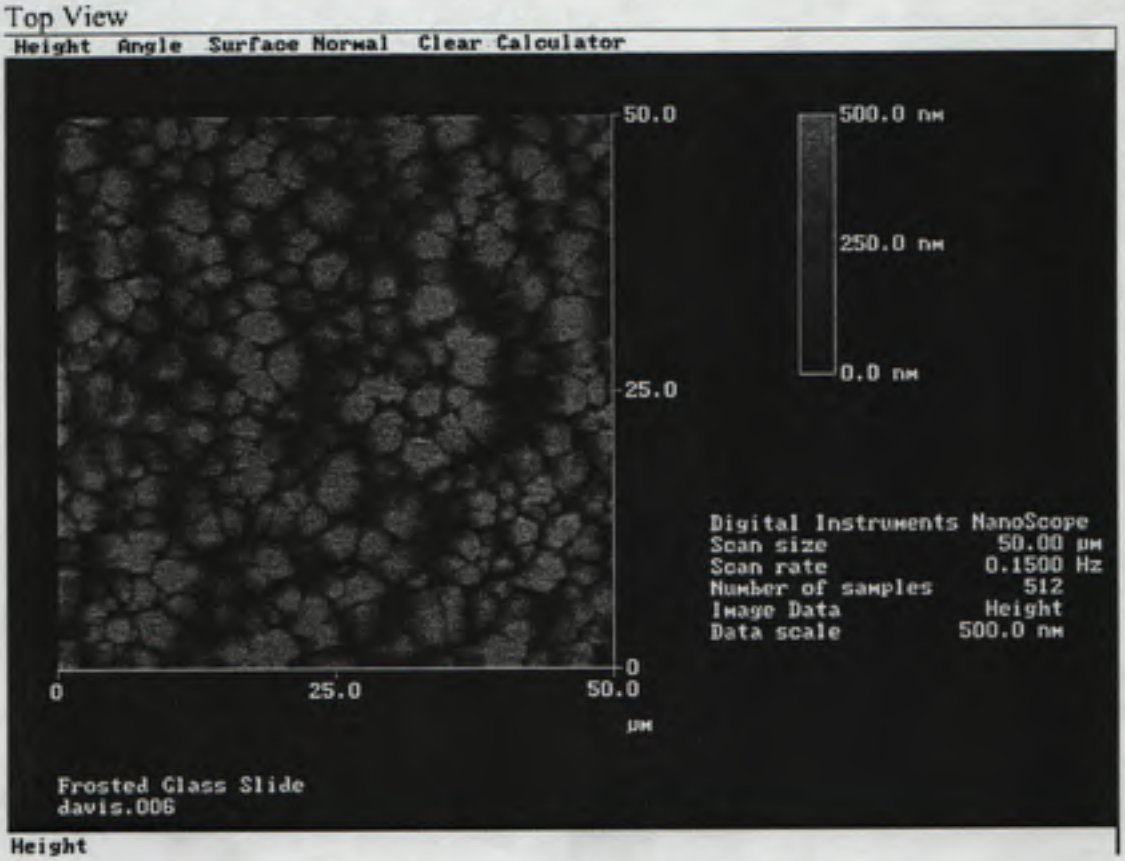

Surface Plot

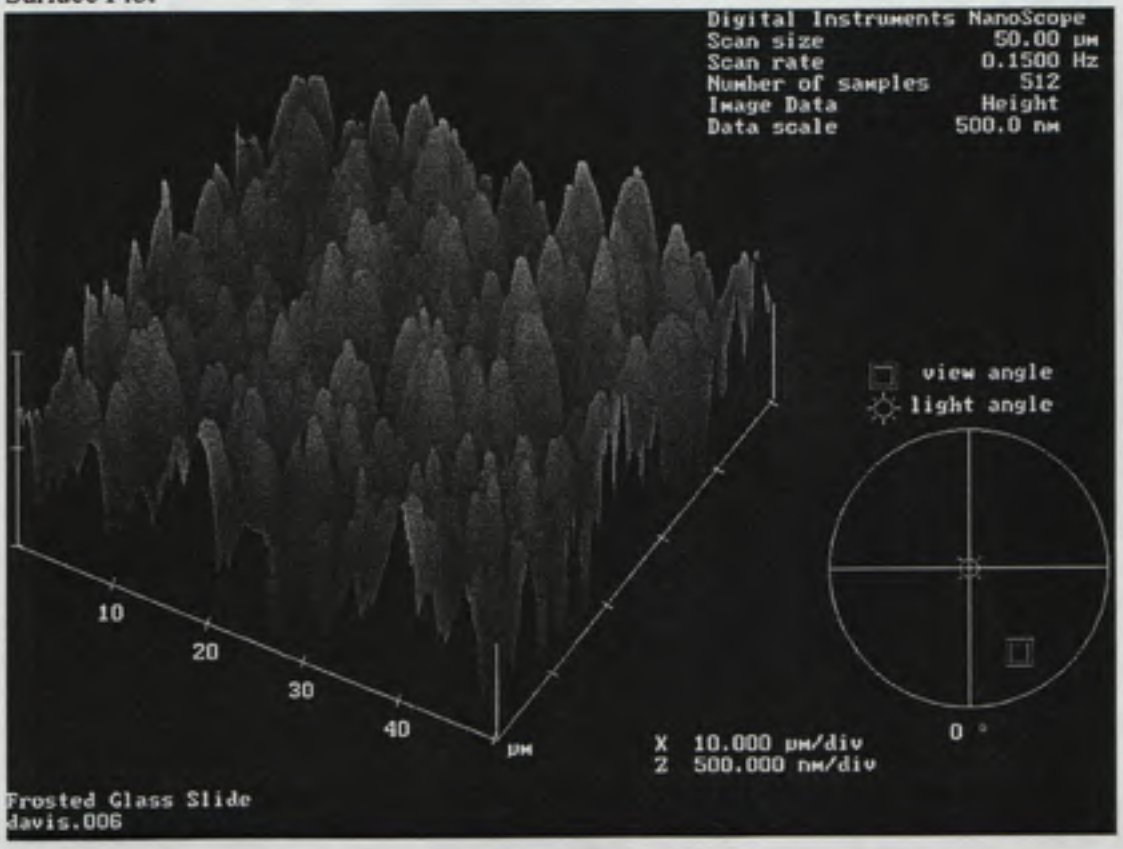

Frosted Glass Slide

Sectional Analysis

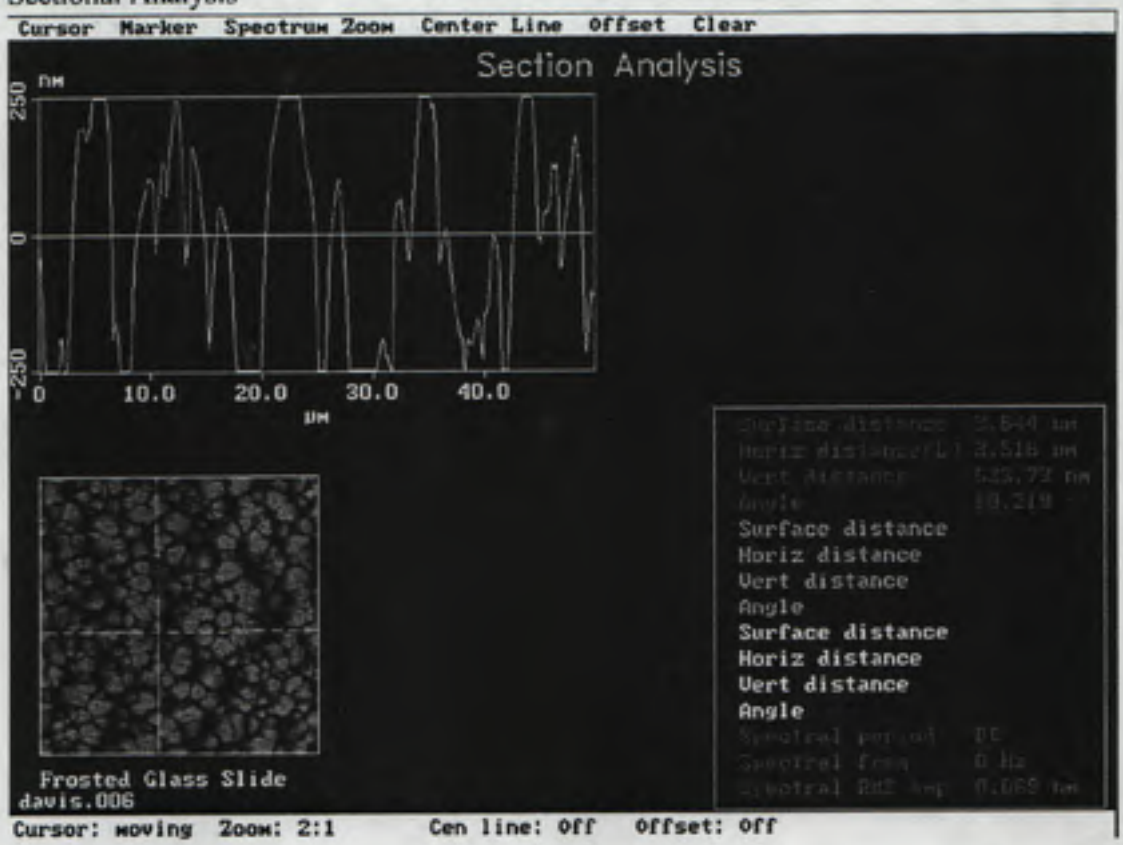

Roughness

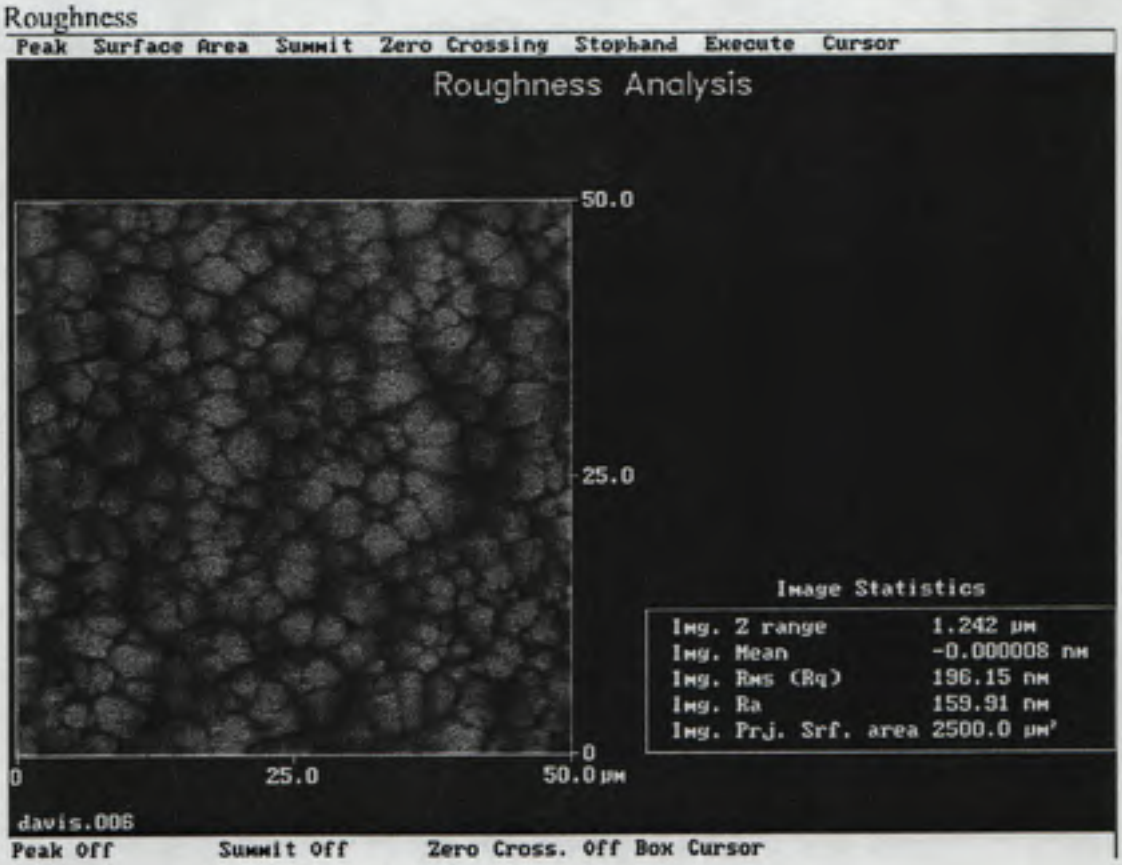

Mica (0.480 um PSL Beads)

Top View

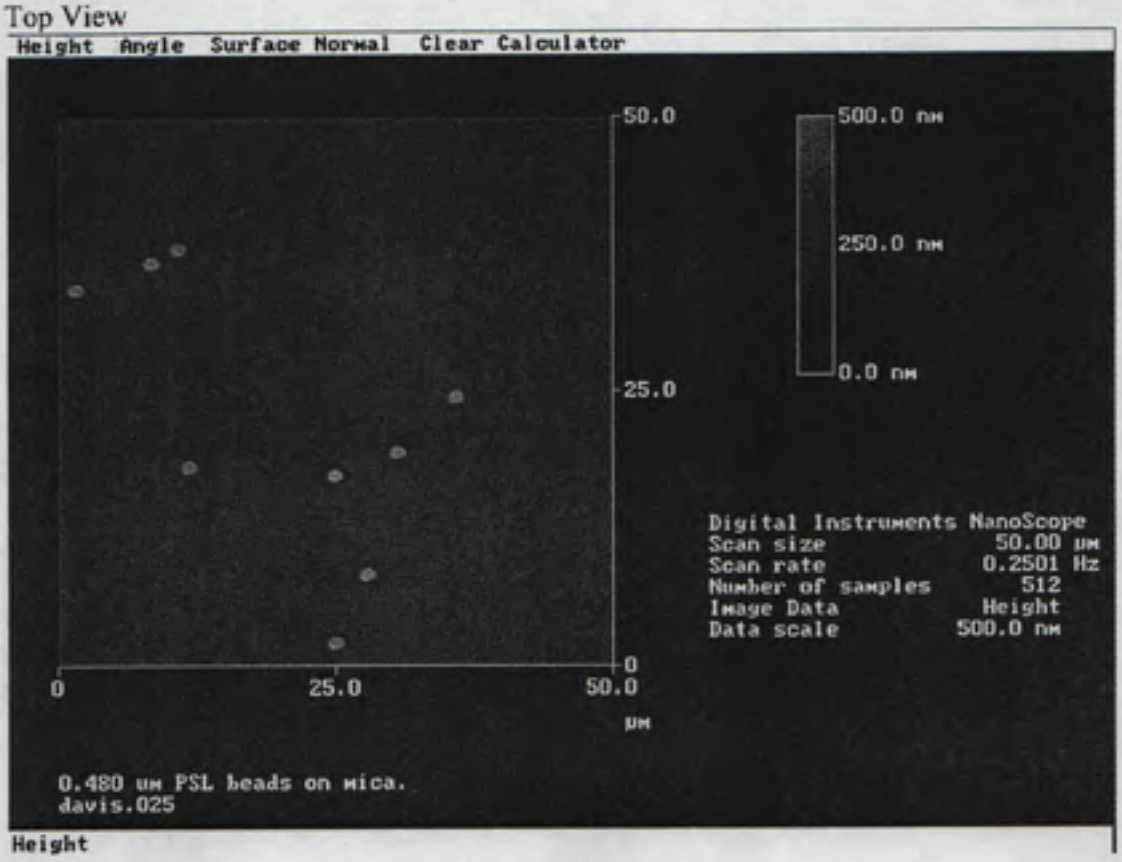

Surface Plot

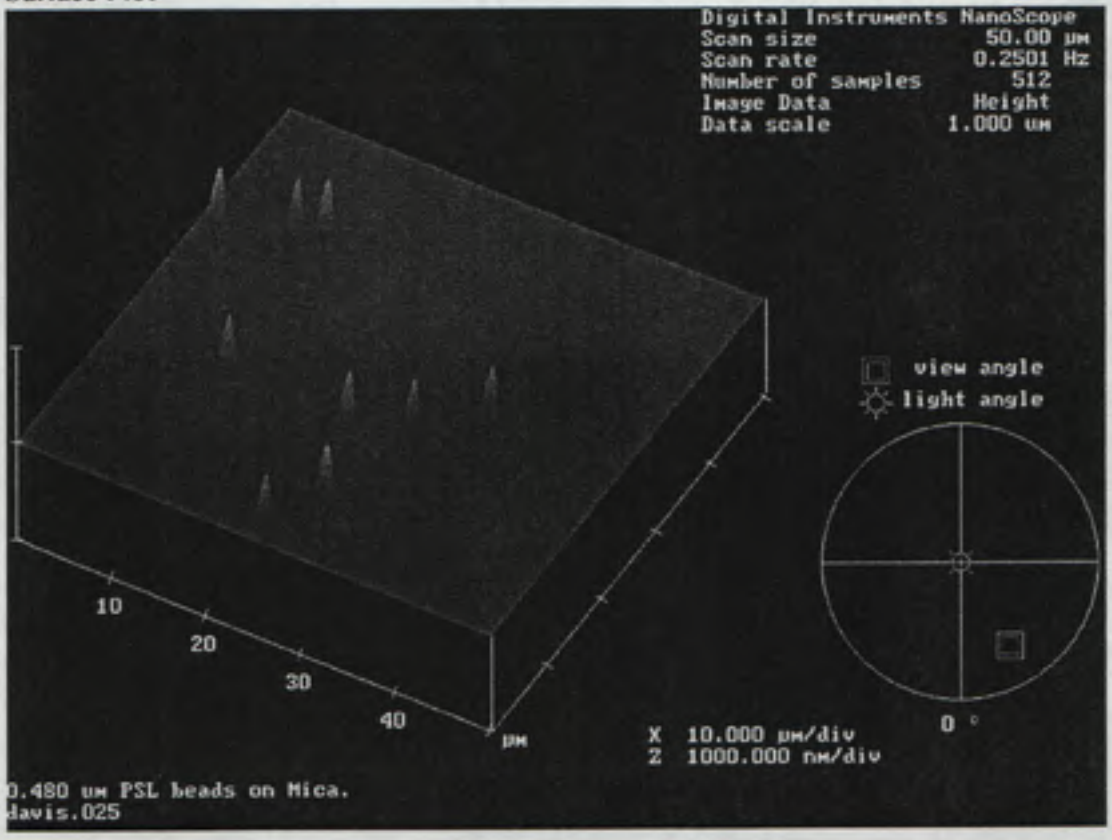

Mica (0.480 um PSL Beads)

Section Analysis

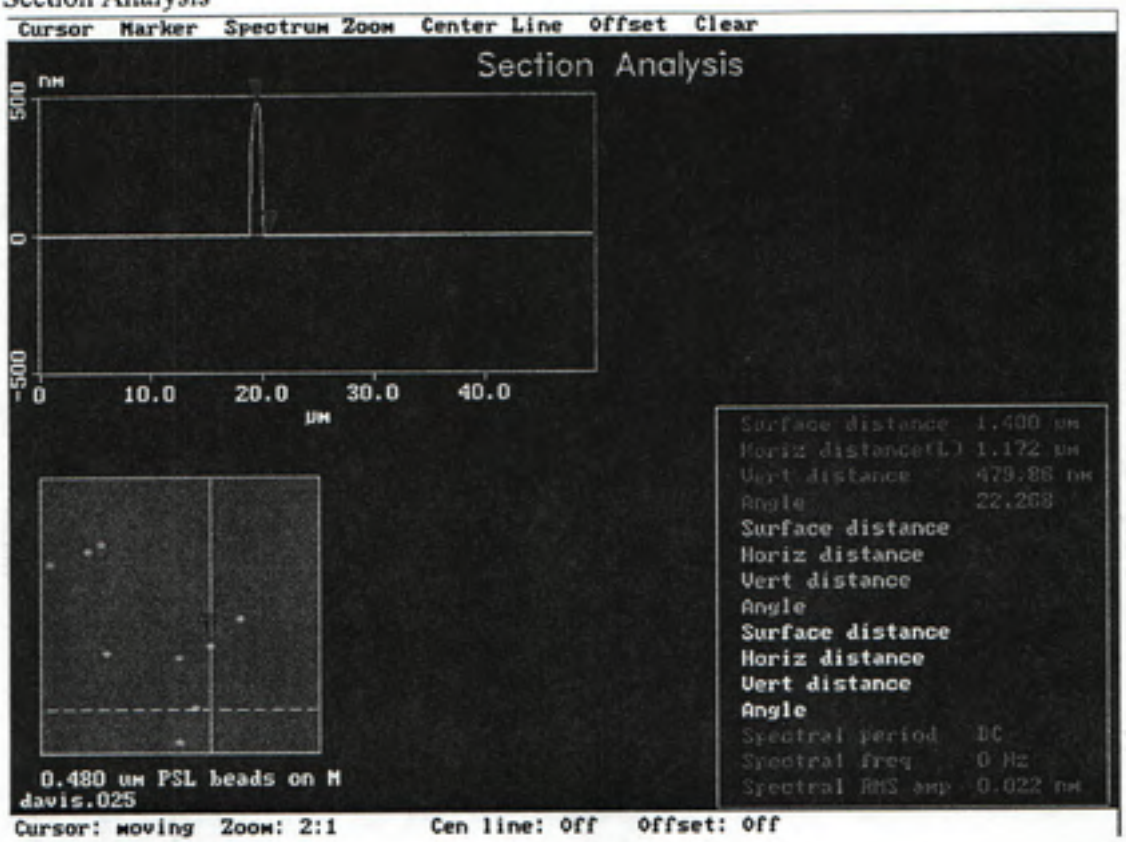

Glass Slide (0.480 um PSL Beads)

Top View

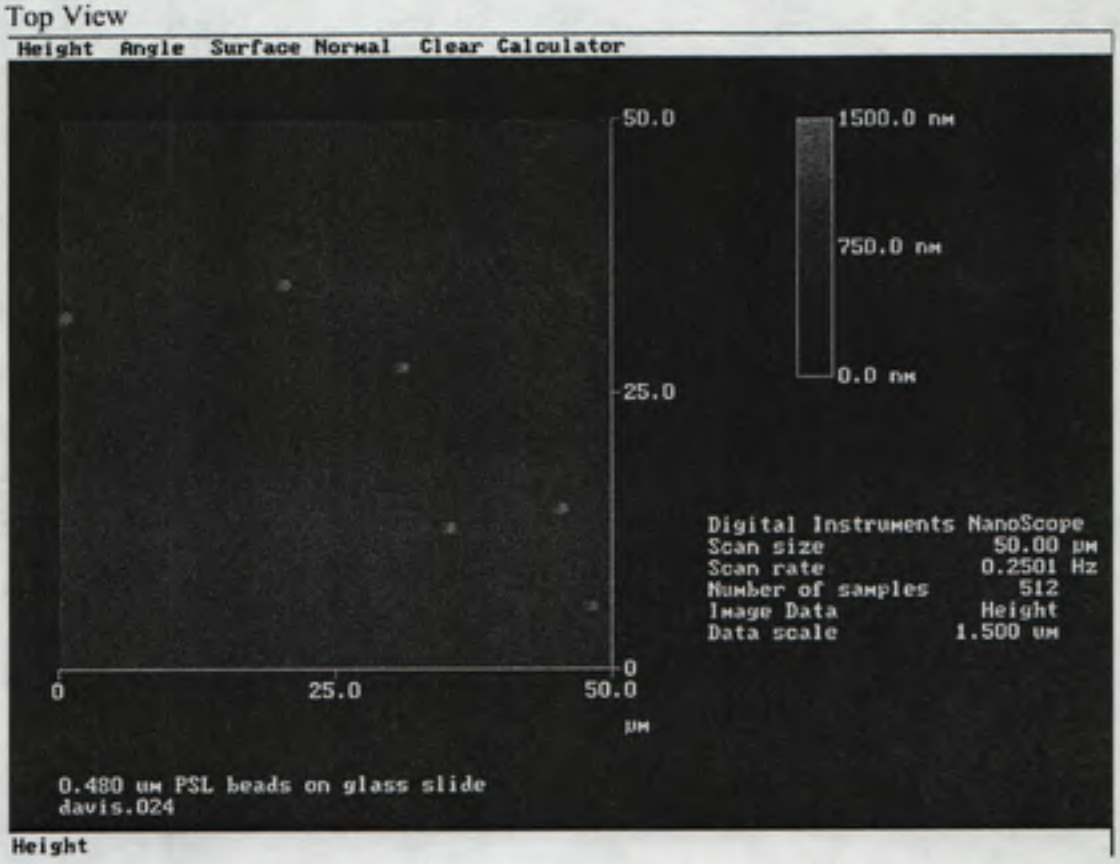

Surface Plot

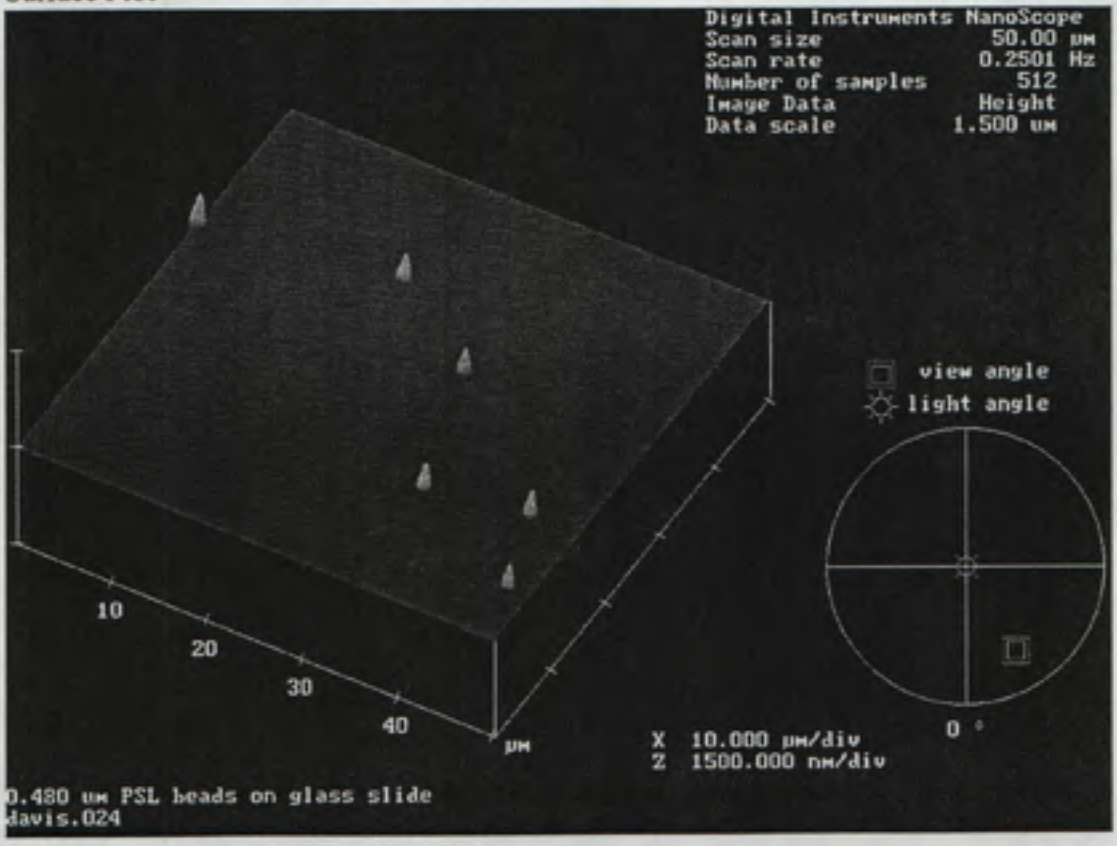

Glass Slide (0.480 um PSL Beads)

Section Analysis

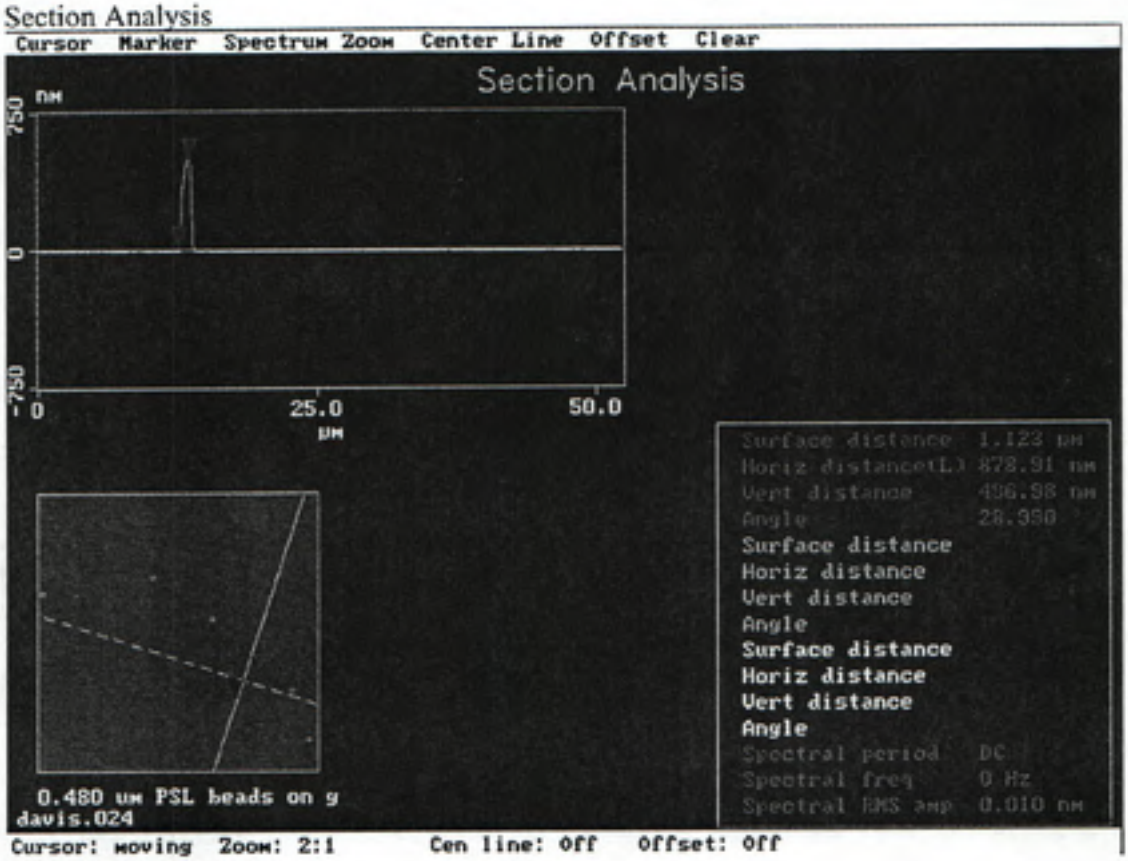

Plastic (0.480 um PSL Beads)

Top View

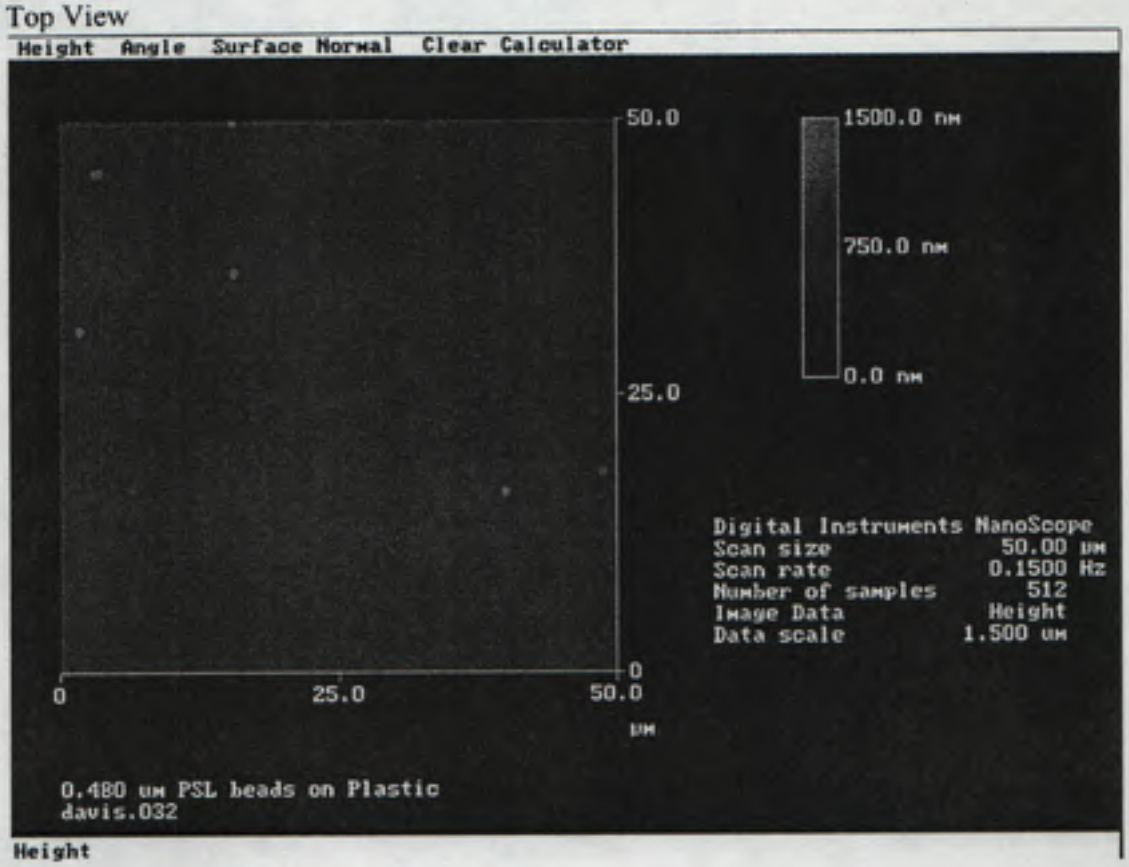

Surface Plot

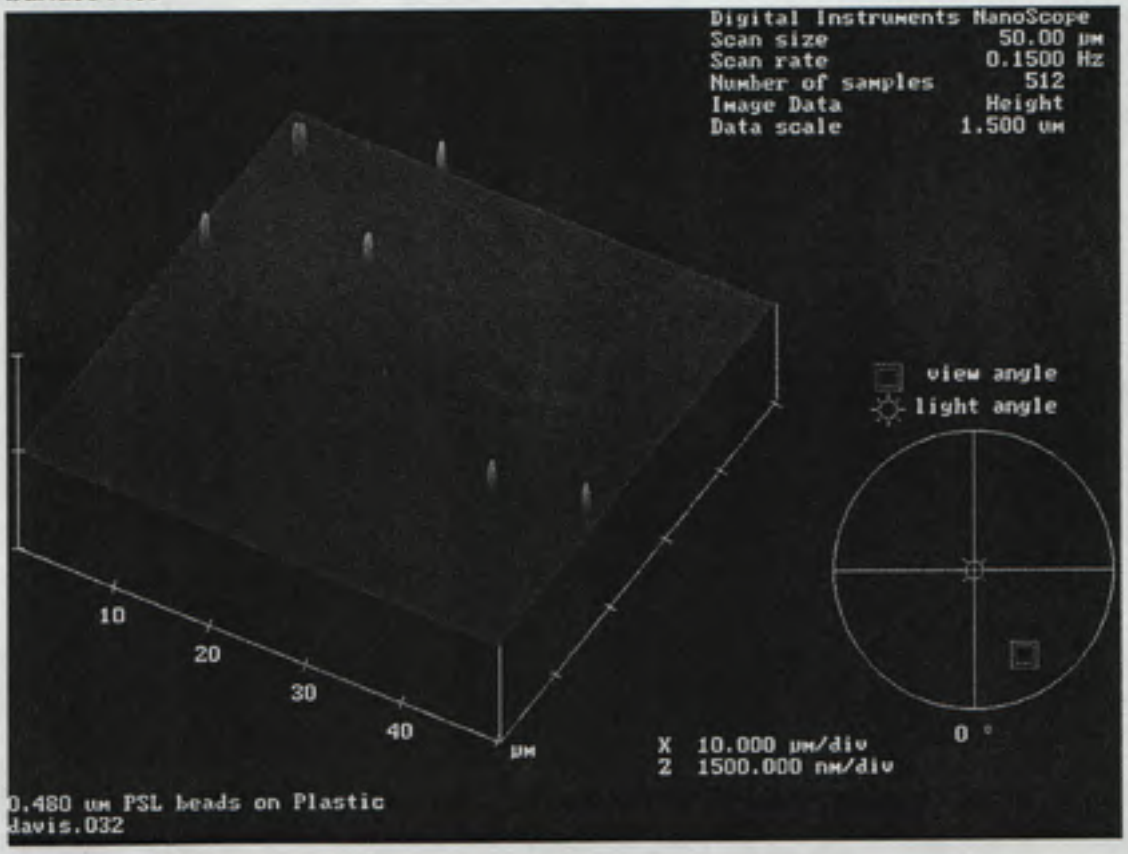

Plastic (0.480 um PSL Beads)

Section Analysis

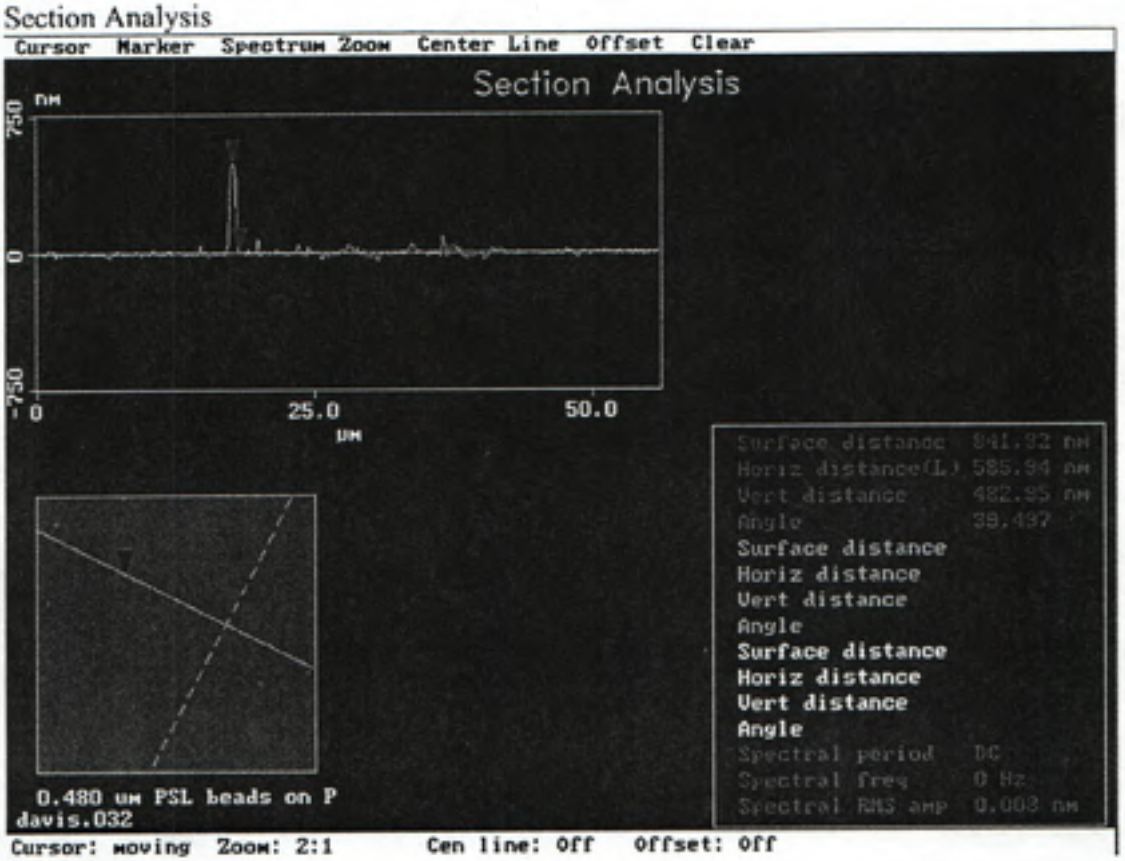

Aluminum (0.480 um PSL Beads)

Top View

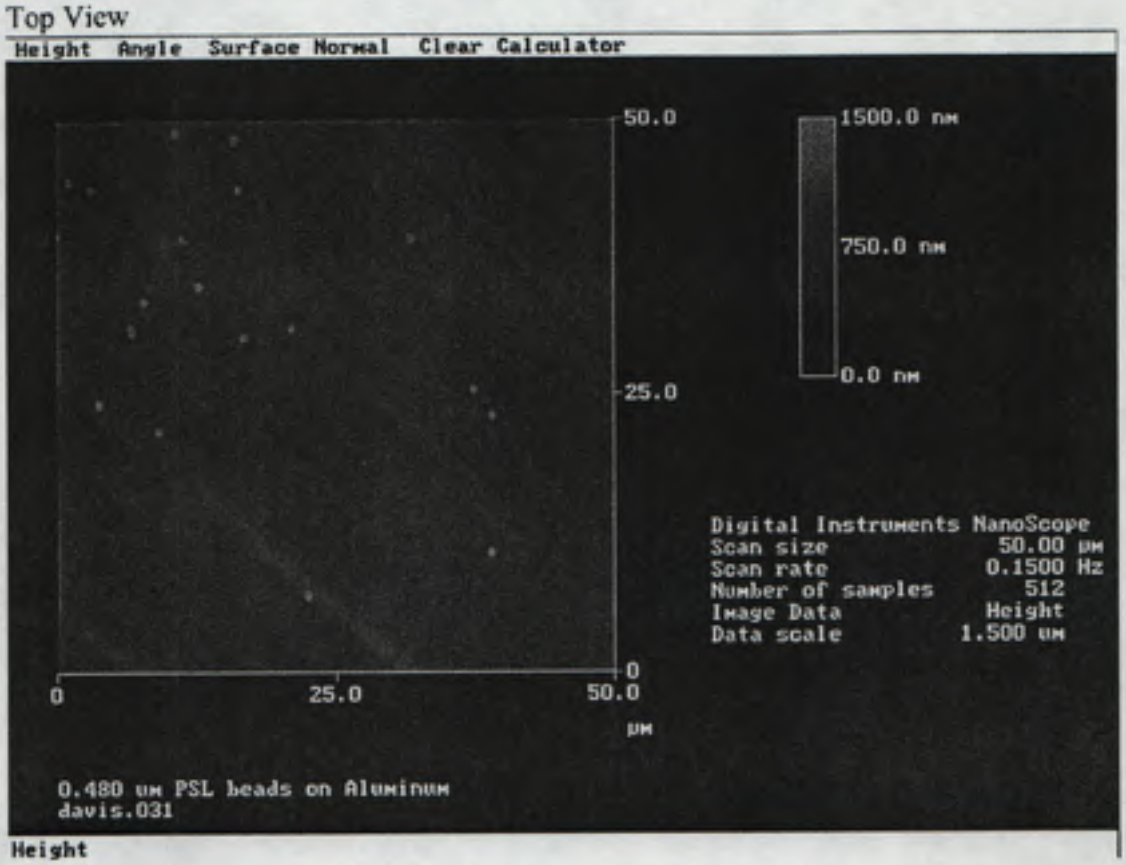

Surface Plot

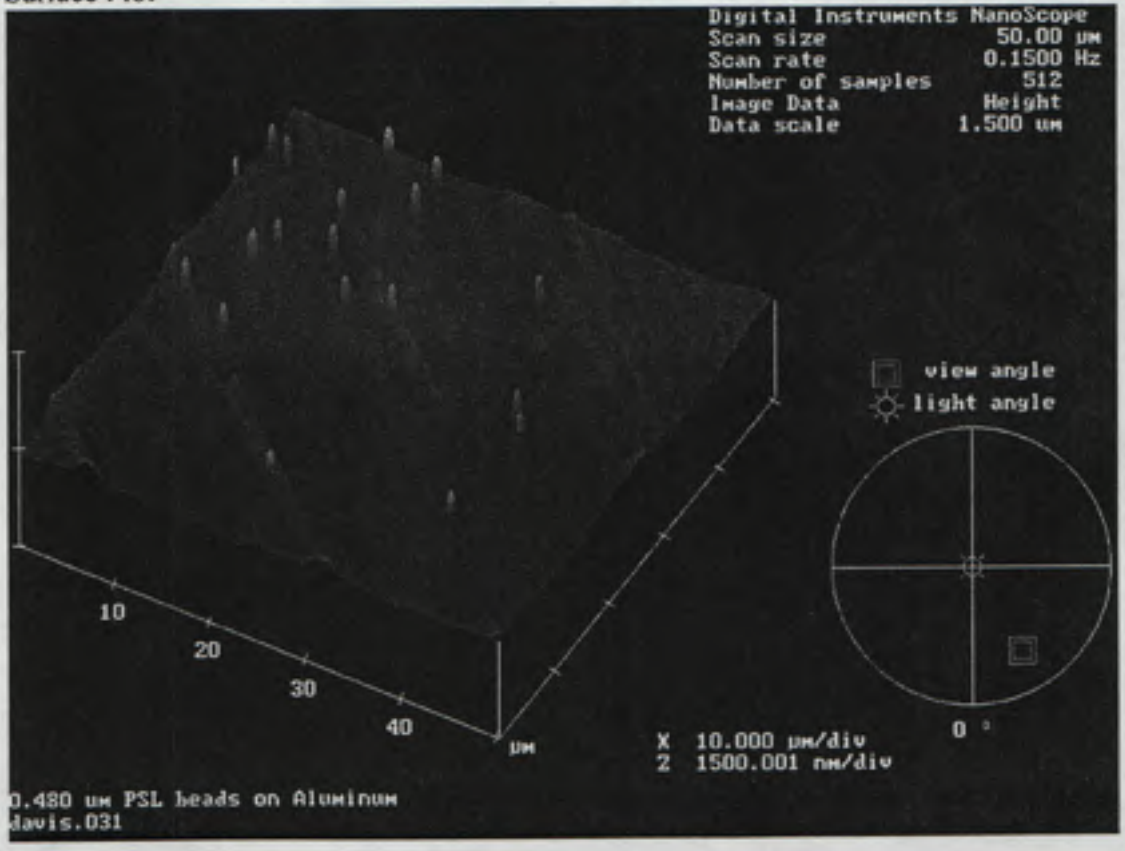

Aluminum (0.480 um PSL Beads)

Section Analysis

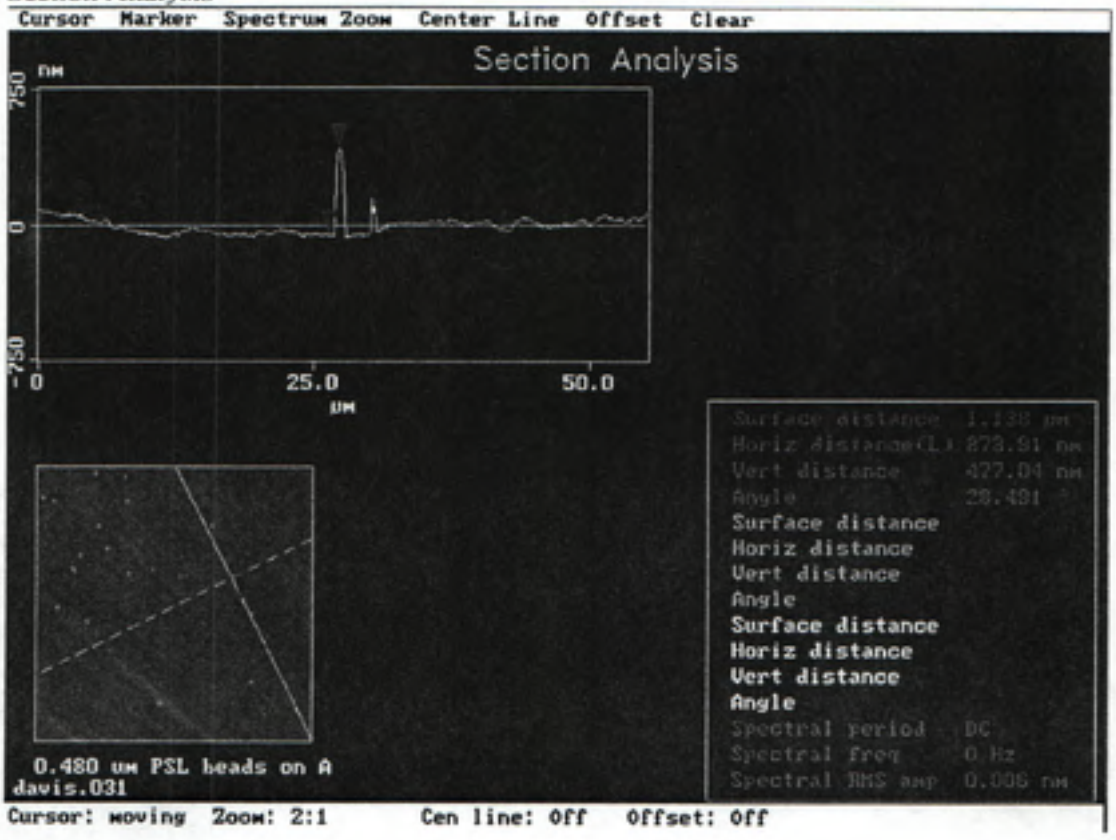

Stainless Steel (0.480 um PSL Beads)

Top View

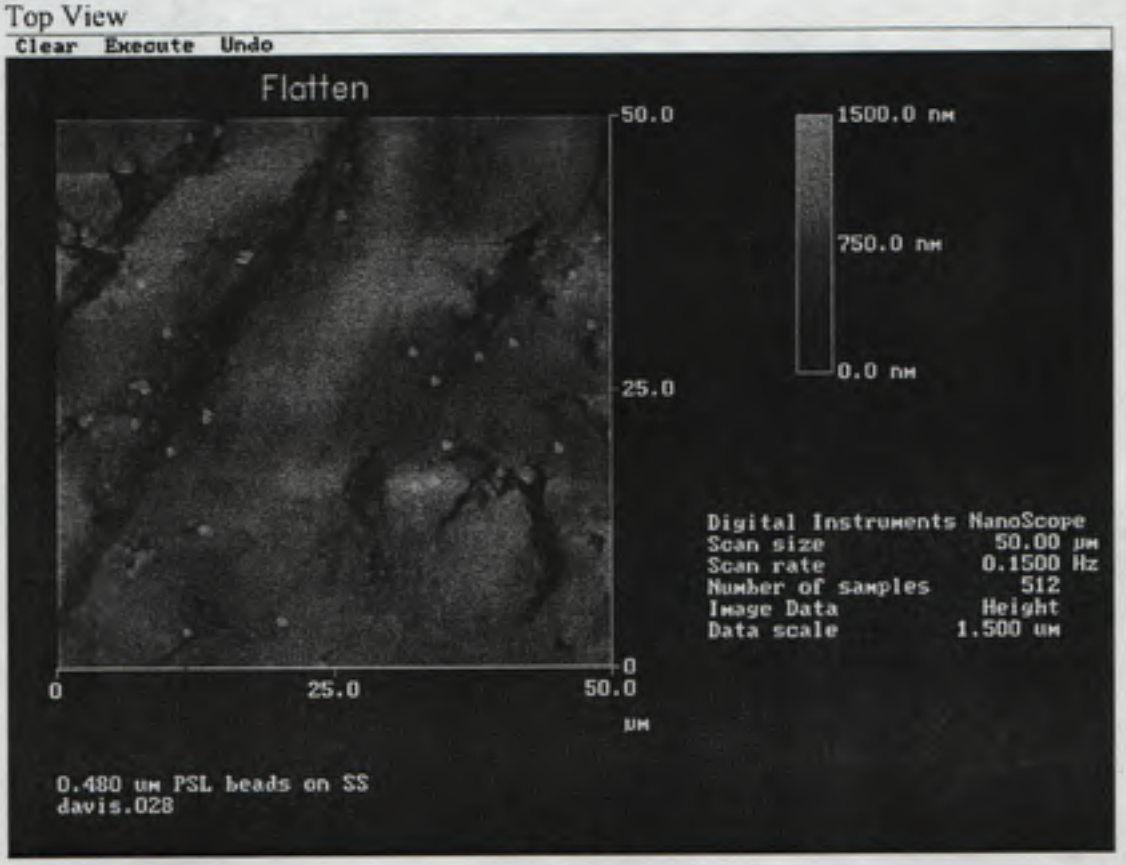

Surface Plot

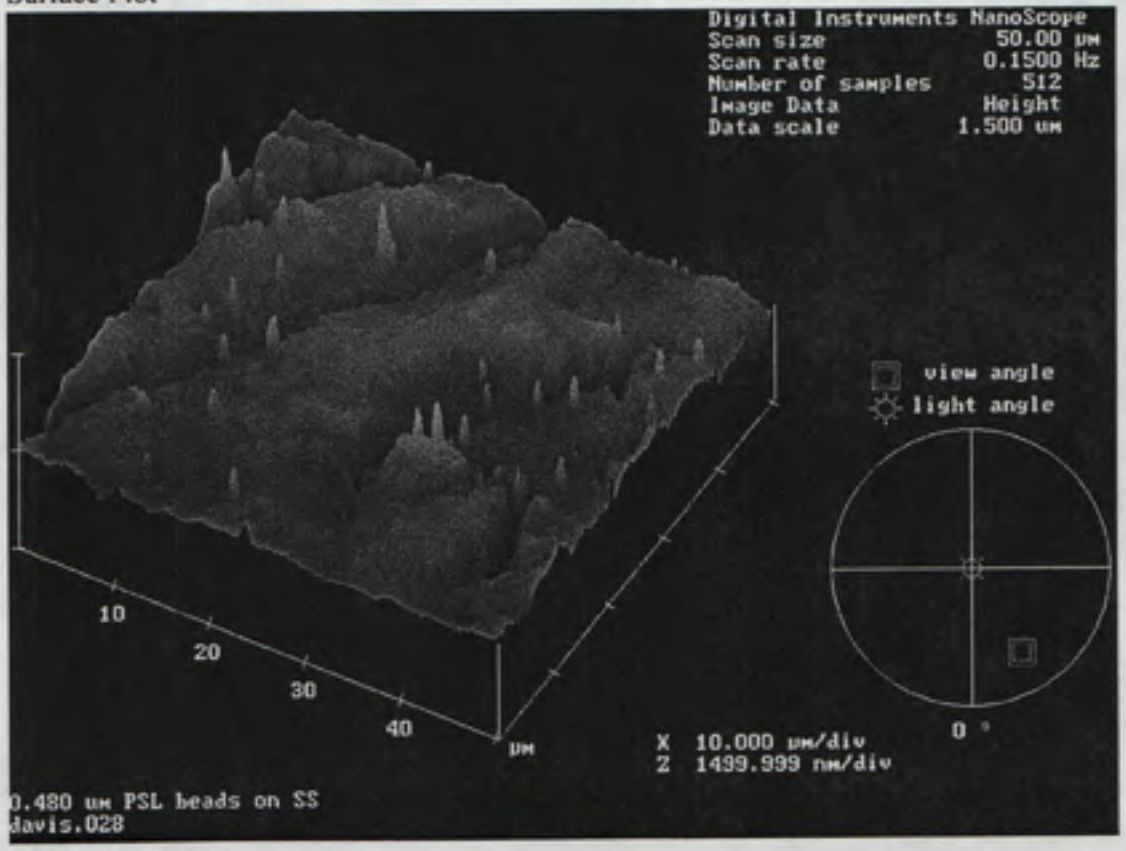

Stainless Steel (0.480 um PSL Beads)

Section Analysis

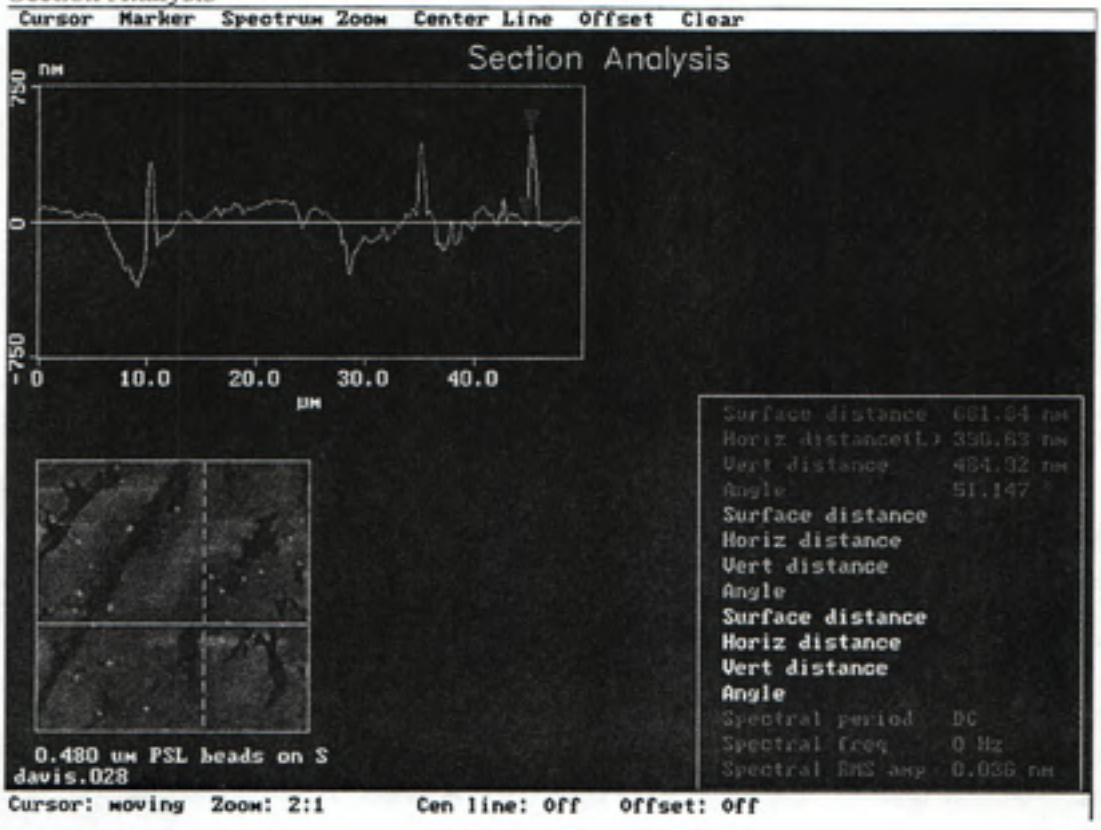

Frosted Glass Slide (0.480 um PSL Beads)

Top View

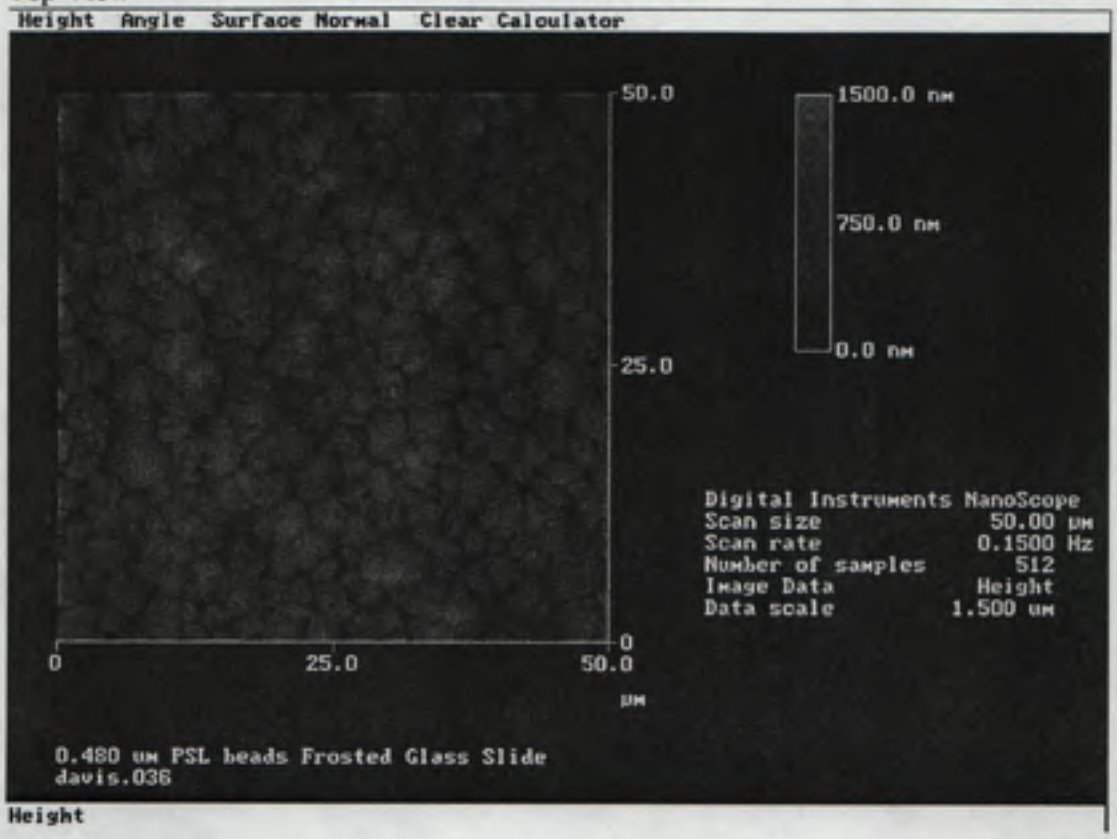

Surface Plot

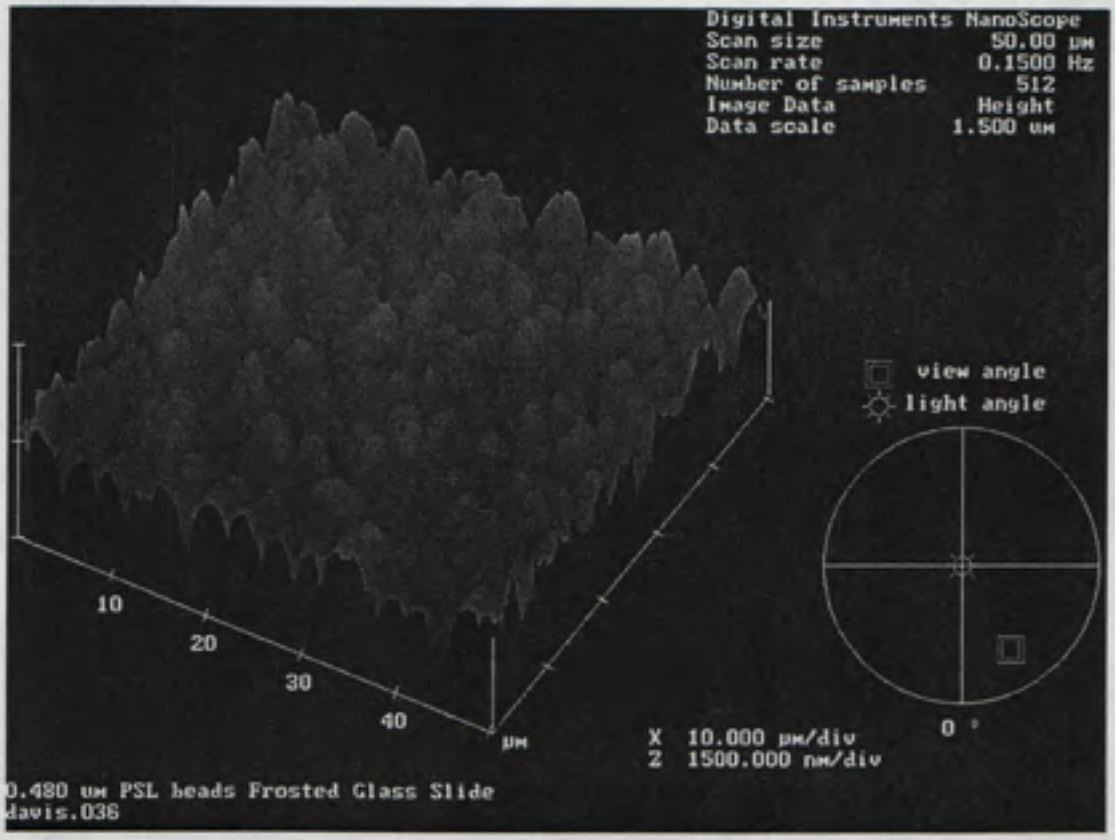

Frosted Glass Slide (0.480 um PSL Beads)

Section Analysis

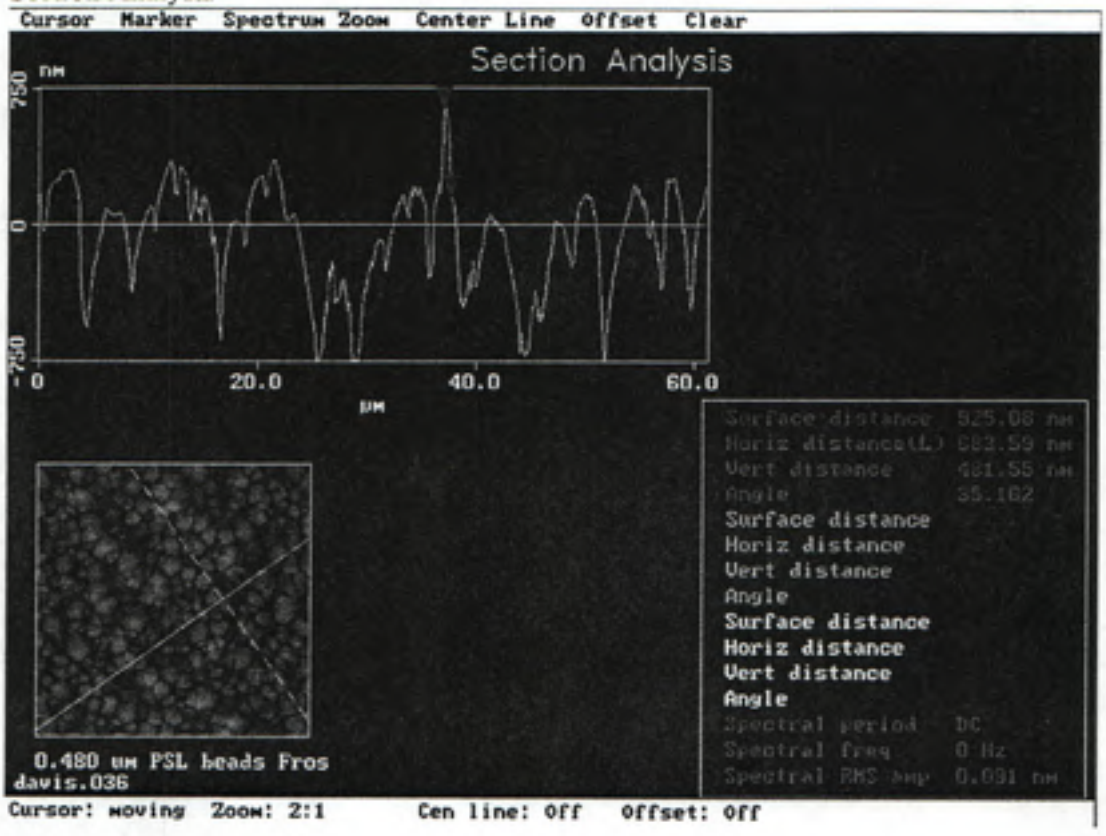

Mica (0.310 um PSL Beads)

Top View

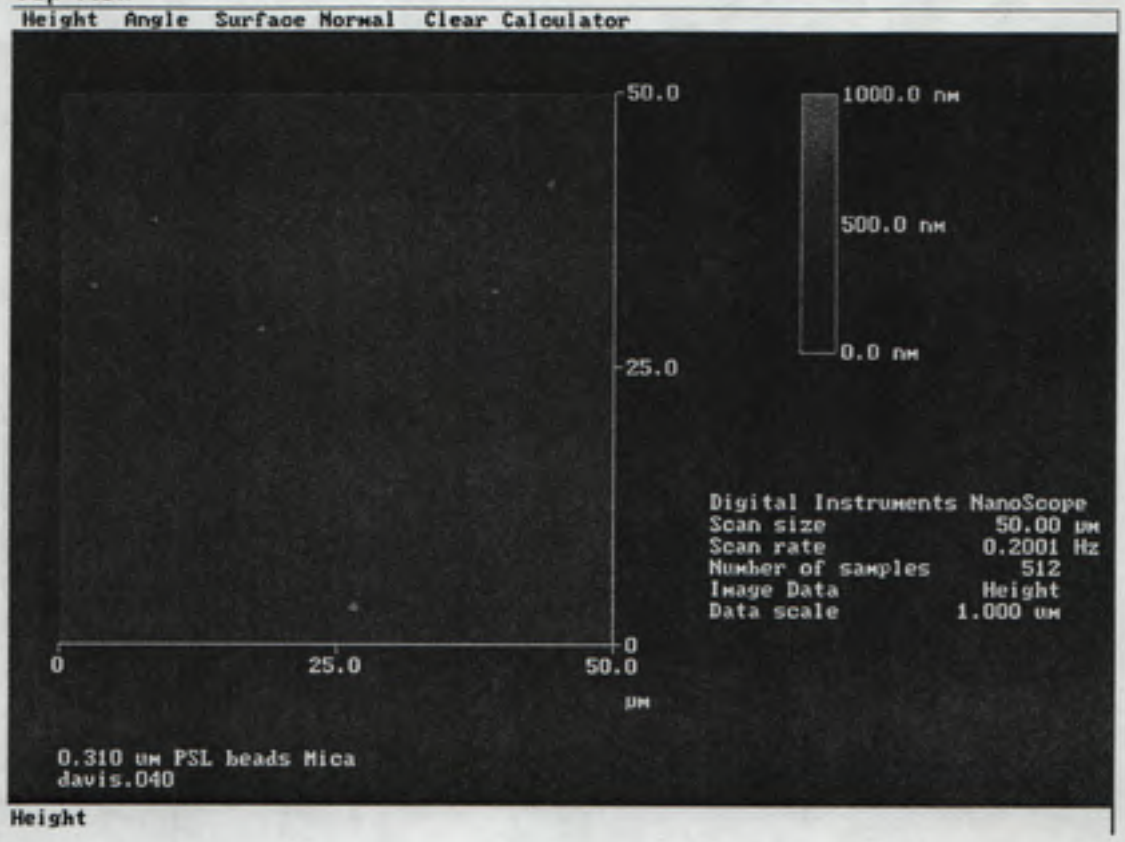

Surface Plot

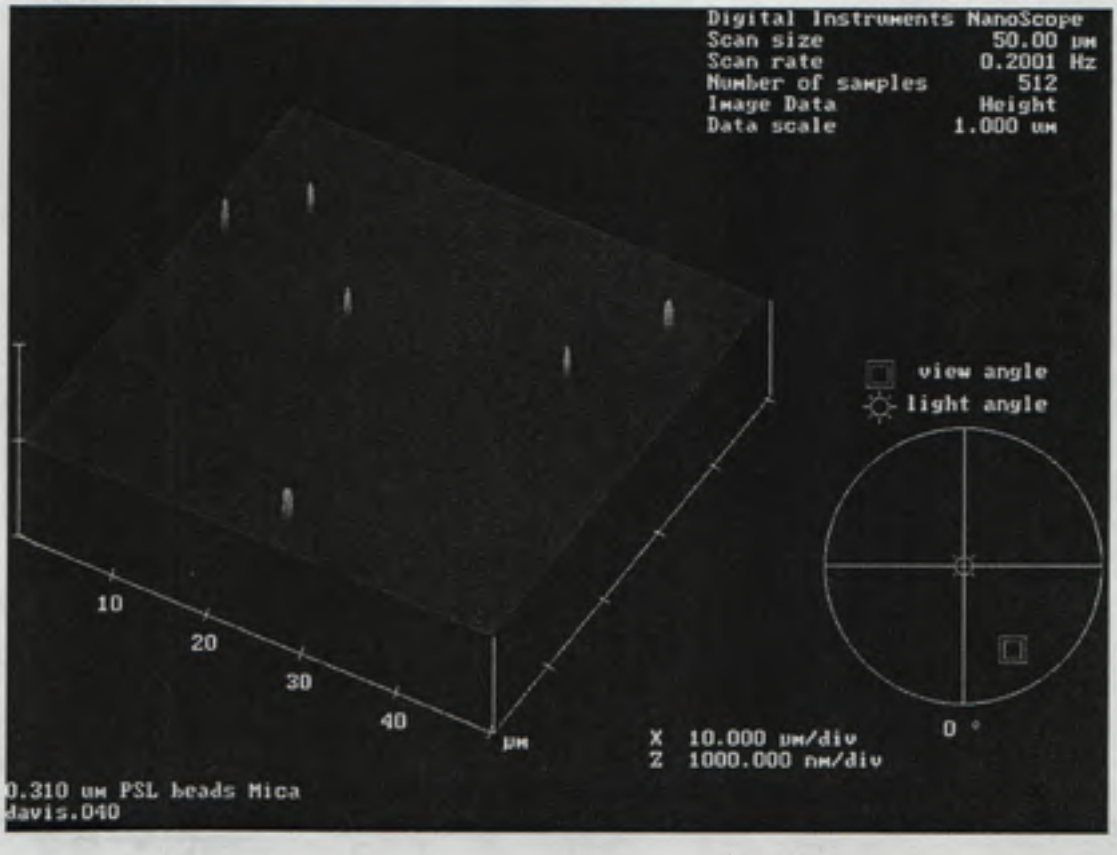

Mica (0.310 um PSL Beads)

Section Analysis

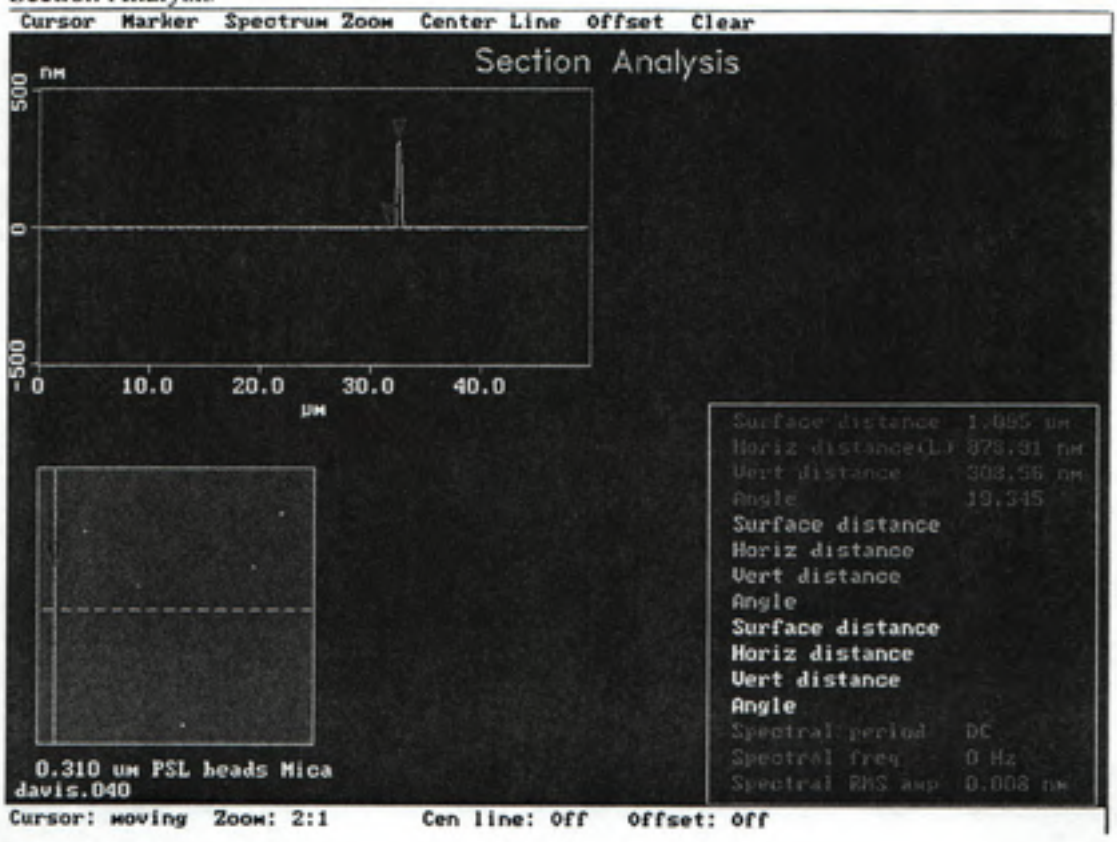

Glass Slide (0.310 um PSL Beads)

Top View

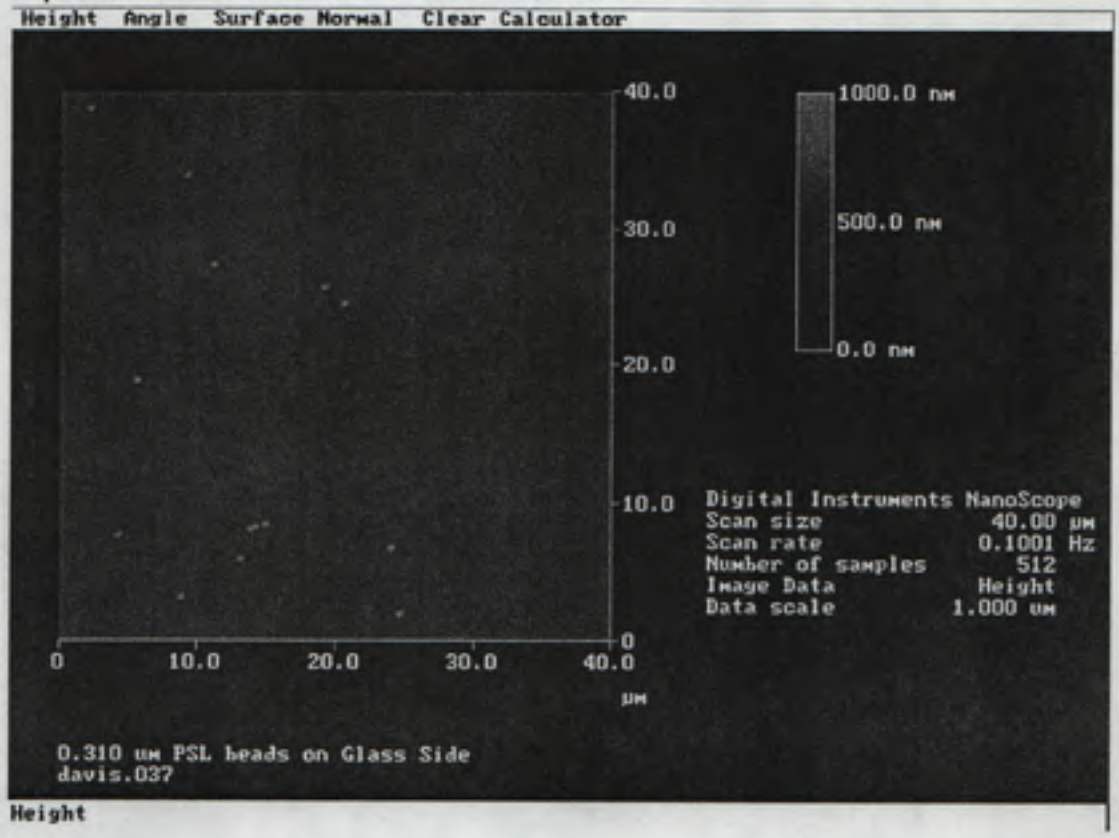

Surface Plot

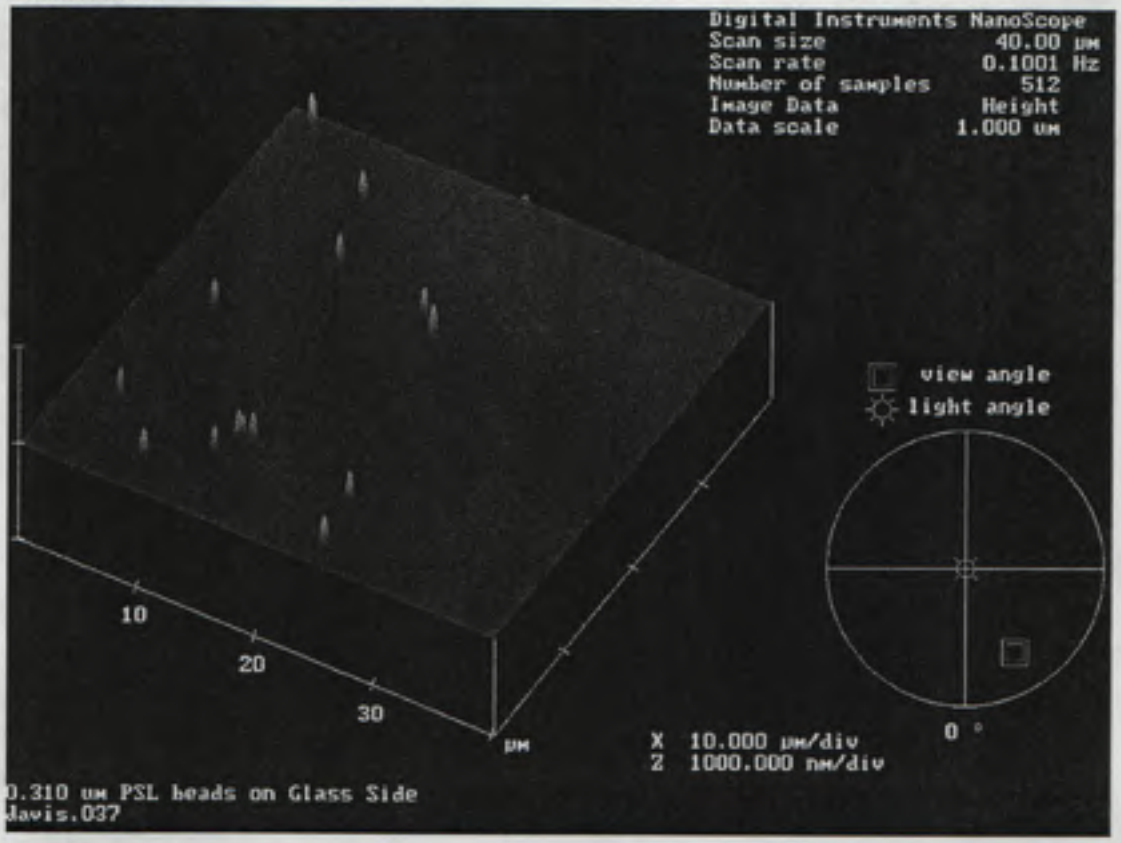

Glass Slide (0.310 um PSL Beads)

Section Analysis

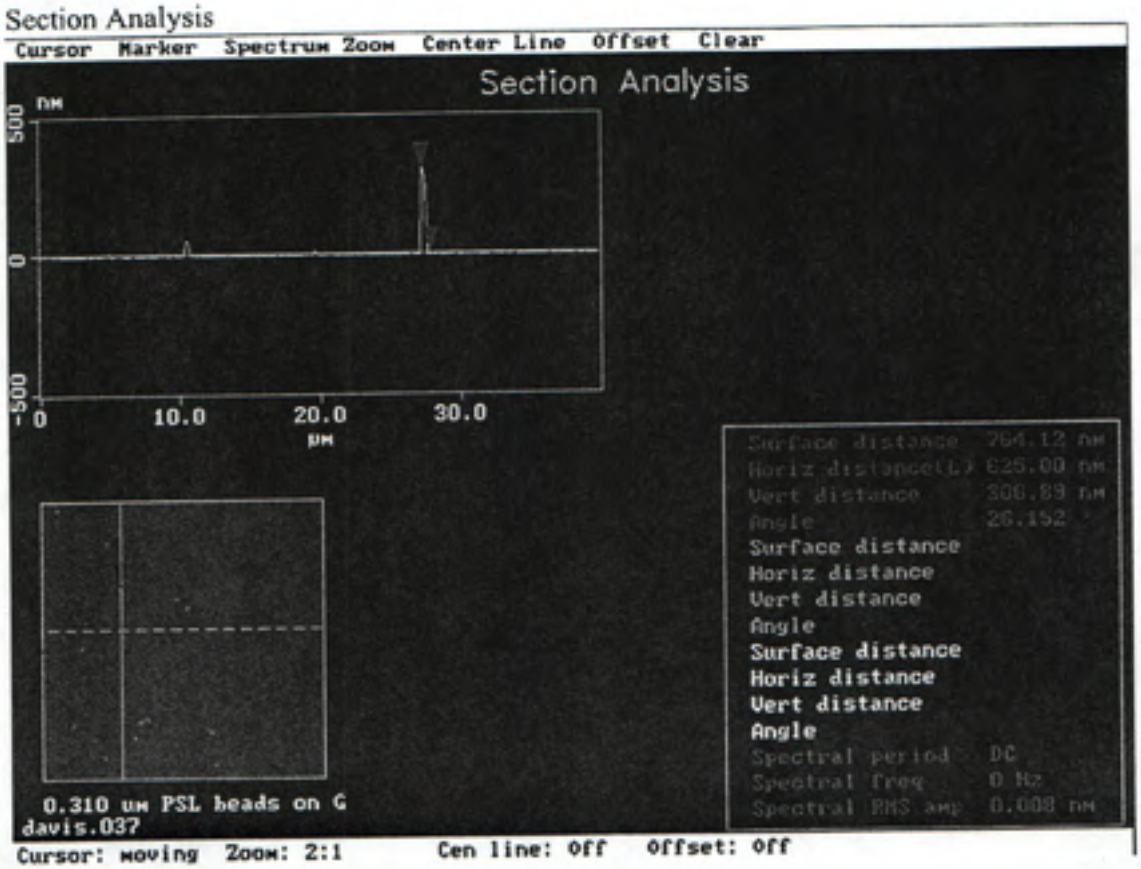

Plastic (0.310 um PSL Beads)

Top View

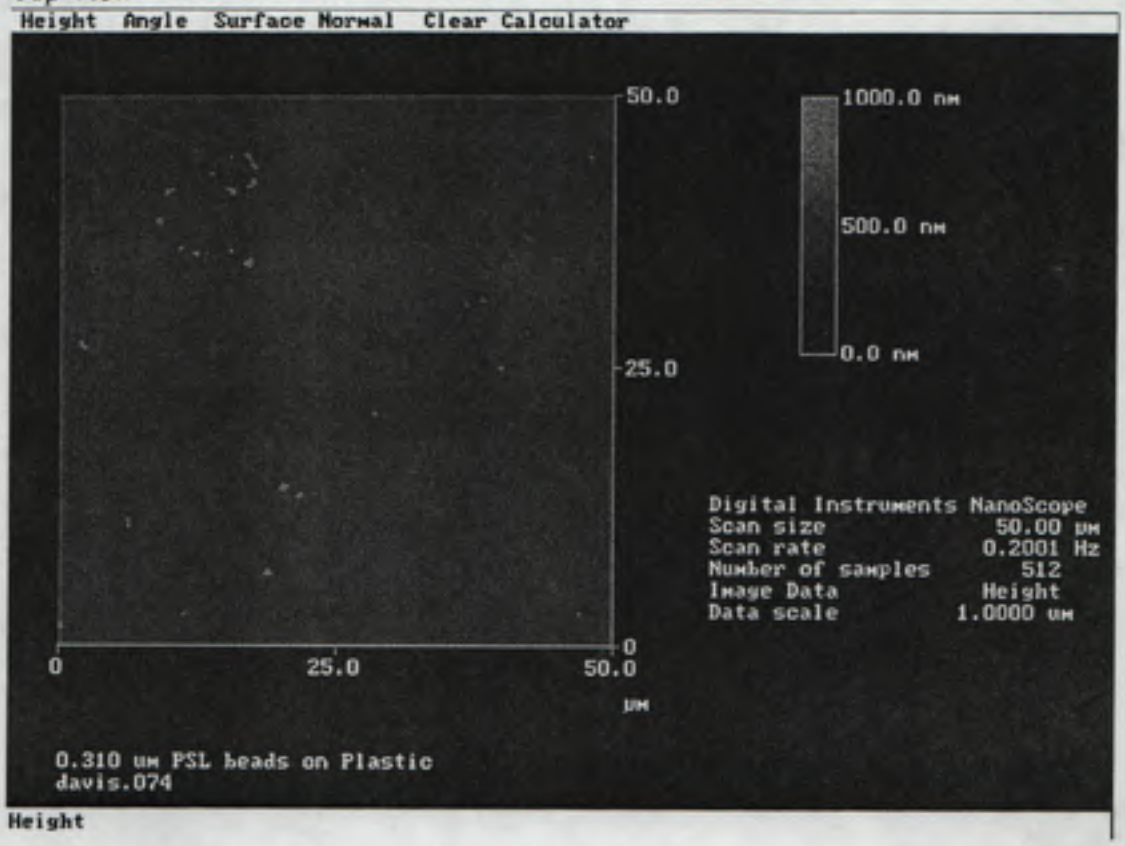

Surface Plot

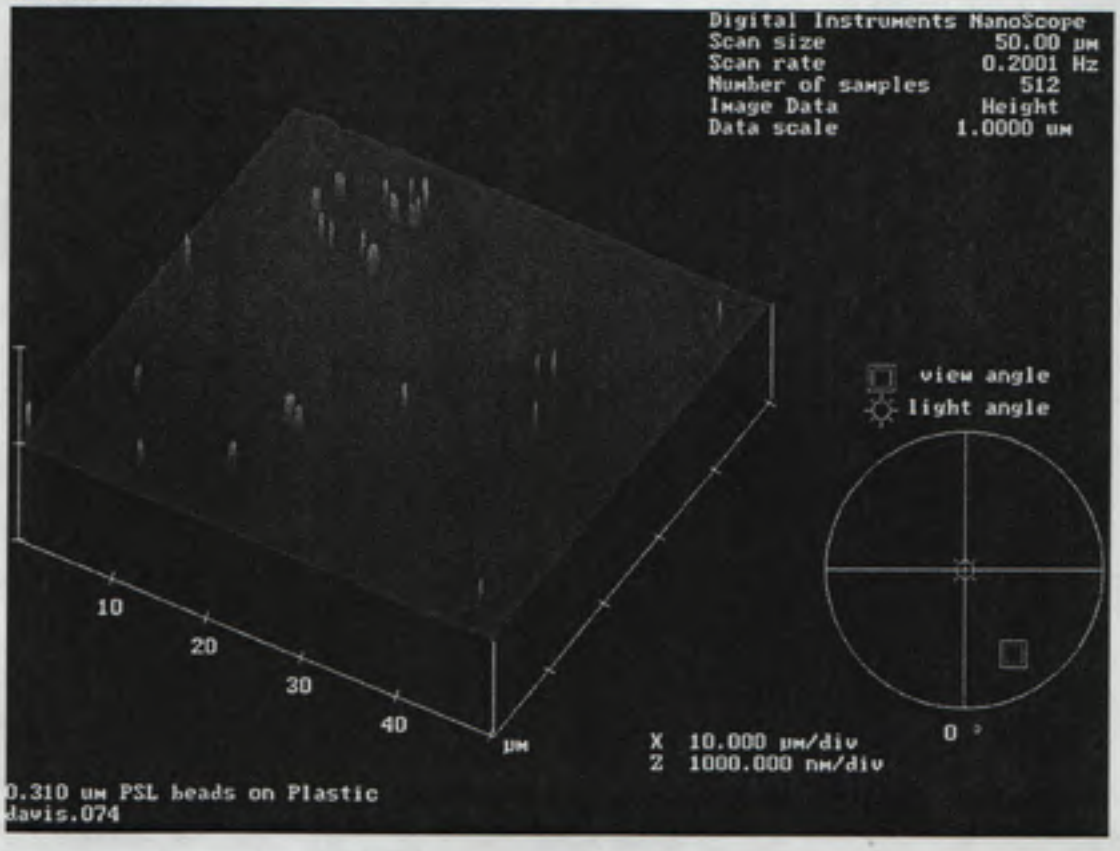

Plastic (0.310 um PSL Beads)

Section Analysis

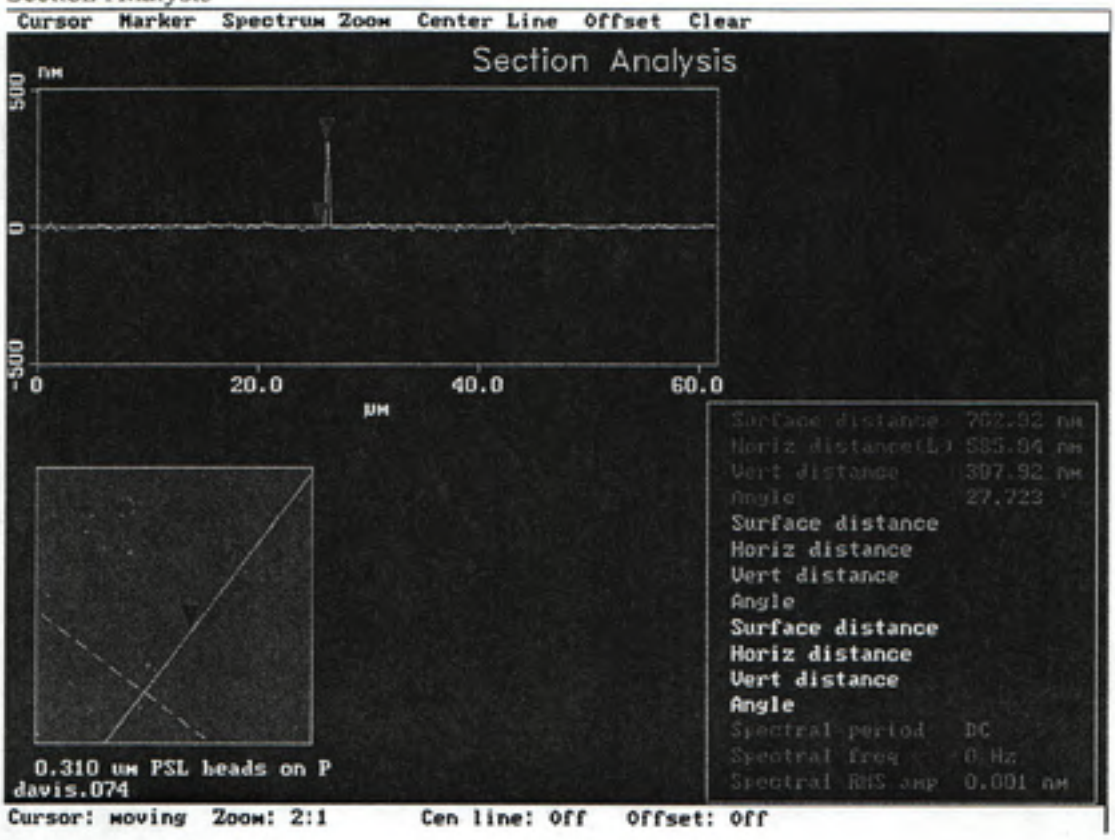

Aluminum (0.310 um PSL Beads)

Top View

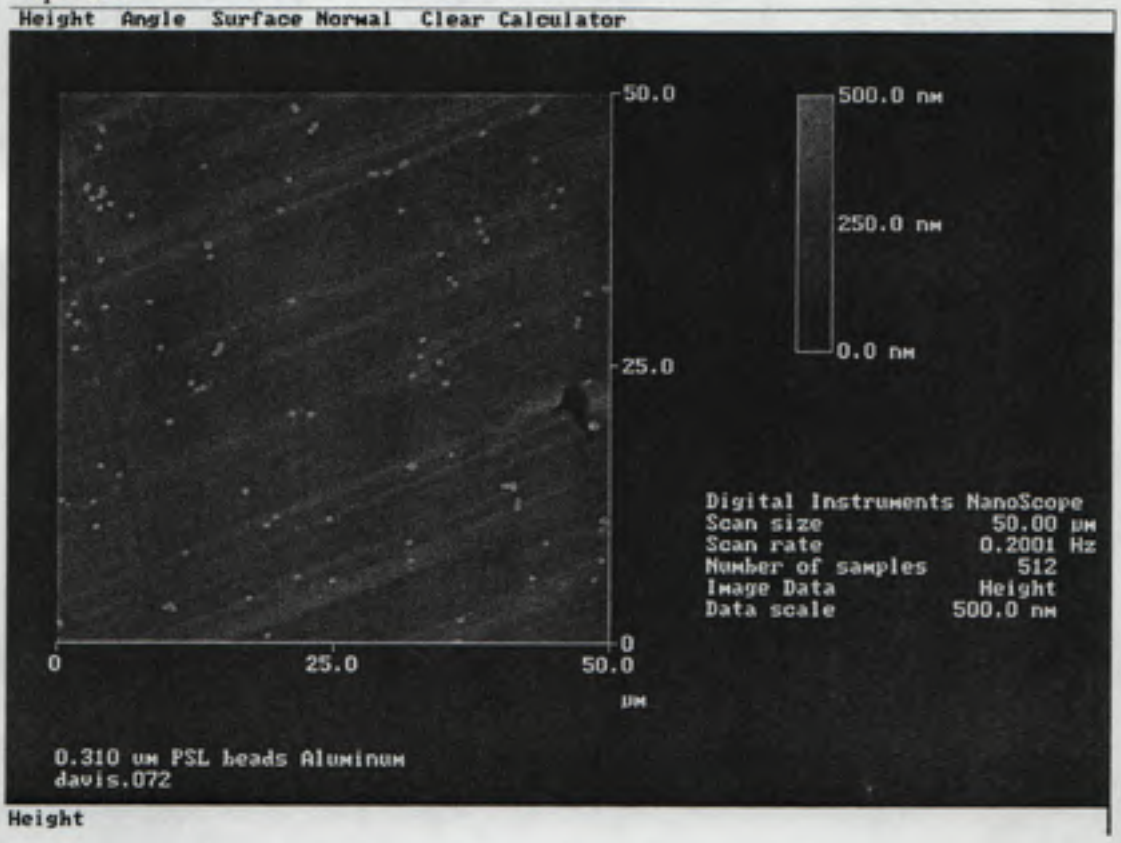

Surface Plot

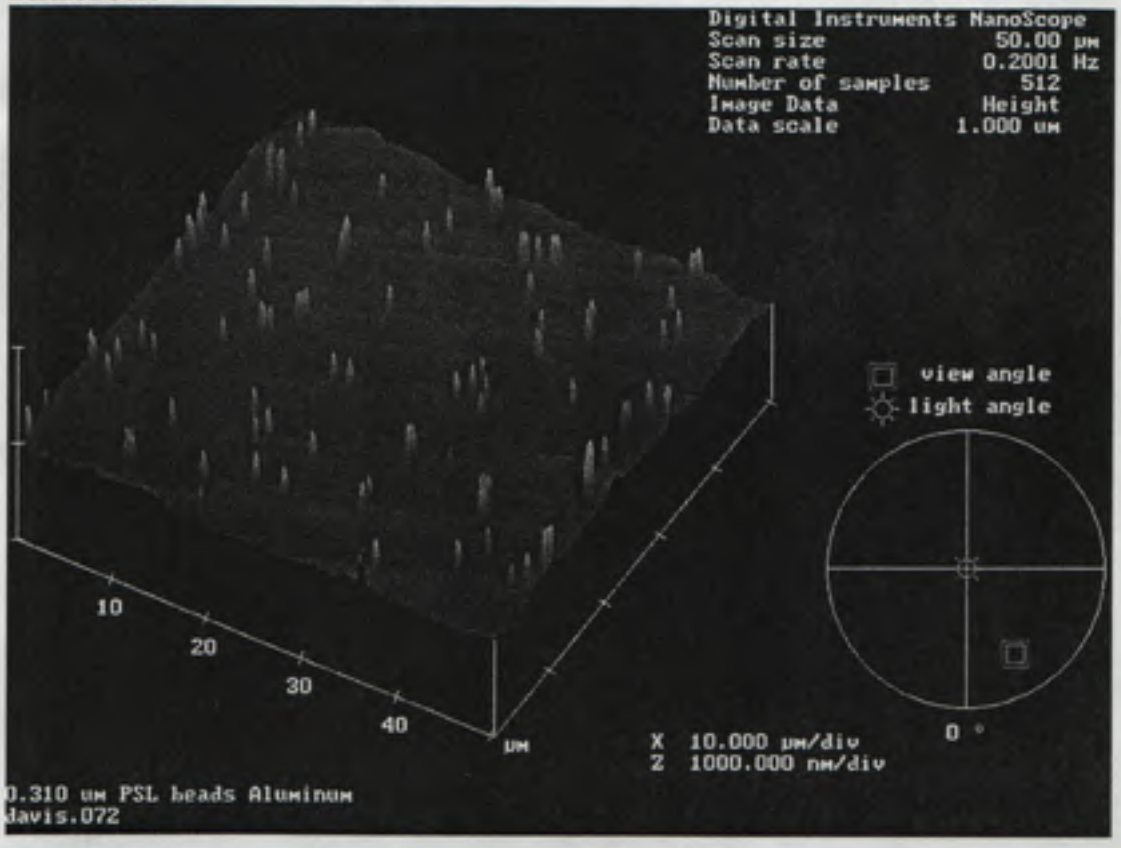

Aluminum (0.310 um PSL Beads)

Section Analysis

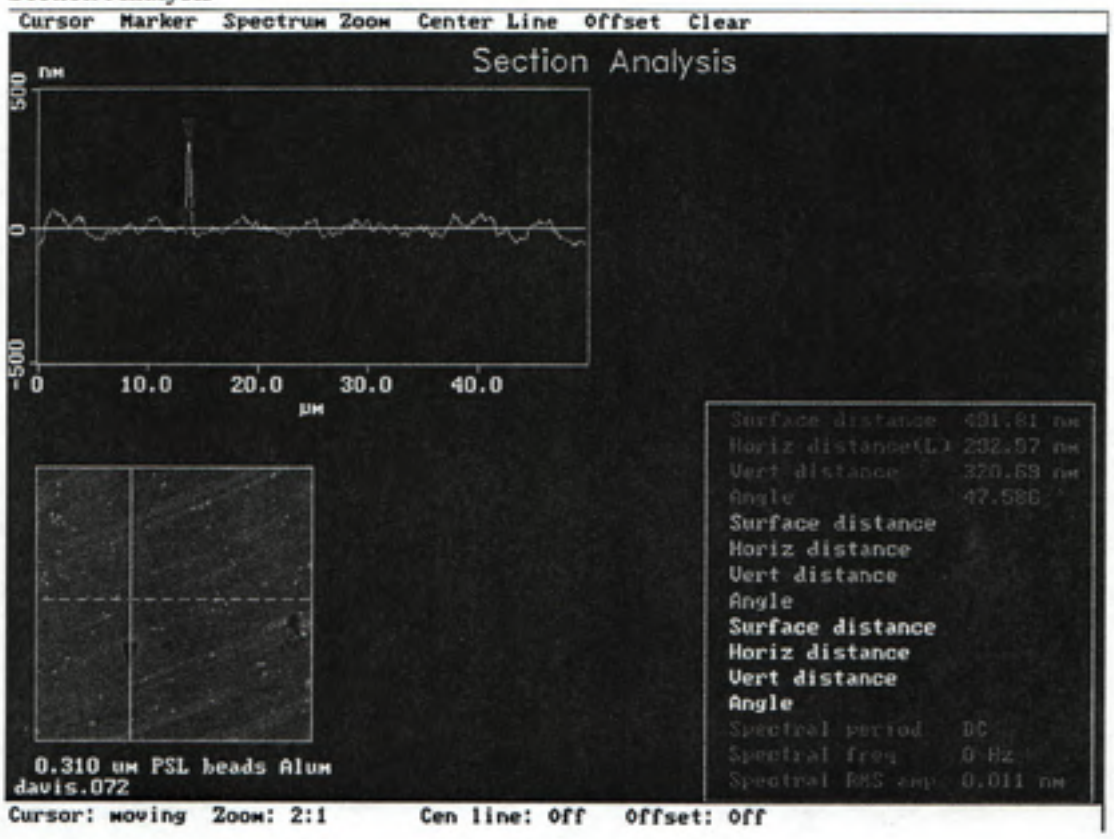

Frosted Glass Slide (0.310 um PSL Beads)

Top View

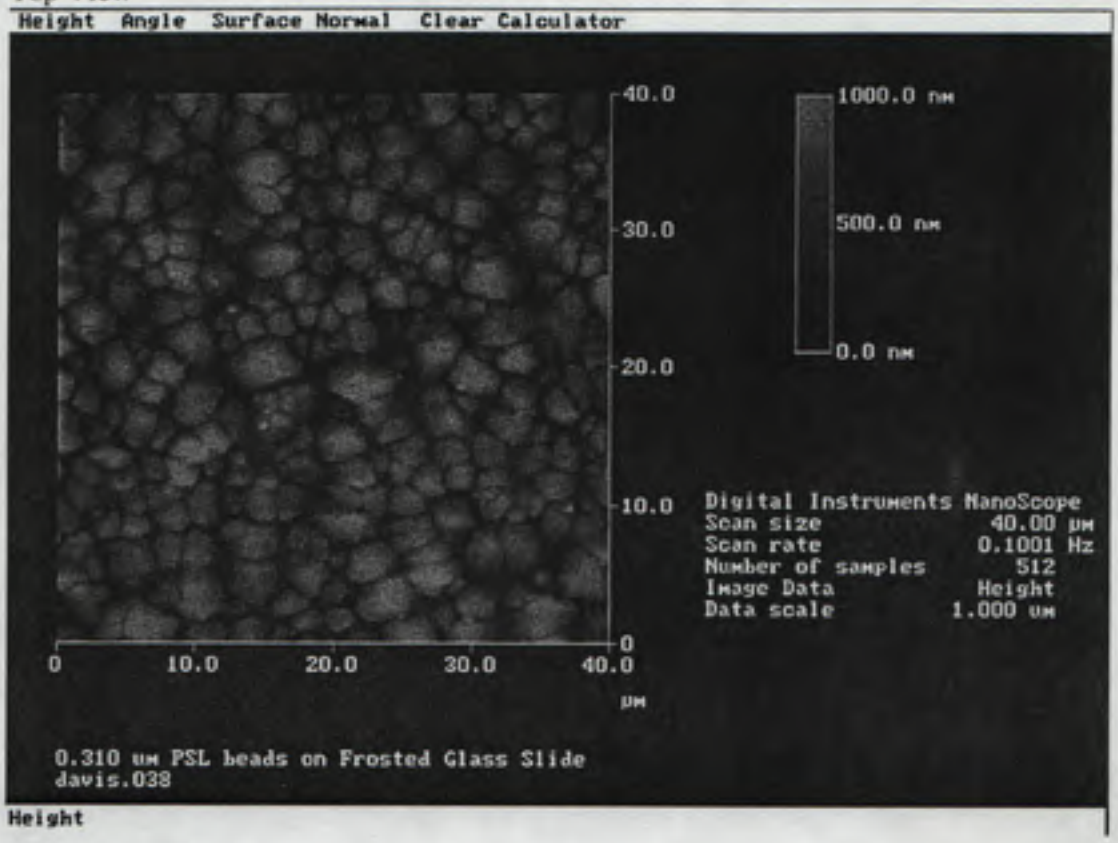

Surface Plot

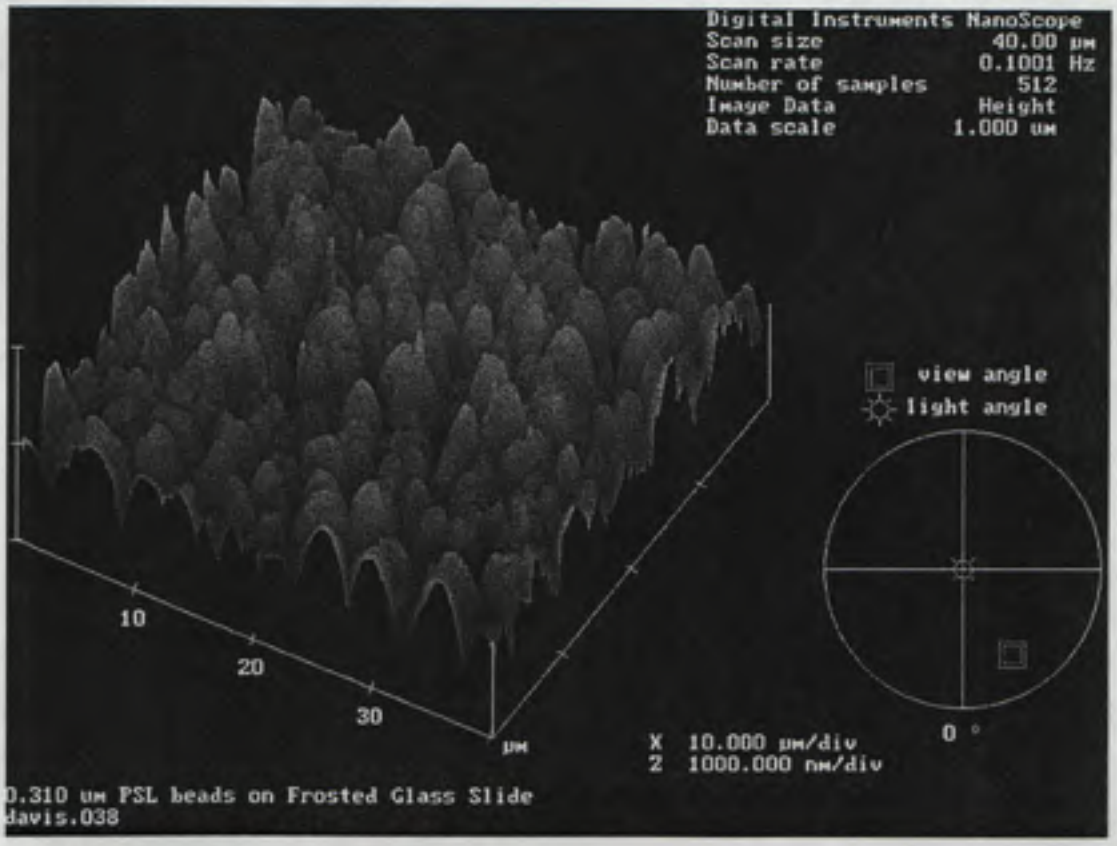

Frosted Glass Slide (0.310 um PSL Beads)

Section Analysis

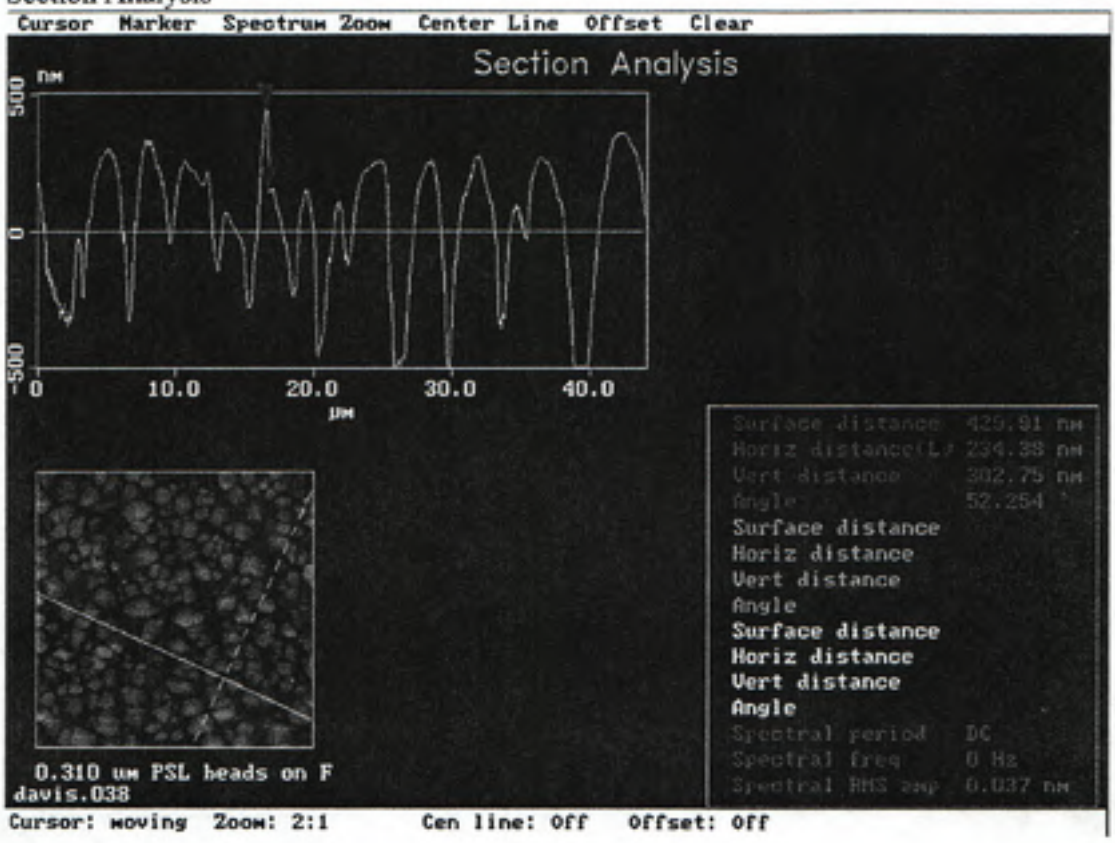

Mica (0.200 um PSL Beads)

Top View

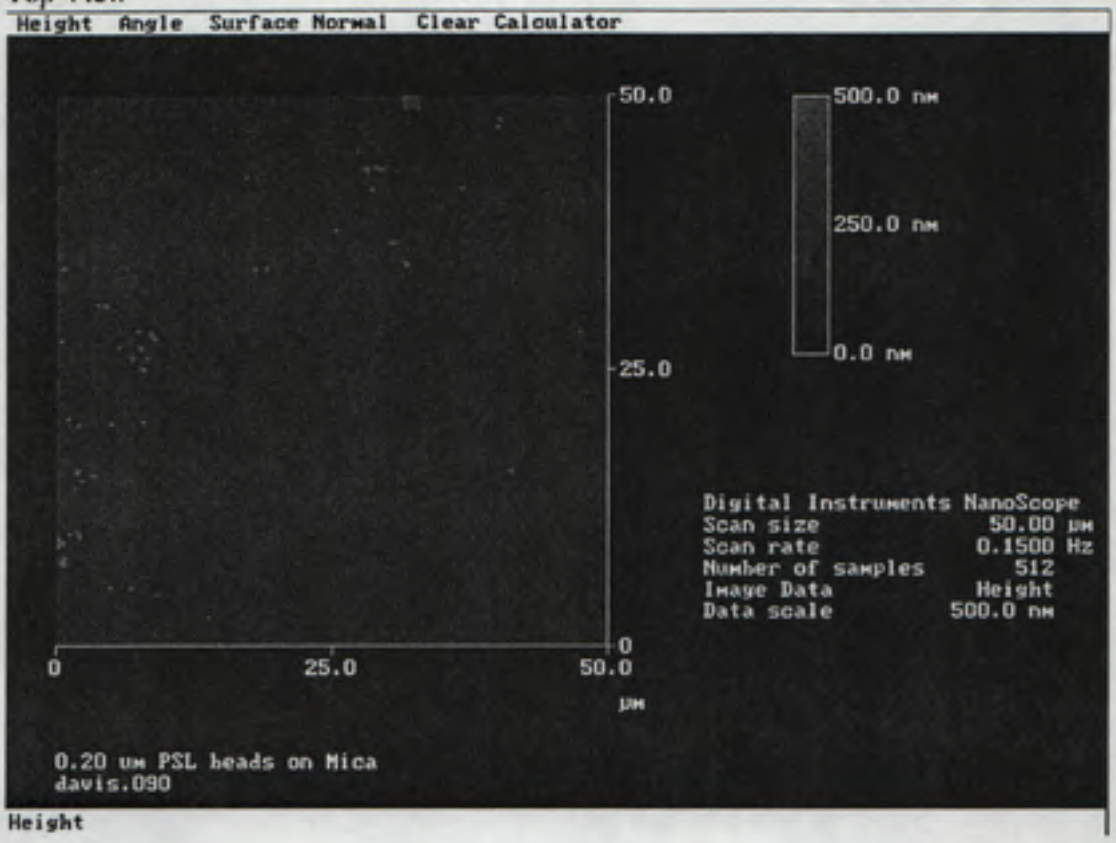

Surface Plot

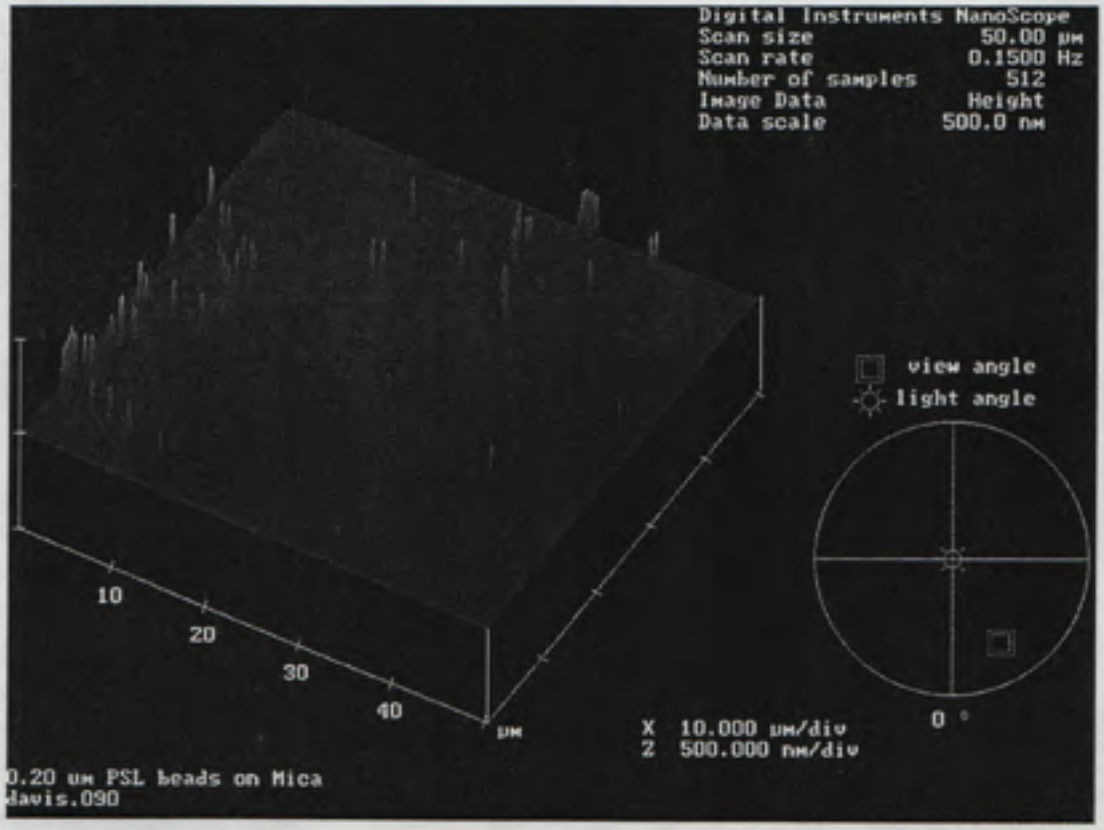

Mica (0.200 um PSL Beads)

Section Analysis

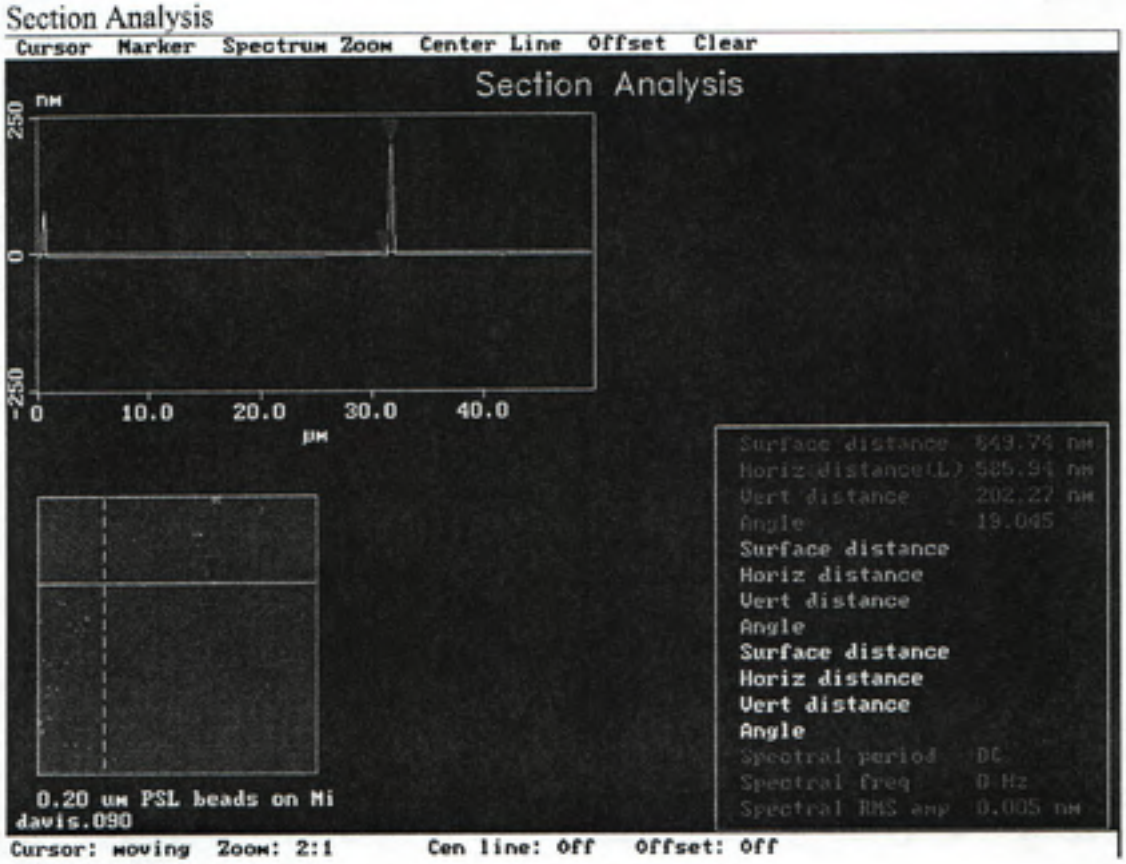

Glass Slide (0.200 um PSL Beads)

Top View

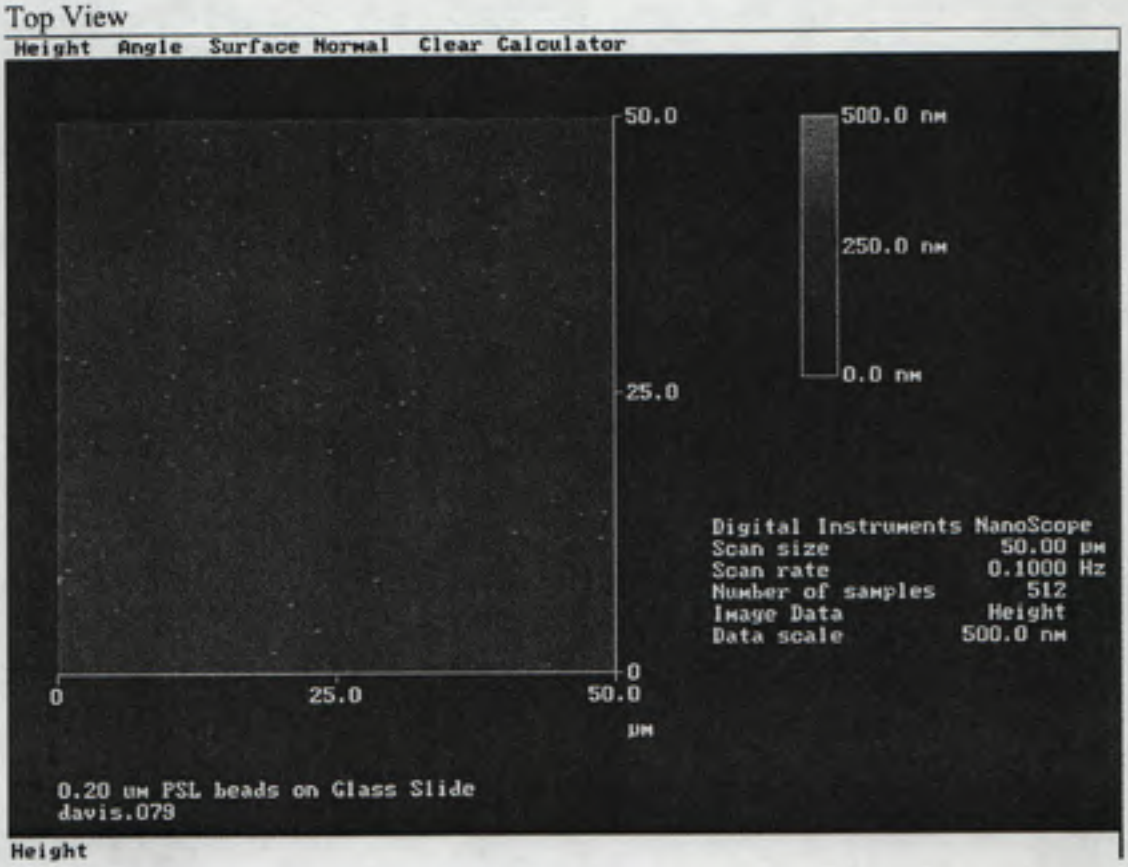

Surface Plot

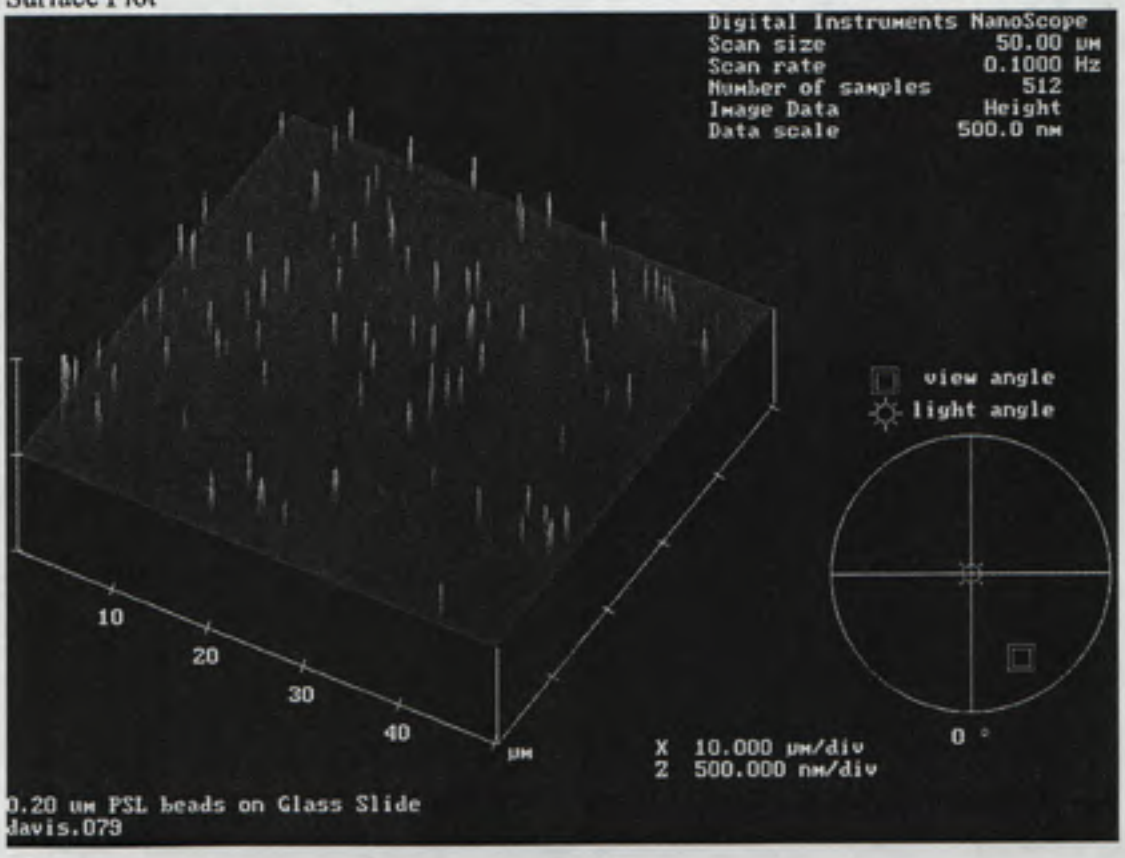

Glass Slide (0.200 um PSL Beads)

Section Analysis

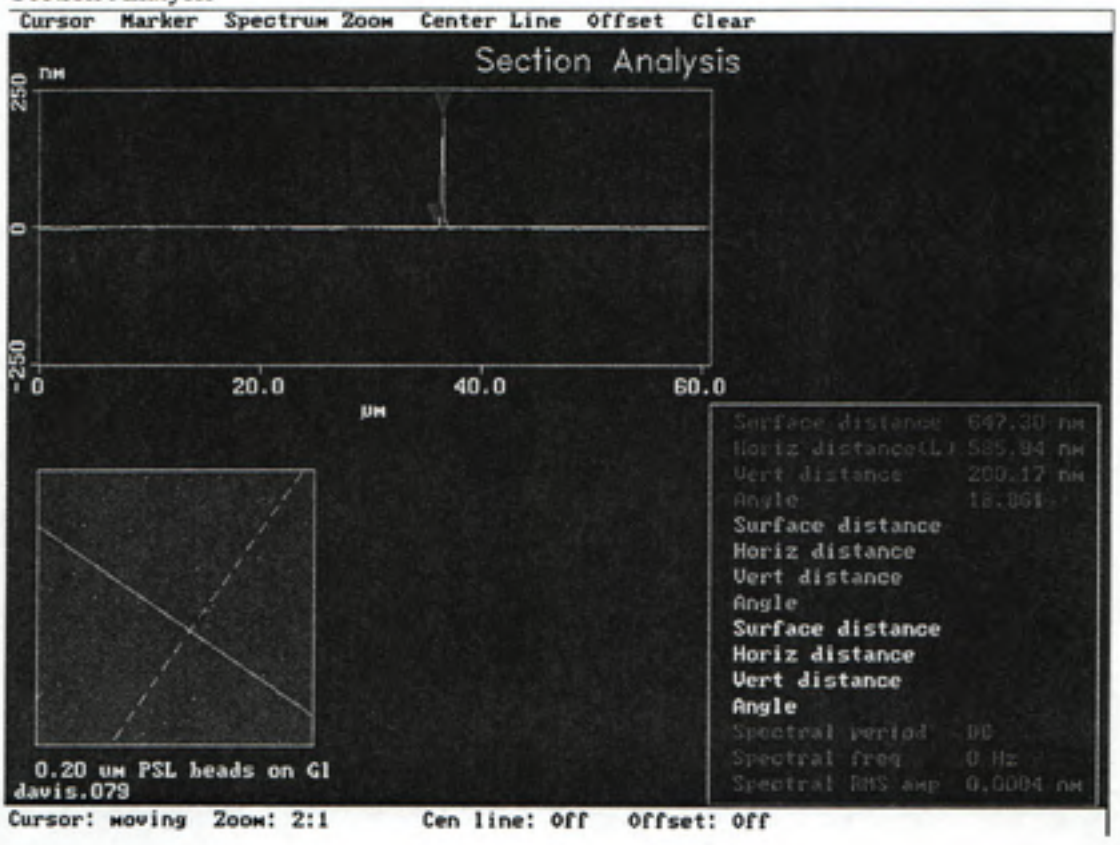

Plastic (0.200 um PSL Beads)

Top View

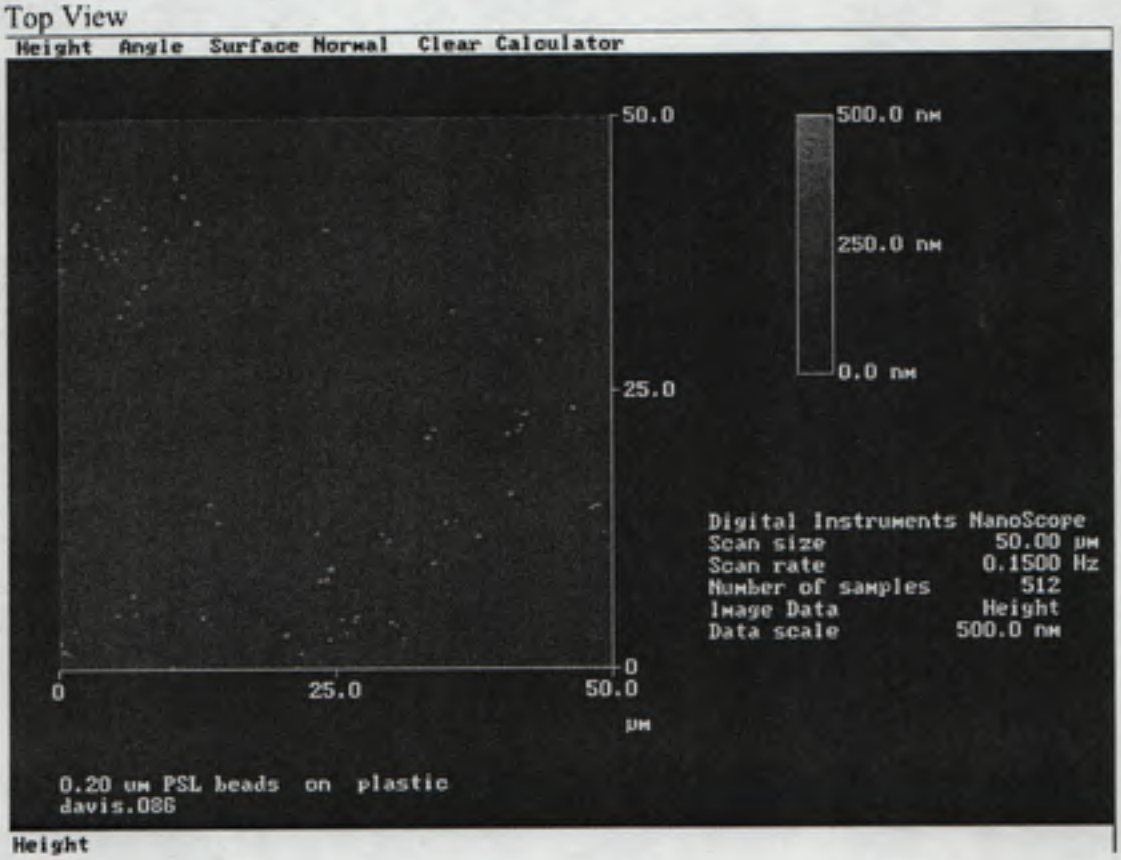

Surface Plot

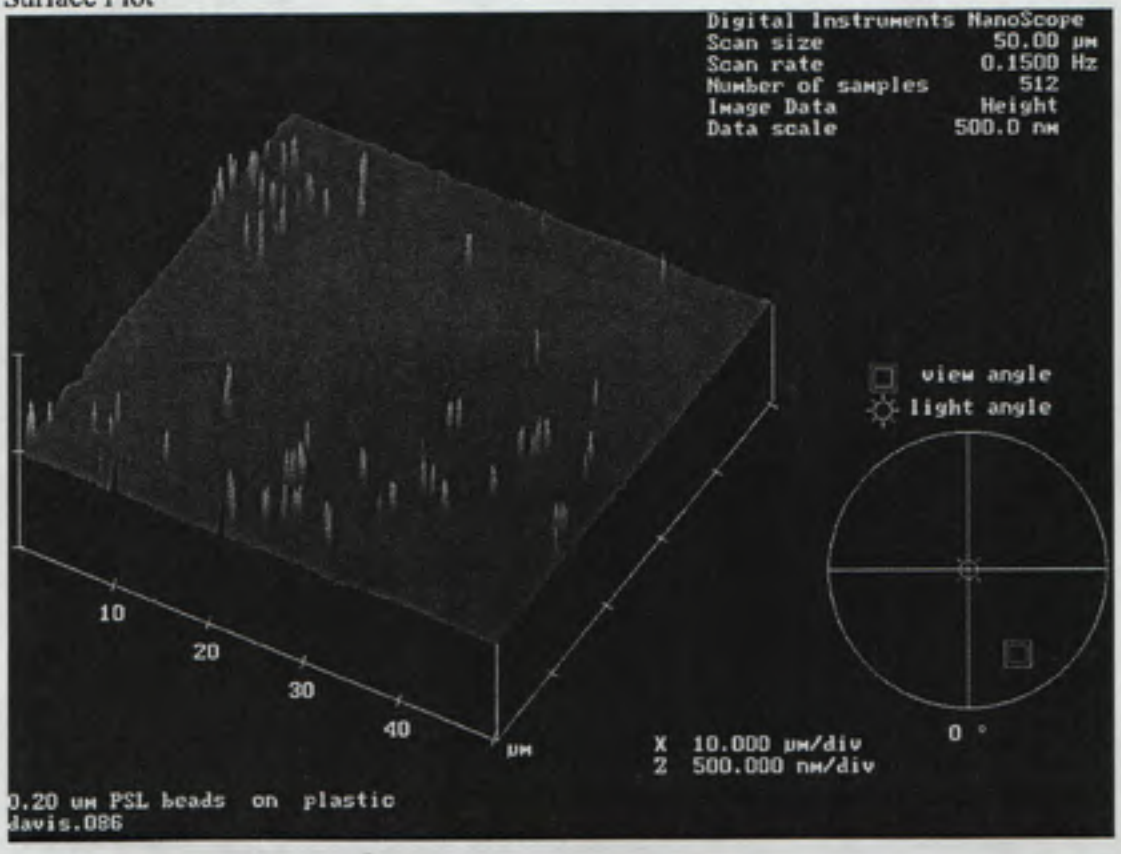

Plastic (0.200 um PSL Beads)

Section Analysis

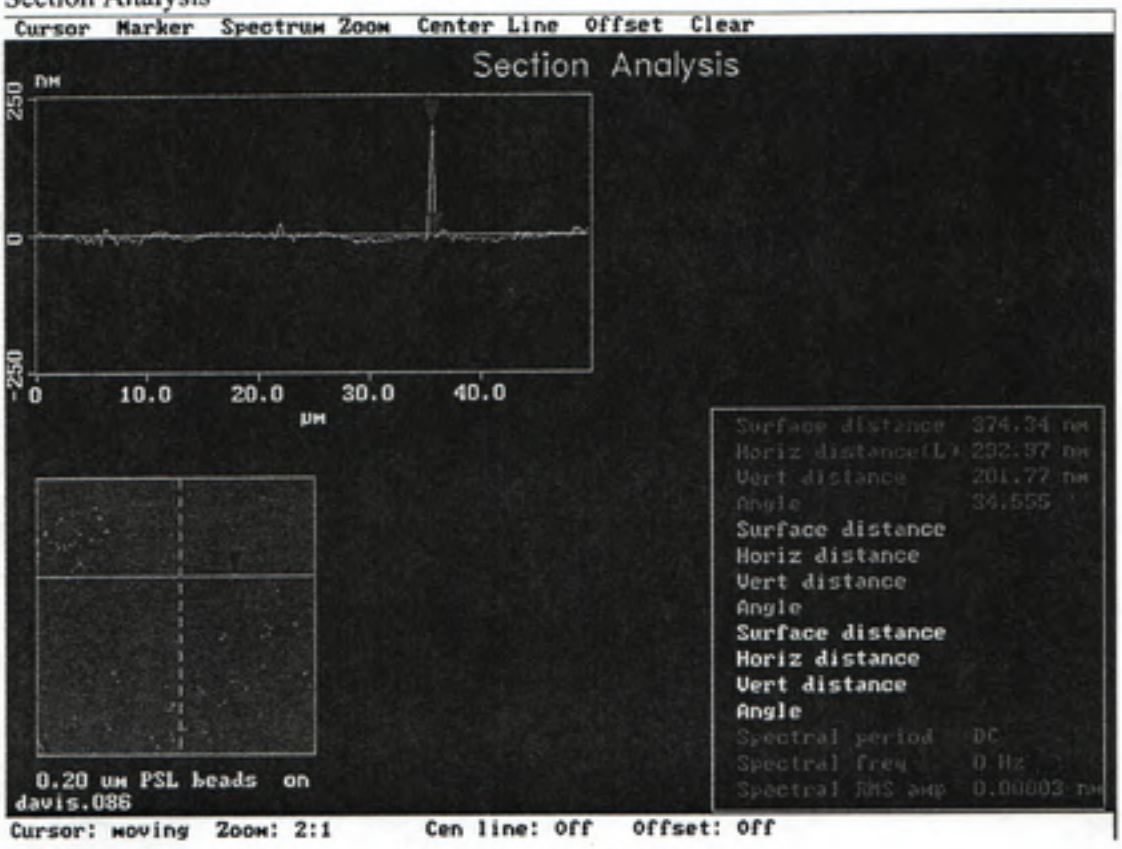

Aluminum (0.200 um PSL Beads)

Top View

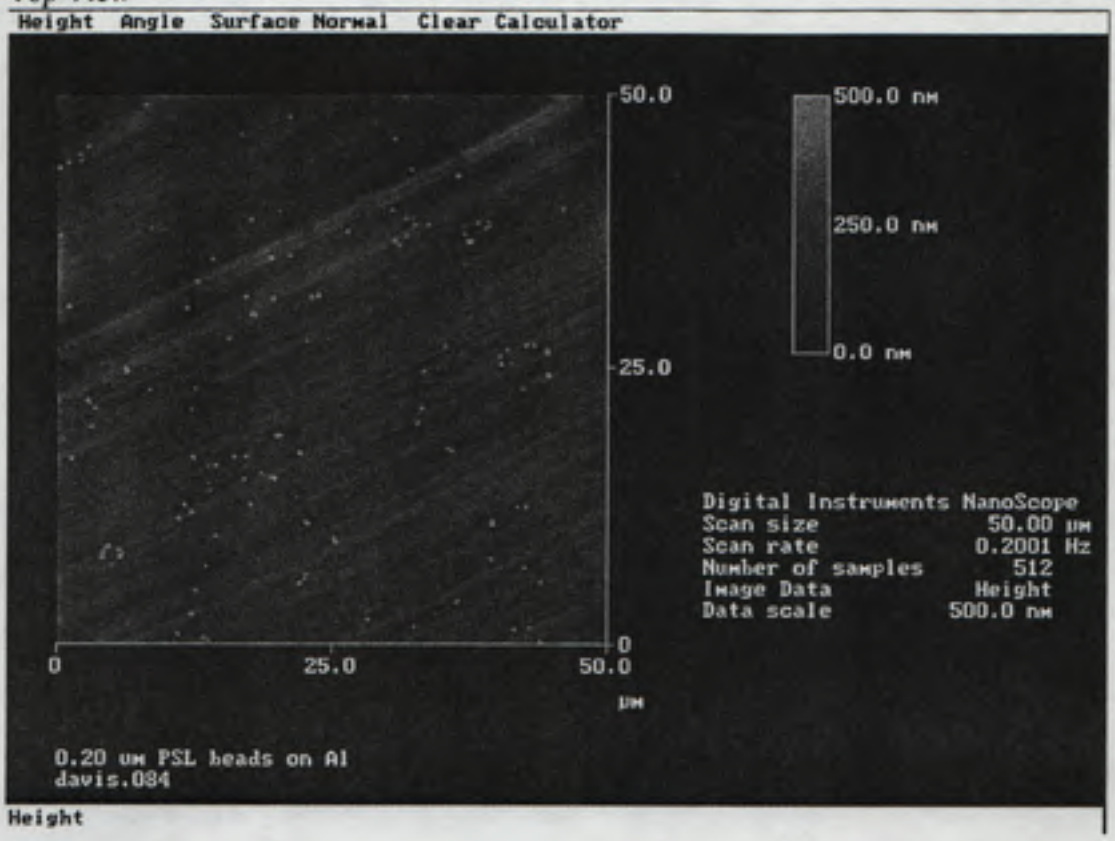

Surface Plot

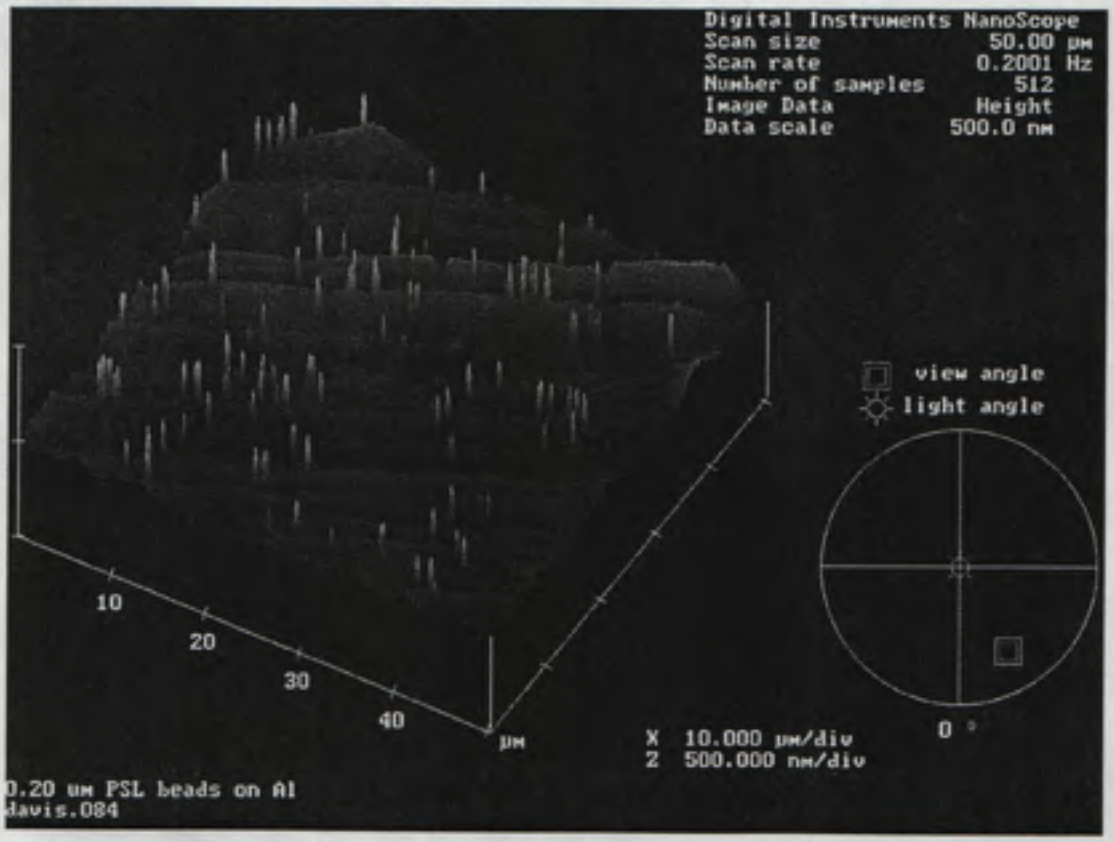

Aluminum (0.200 um PSL Beads)

Section Analysis

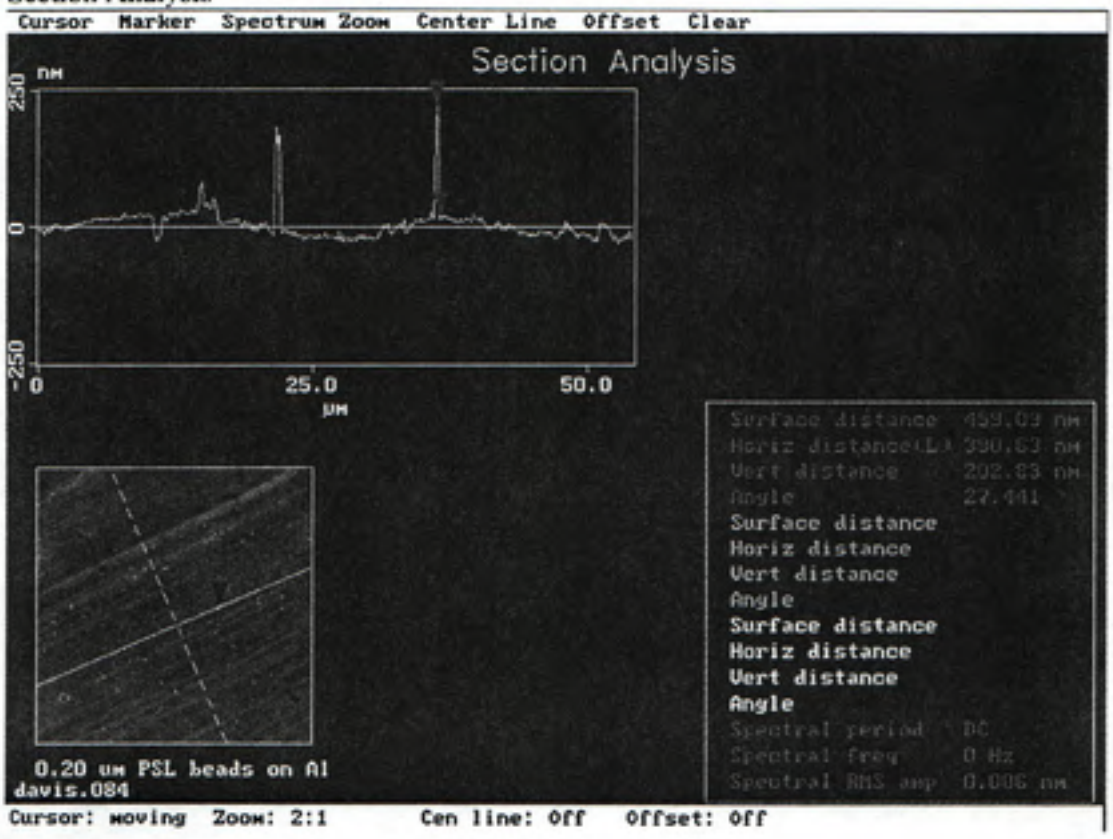

Stainless Steel (0.200 um PSL Beads)

Top View

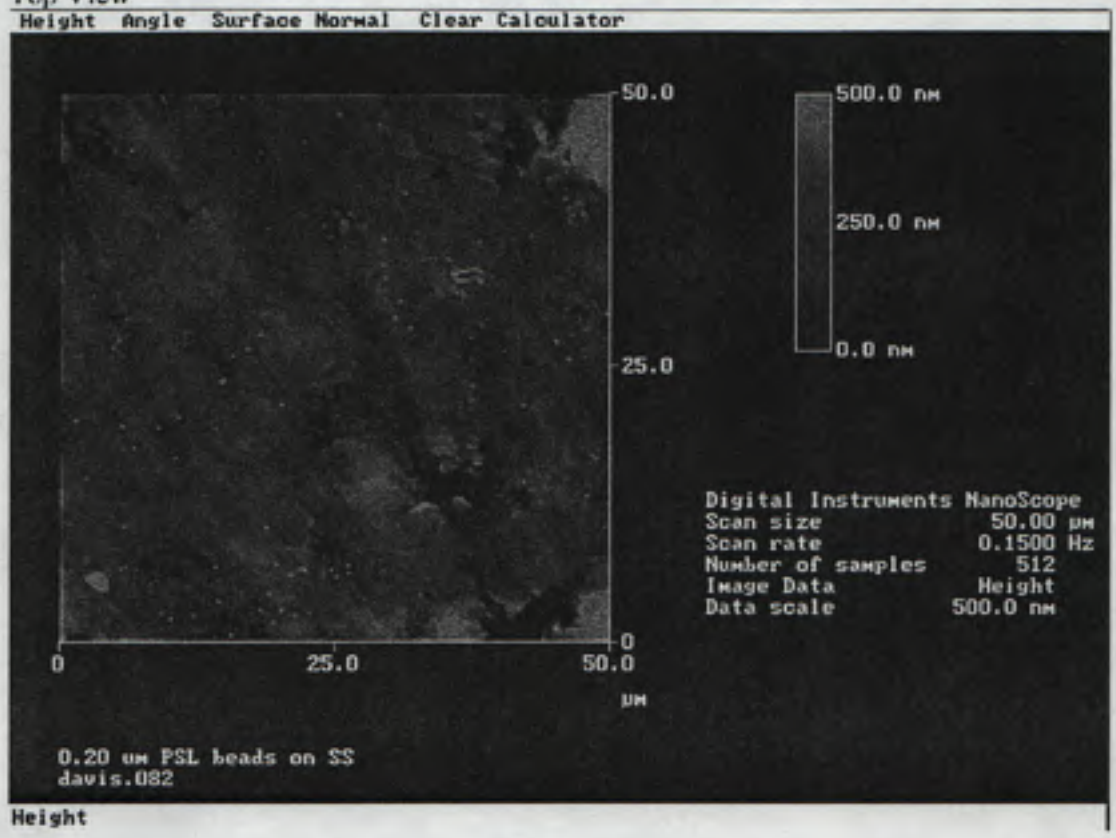

Surface Plot

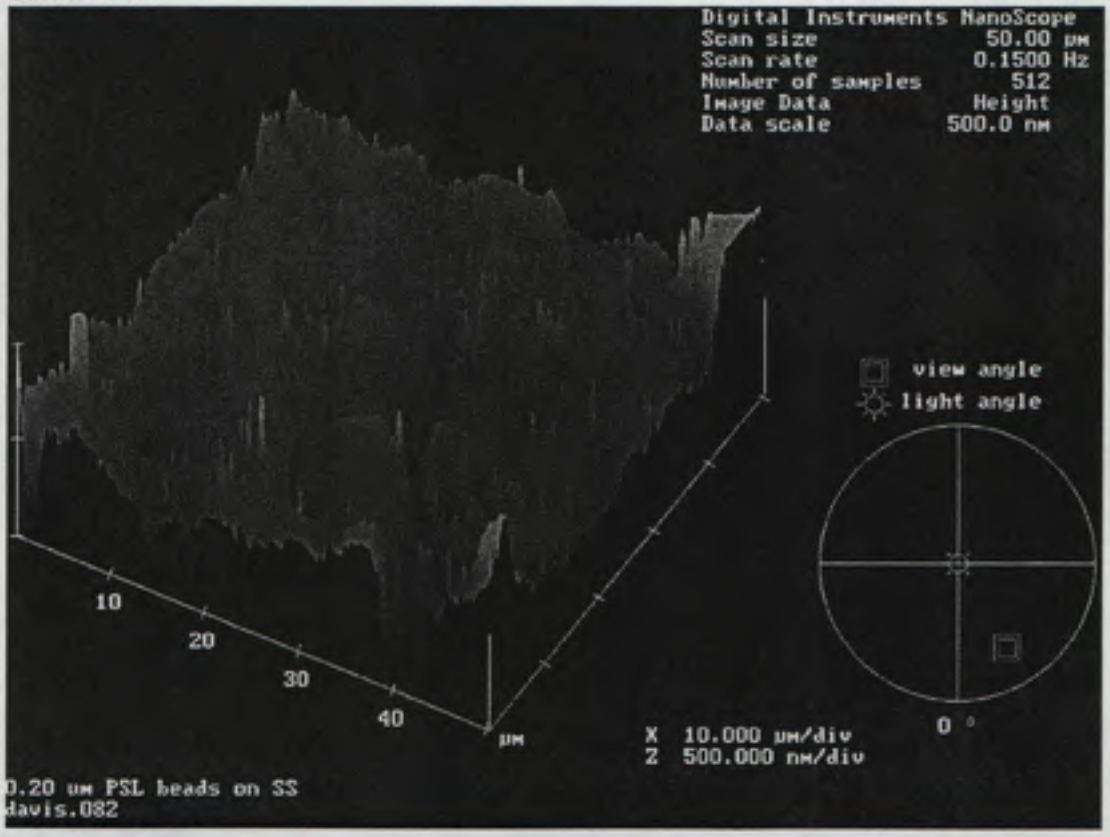

Stainless Steel (0.200 um PSL Beads)

Section Analysis

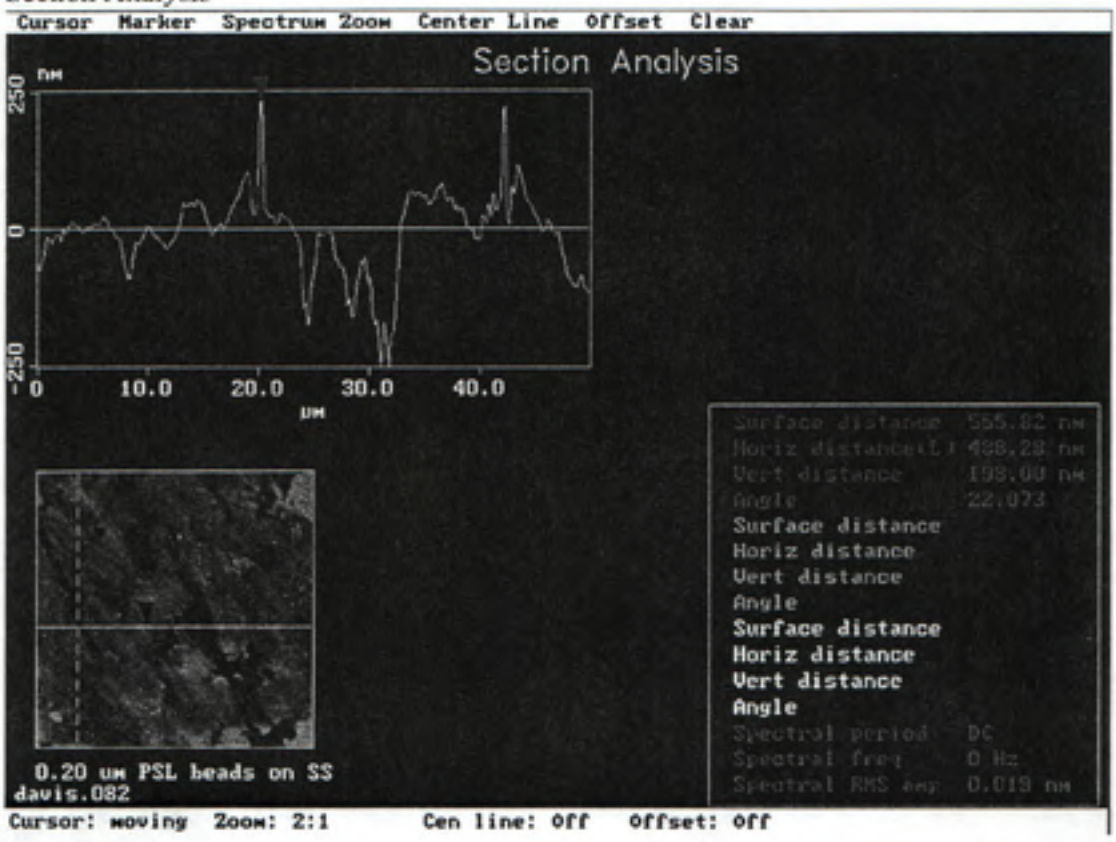

Frosted Glass Slide (0.200 um PSL Beads)

Top View

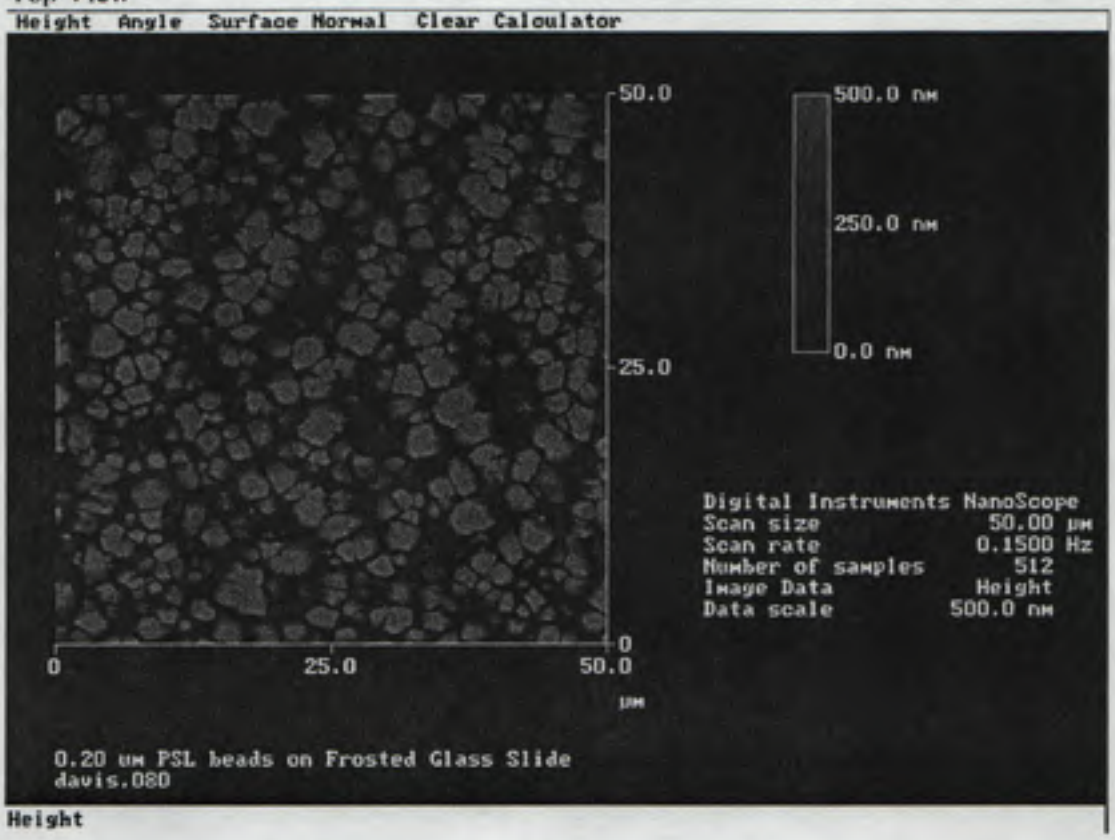

Surface Plot

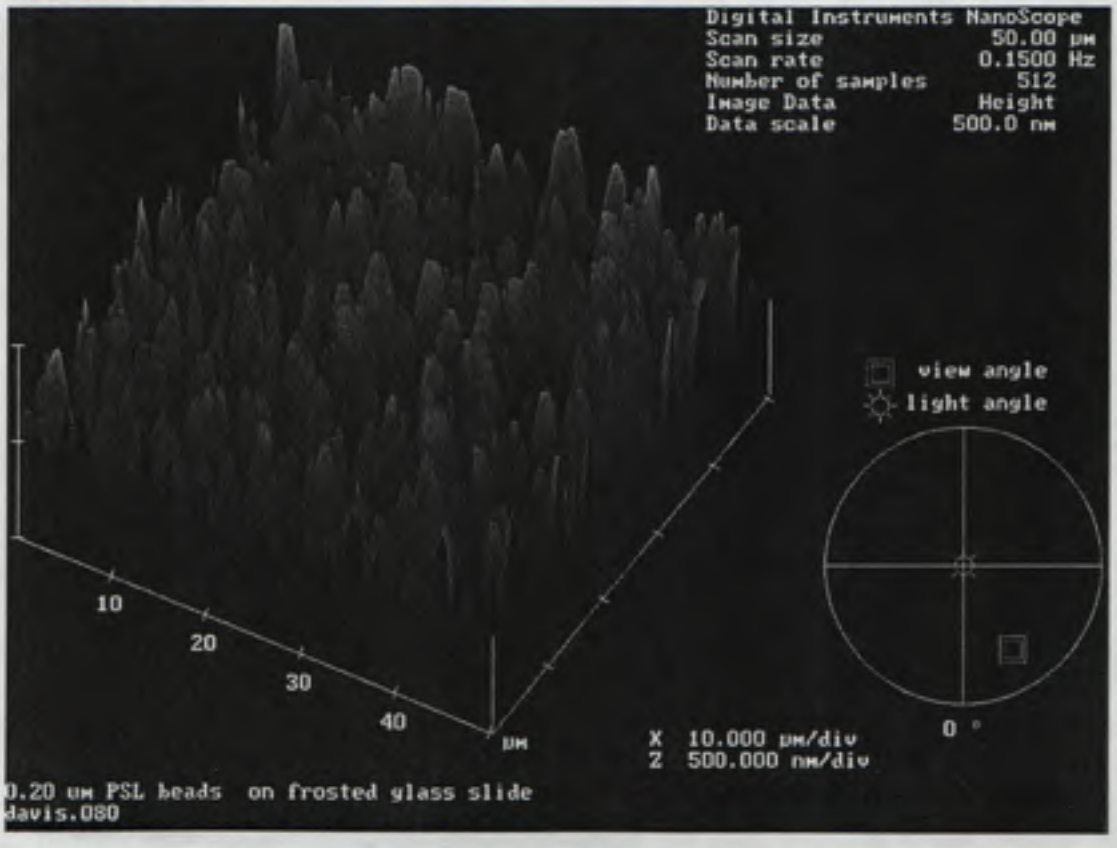

Frosted Glass Slide (0.200 um PSL Beads)

Section Analysis

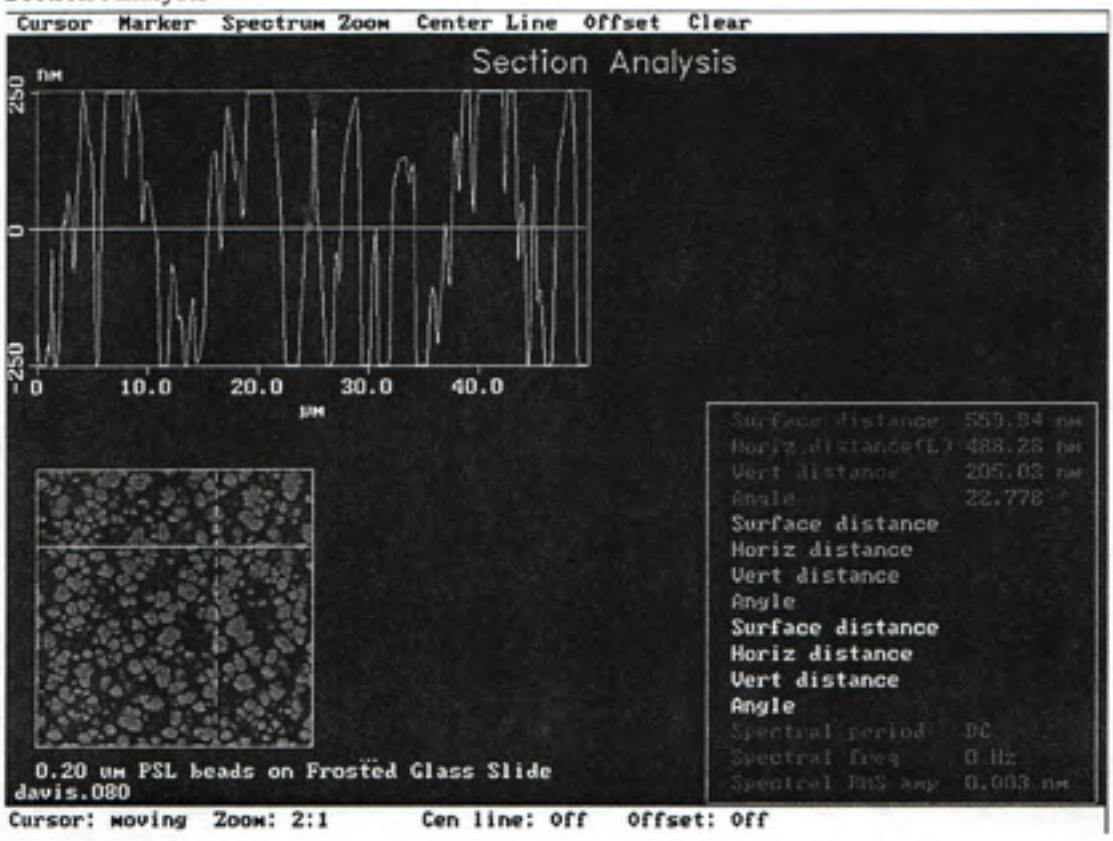

Slide 5 (1.00 um PSL Beads)

Top View

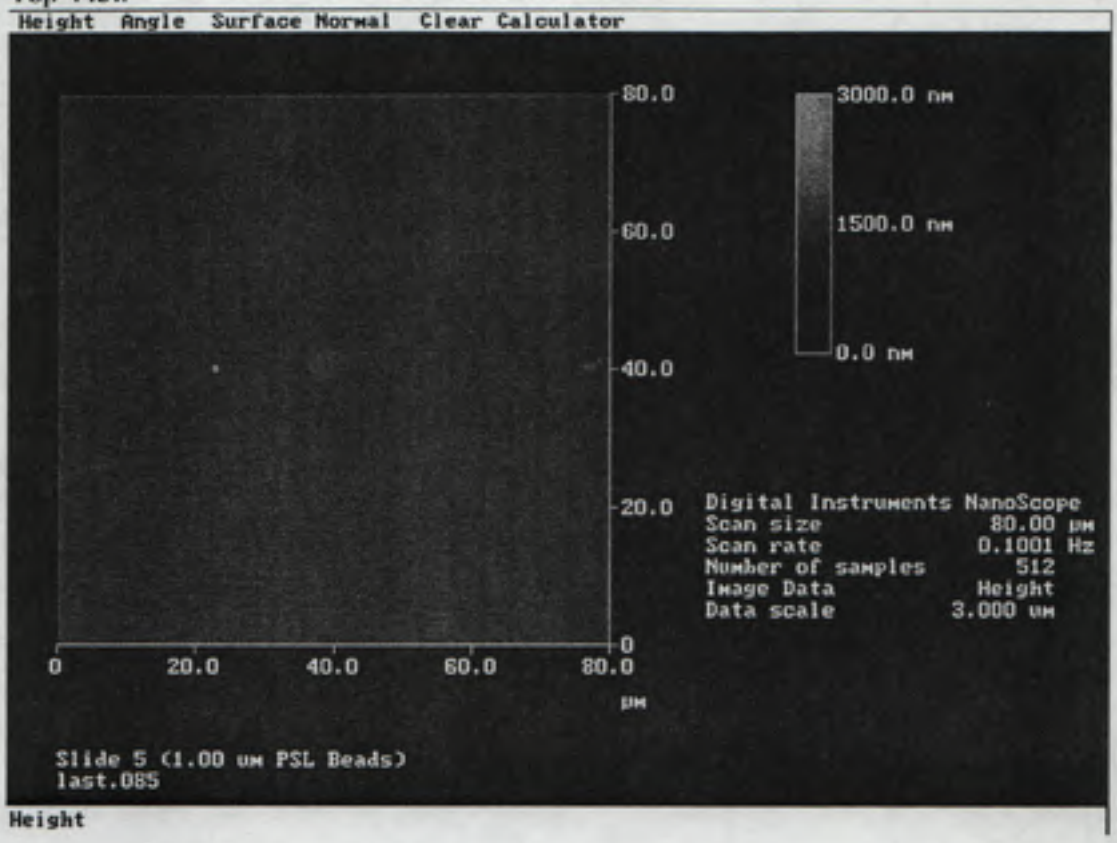

Surface Plot

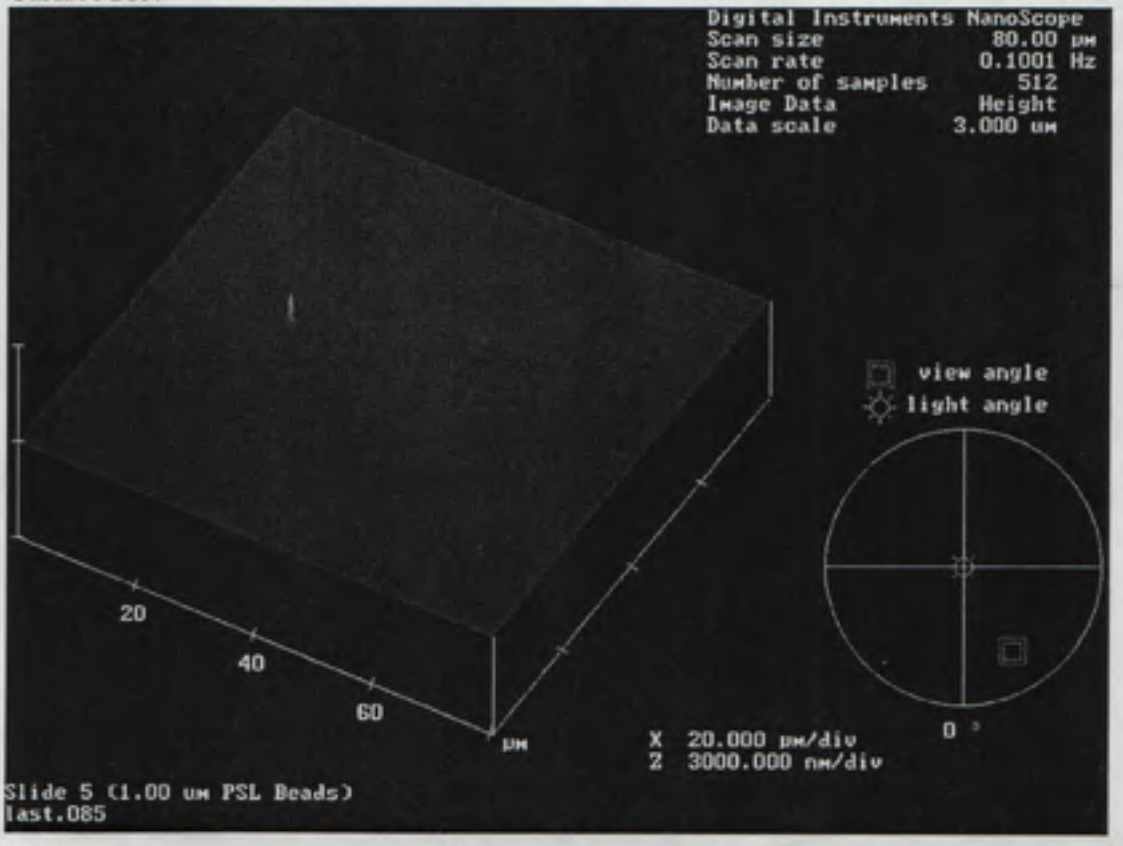

Slide 5 (1.00 um PSL Beads)

Section Analysis

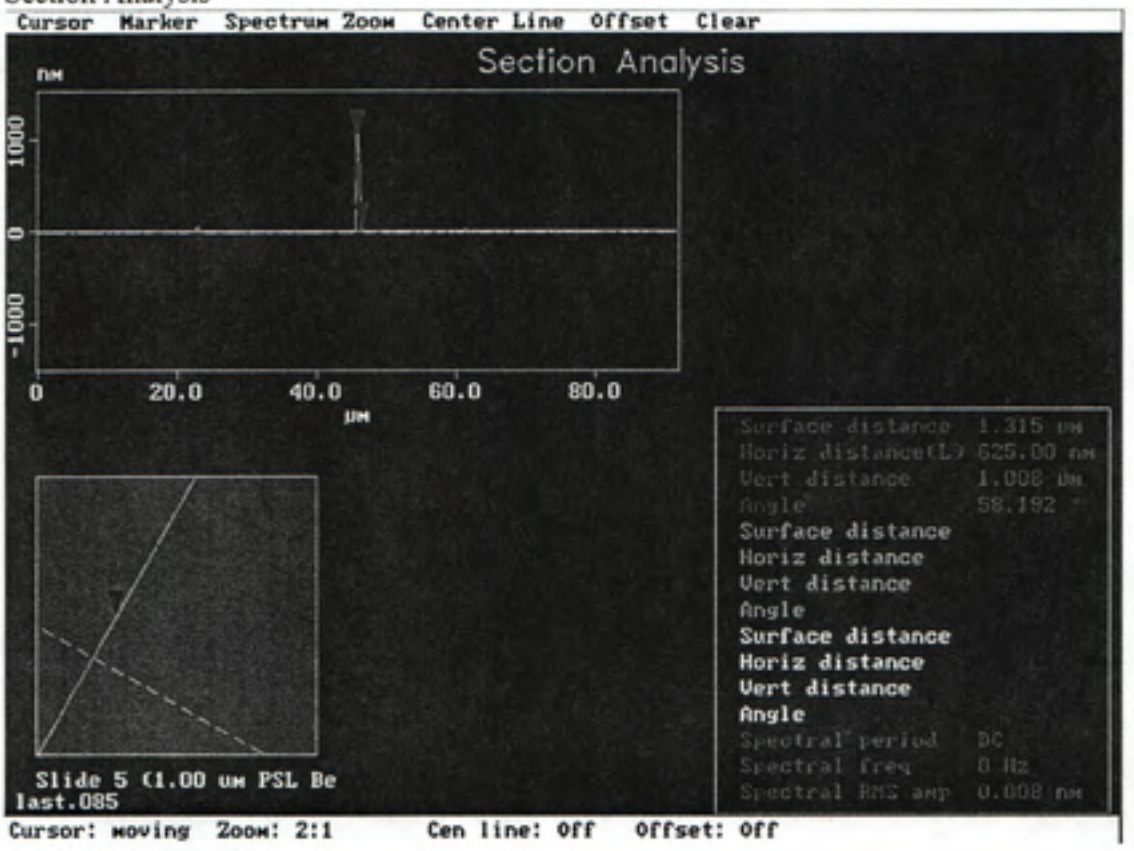

Slide 5 (0.480 um PSL Beads)

Top View

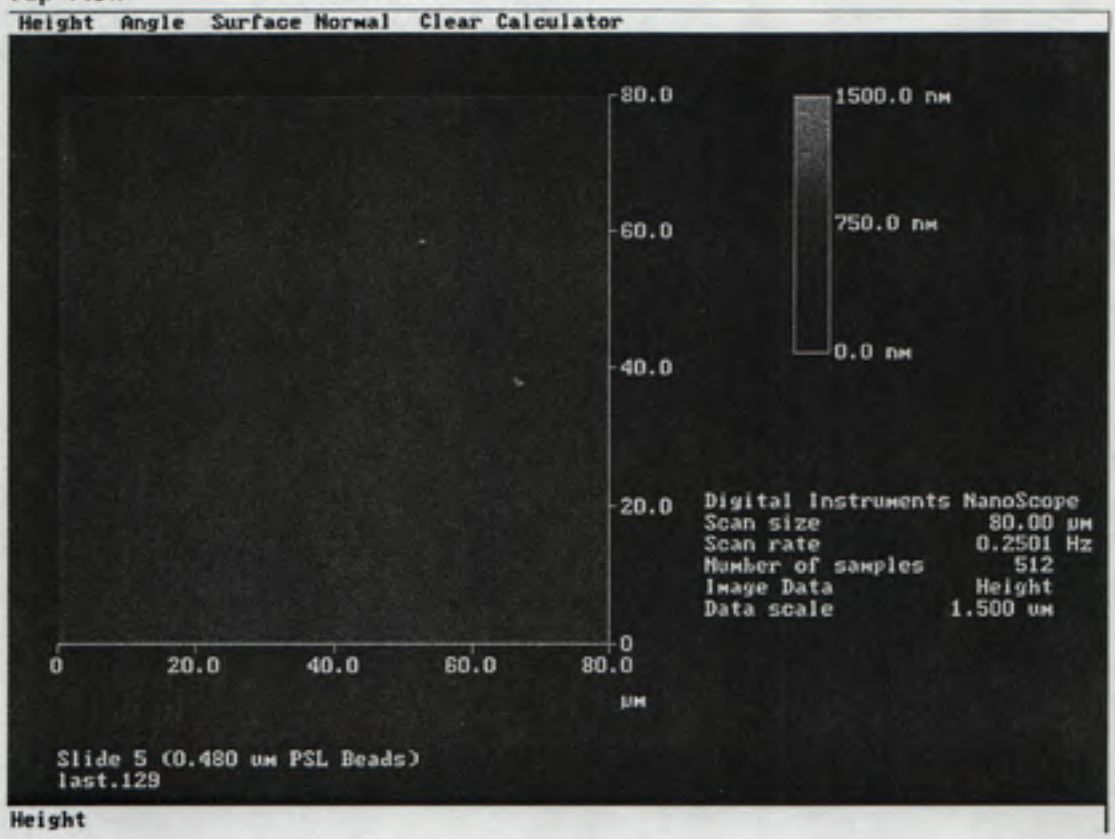

Surface Plot

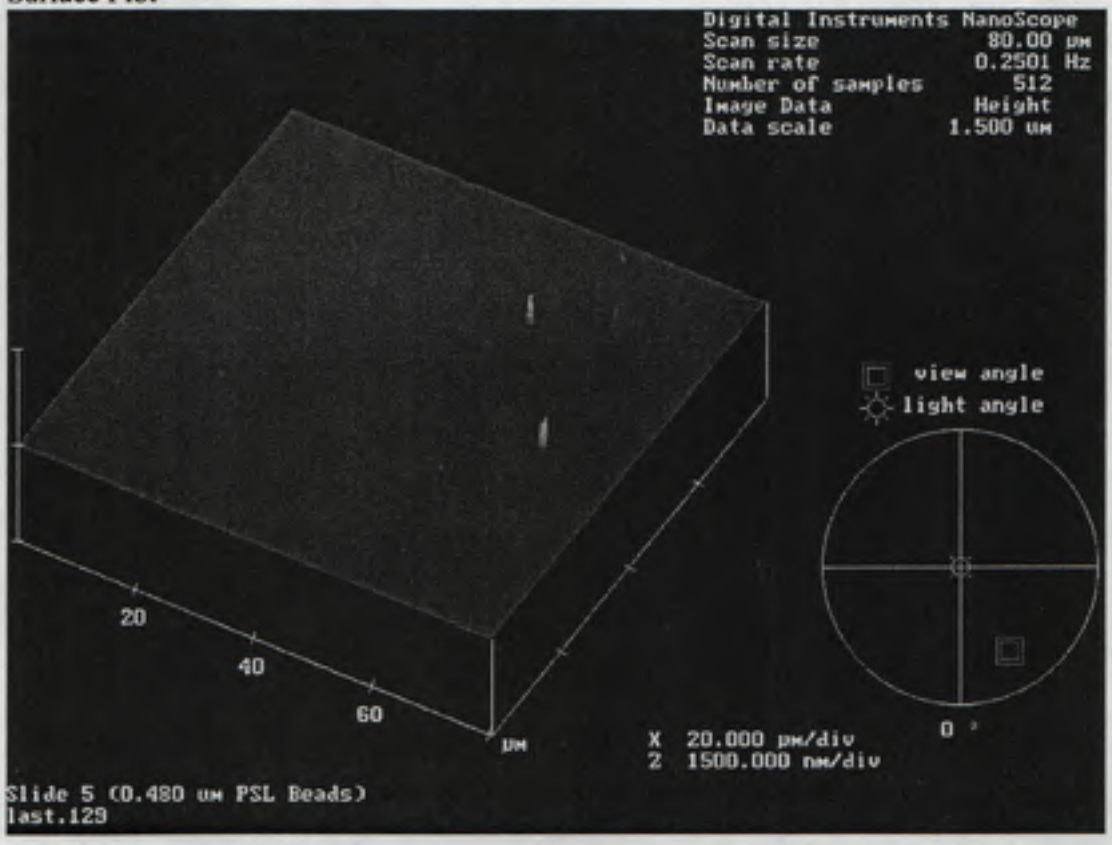

Slide 5 (0.480 um PSL Beads)

Section Analysis

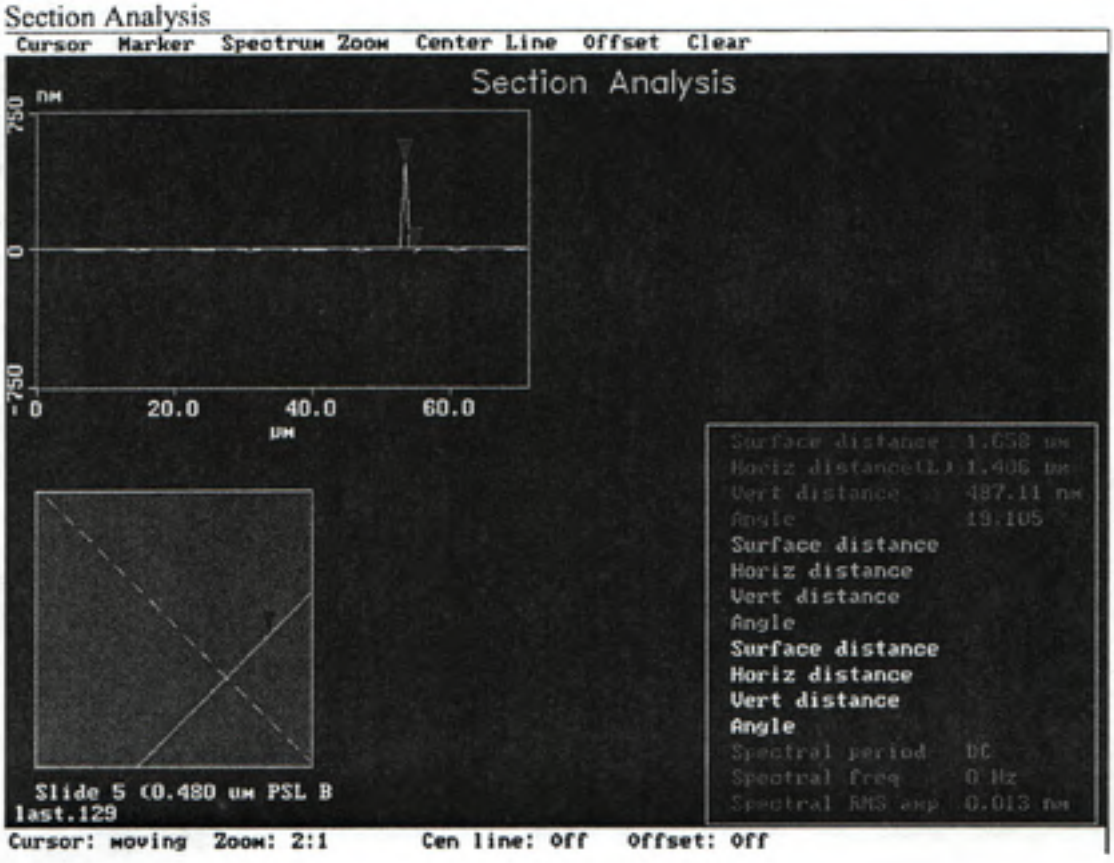

Slide 5 (0.310 um PSL Beads)

Top View

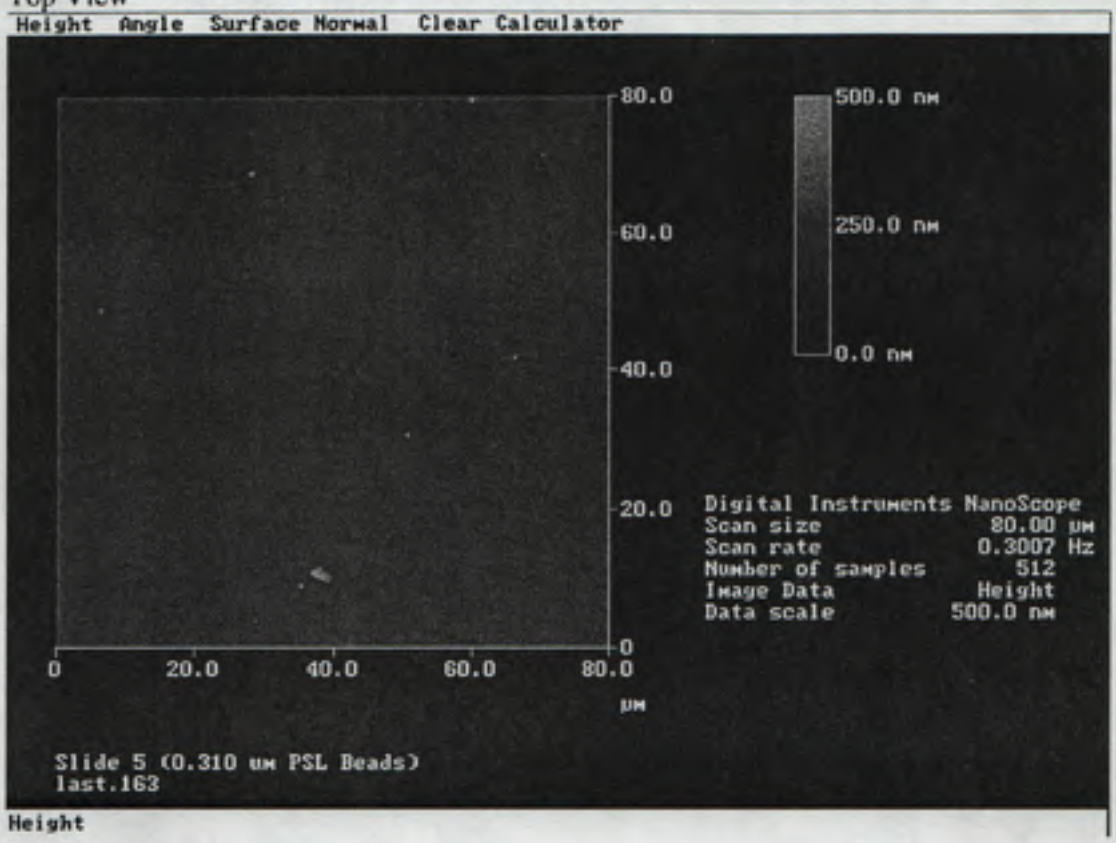

Surface Plot

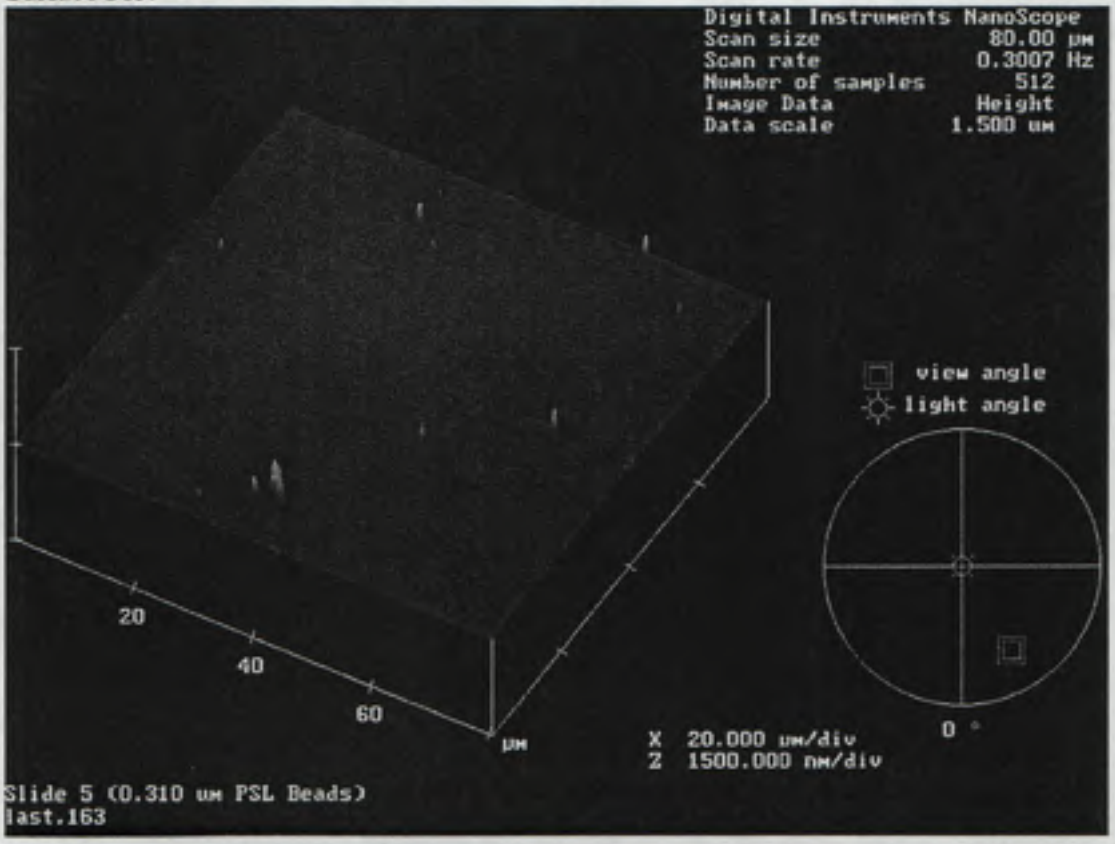

Slide 5 (0.310 um PSL Beads)

Sectional Analysis

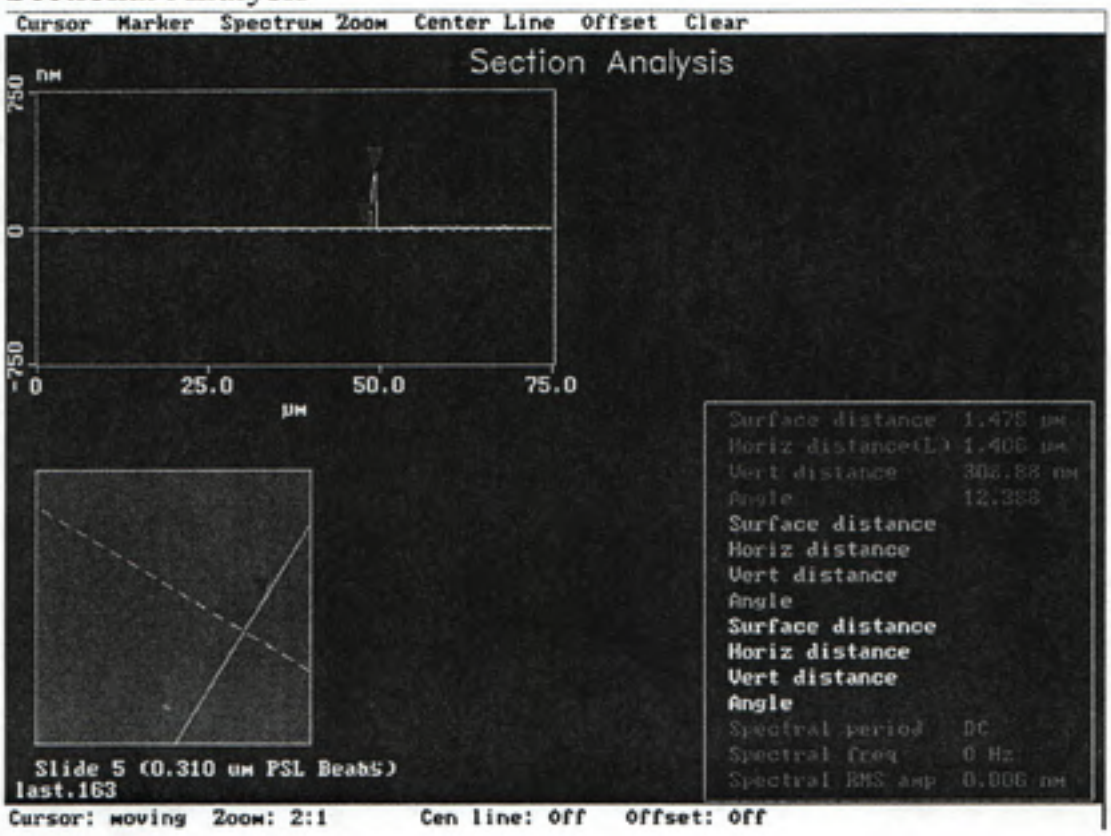

Slide 4 (0.200 um PSL Beads)

Top View

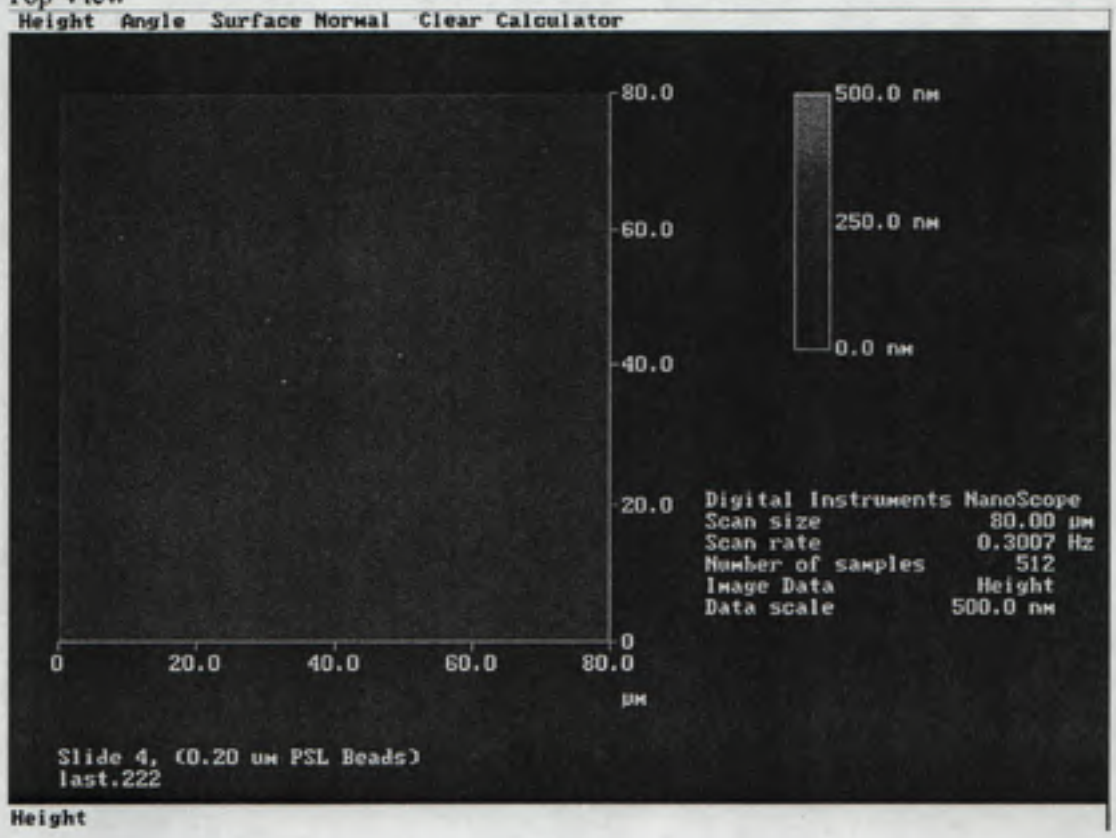

Surface Plot

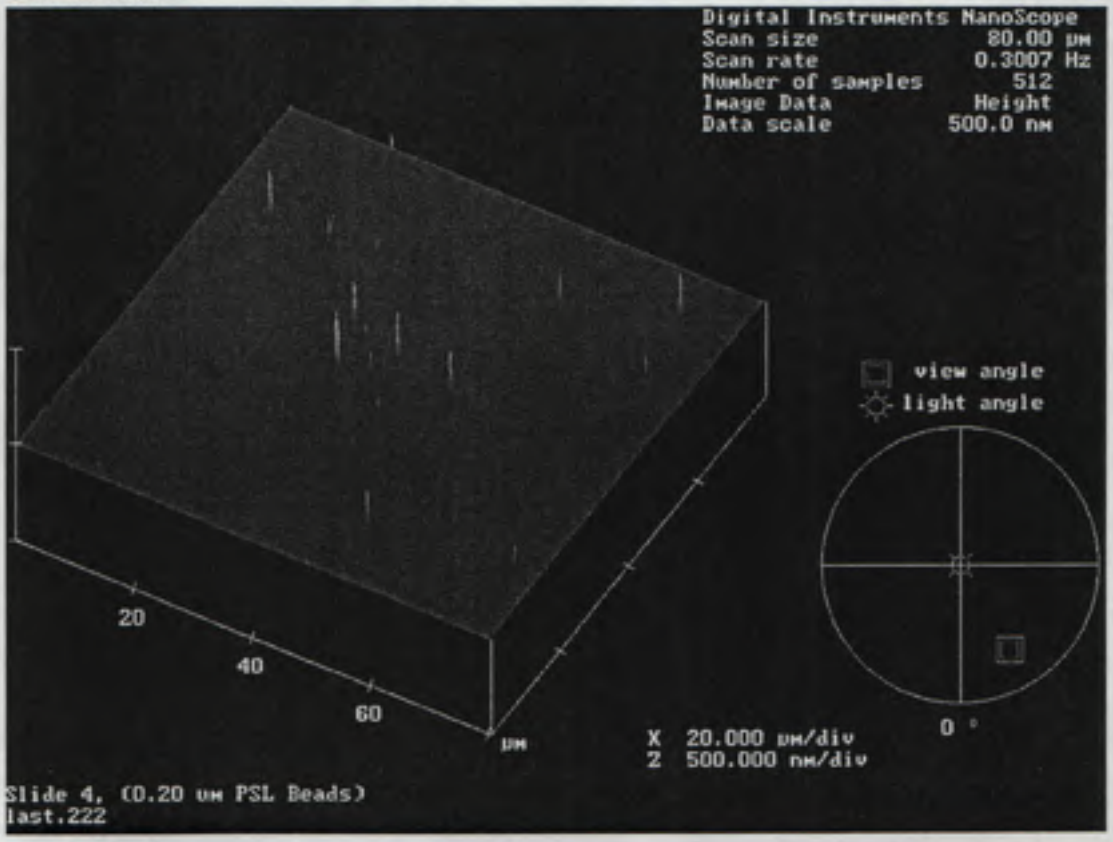

Slide 4 (0.200 um PSL Beads)

Sectional Analysis

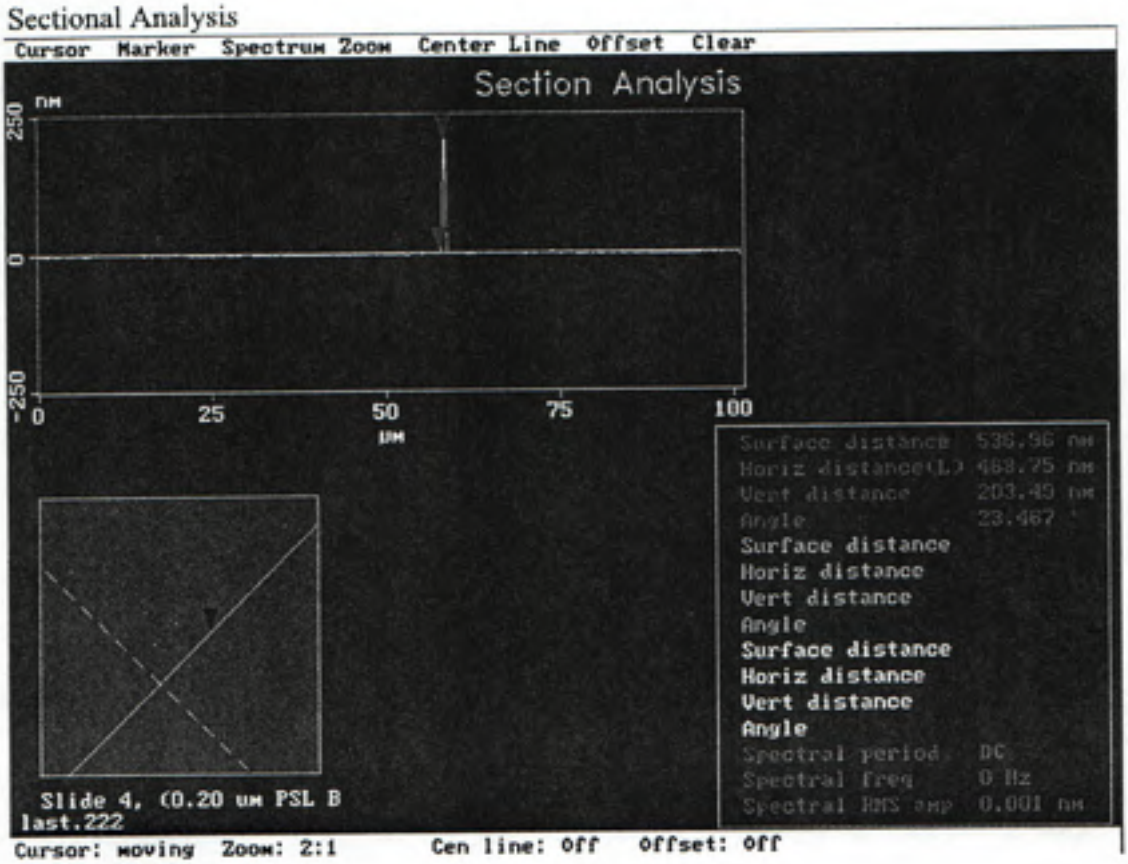

Slide 3 (0.100 um PSL Beads)

Top View

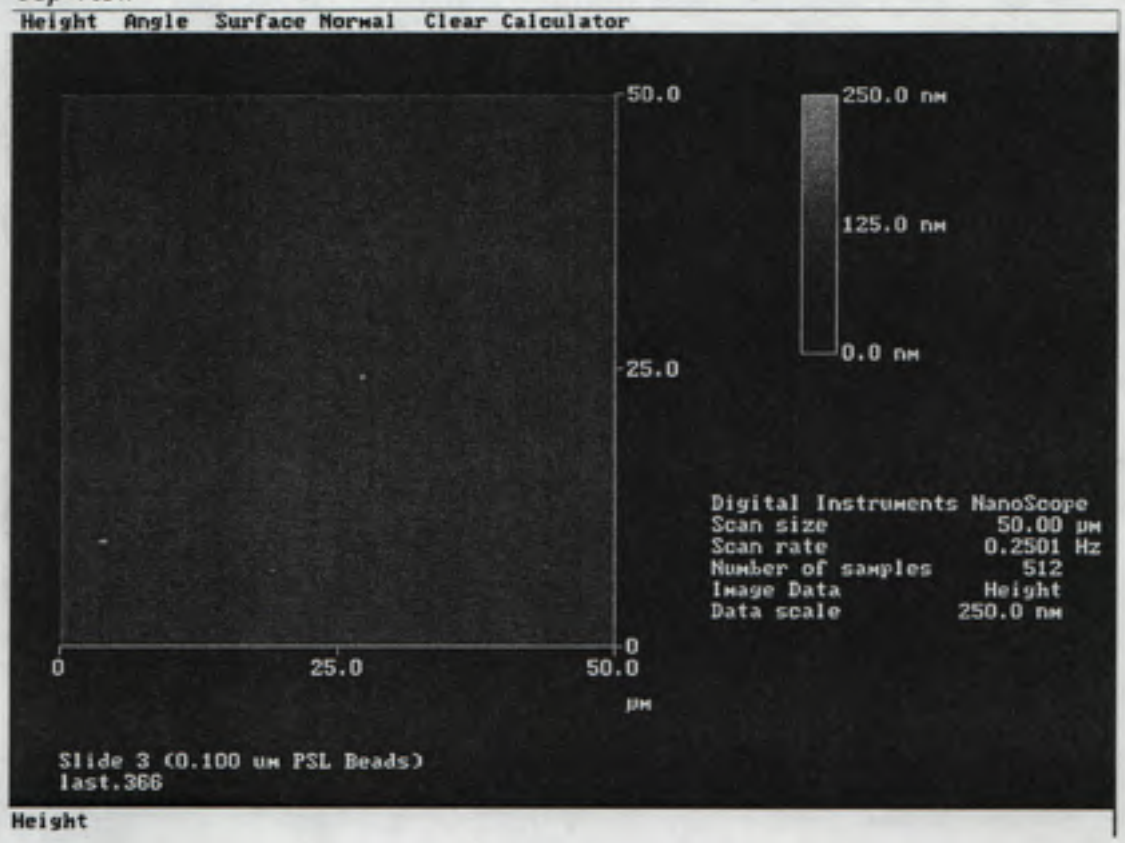

Surface Plot

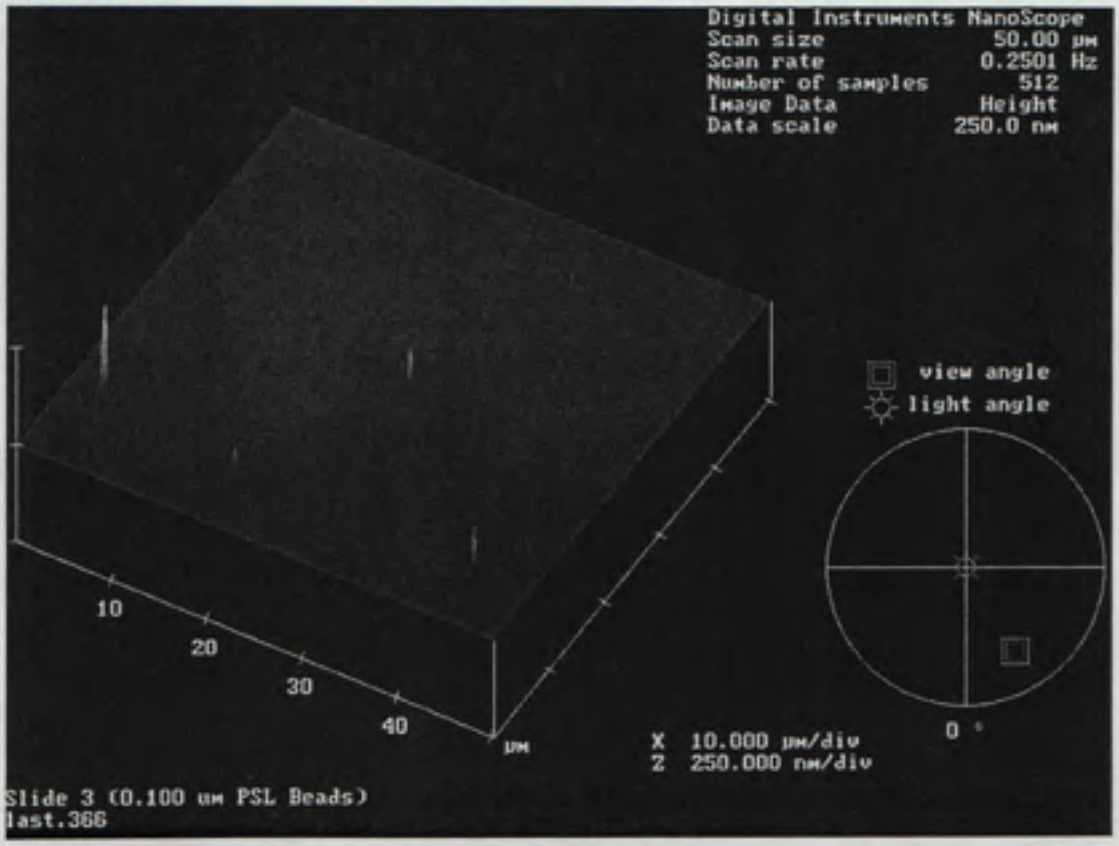

Slide 3 (0.100 um PSL Beads)

Section Analysis

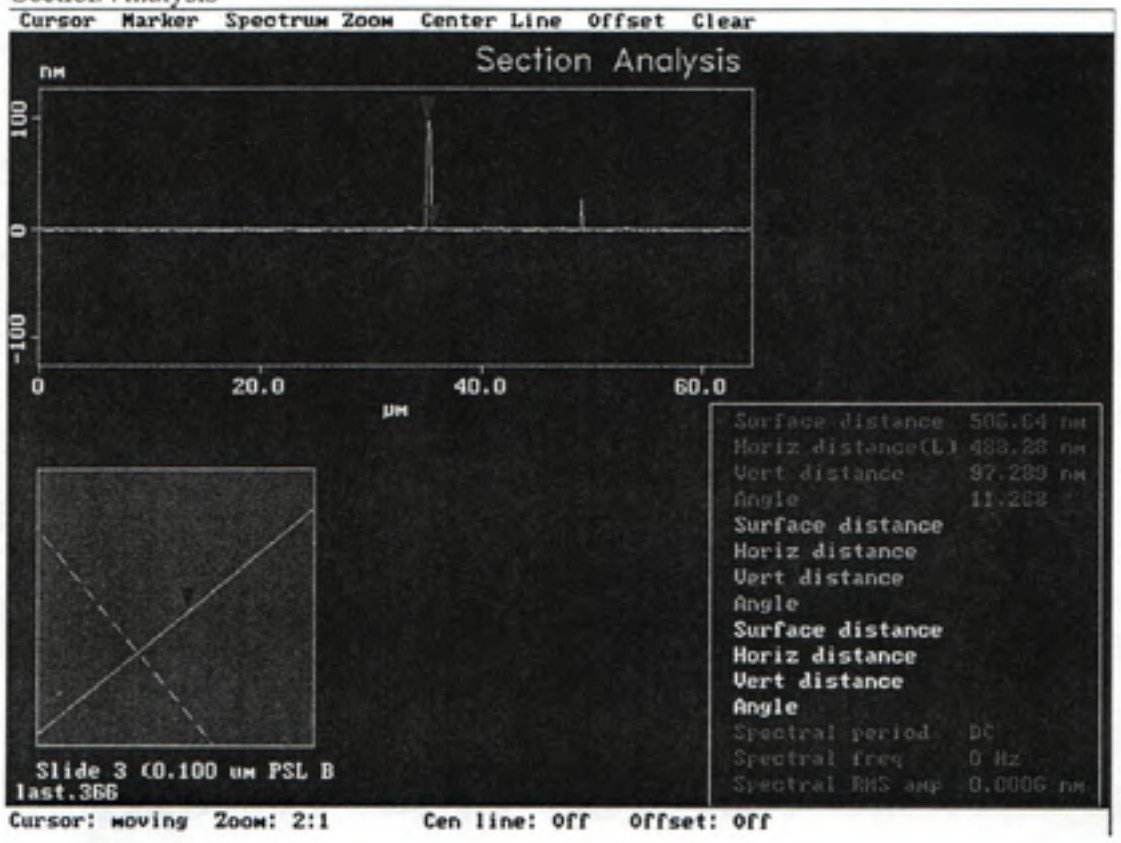

Slide 2 (0.049 um PSL Beads)

Top View

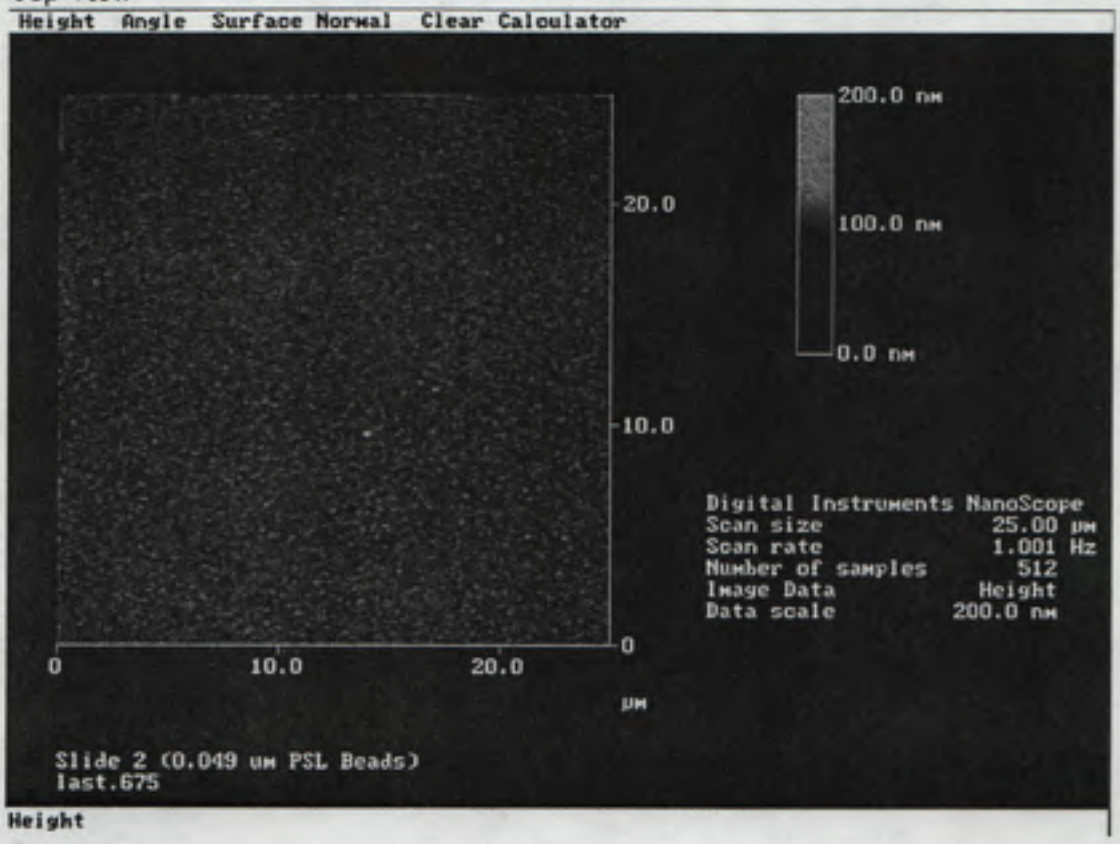

Surface Plot

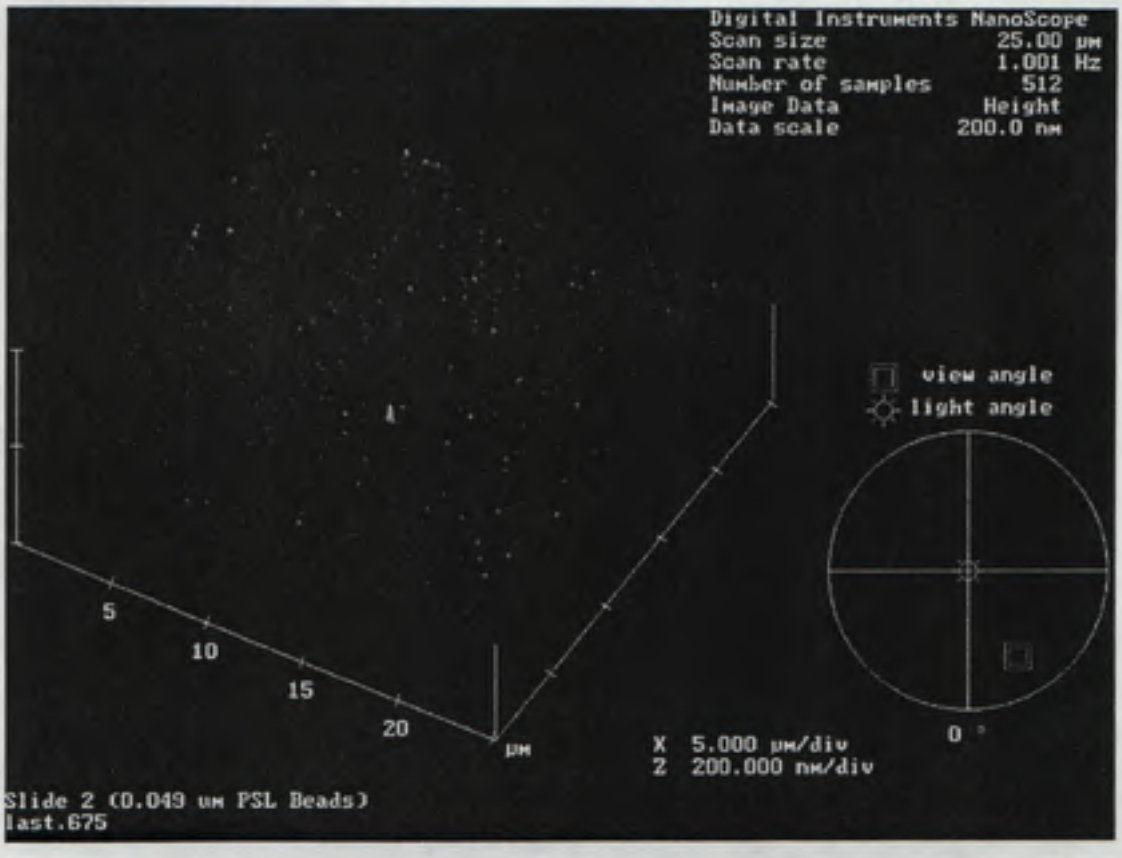

Slide 2 (0.049 um PSL Beads)

Section Analysis

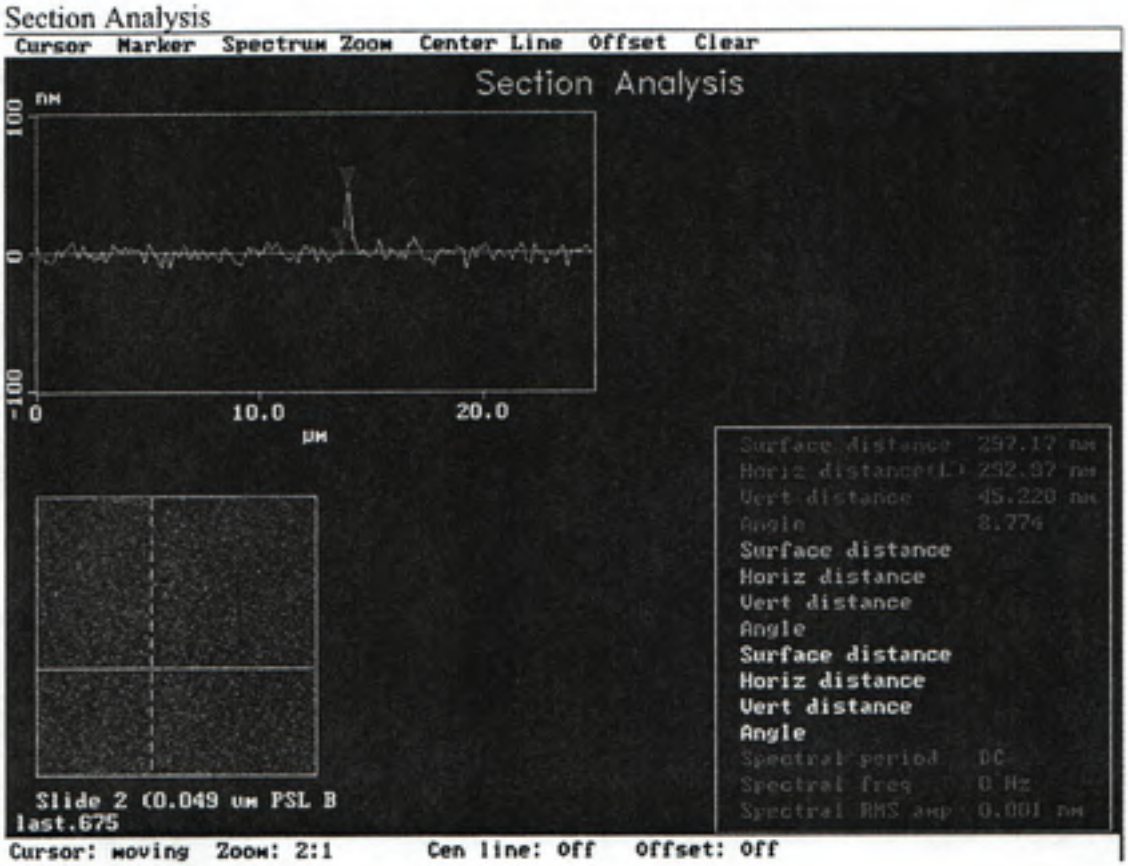

1.0 um diameter PSL beads

Scan Size: 80um x 80um
Sample/Line: 512

Scan #	Slide 1	Slide 2	Slide 3	Slide 4	Slide 5
1	0	0	0	0	1
2	0	0	0	0	2
3	0	0	0	0	0
4	0	0	0	0	0
5	0	0	0	0	3
6	0	0	0	0	2
7	0	0	0	0	0
8	0	0	0	0	4
9	0	0	0	0	2
10	0	0	0	0	1
11	0	0	0	0	0
12	0	0	0	0	0
13	0	0	0	0	2
14	0	0	0	0	1
15	0	0	0	0	1
16	0	0	0	0	1
17	0	0	0	0	0
18	0	0	0	0	3
19	0	0	0	0	0
20	0	0	0	0	2
Total	0	0	0	0	25
#/cm^2	0	0	0	0	1.95×10^4

0.48 um diameter PSL beads

Scan Size: 80um x 80um
Sample/Line: 512

Scan #	Slide 1	Slide 2	Slide 3	Slide 4	Slide 5
1	0	0	0	0	1
2	0	0	0	0	3
3	0	0	0	0	2
4	0	0	0	1	0
5	0	0	1	0	1
6	0	0	0	0	2
7	0	0	0	0	1
8	0	0	0	0	3
9	0	0	0	0	2
10	0	0	0	0	2
11	0	0	0	0	1
12	0	0	0	0	0
13	0	0	0	0	2
14	0	0	0	1	2
15	0	0	0	0	0
16	0	0	0	0	0
17	0	0	0	0	1
18	0	0	0	0	3
19	0	0	0	0	0
20	0	0	0	0	1
Total	0	0	1	2	27
#/cm^2			7.81×10^2	1.65×10^3	2.11×10^4

0.31 uM diameter PSL beads

Scan Size: 80um x 80um
Sample/Line: 512

Scan #	Slide 1	Slide 2	Slide 3	Slide 4	Slide 5
1	0	0	0	2	3
2	0	1	0	0	1
3	0	0	0	0	1
4	0	0	0	1	1
5	0	0	0	0	2
6	0	0	0	0	1
7	0	0	0	0	2
8	0	0	0	2	0
9	0	0	0	0	2
10	0	0	1	1	4
11	0	0	0	0	1
12	0	0	0	0	3
13	0	0	0	0	1
14	0	0	0	0	2
15	0	0	2	1	0
16	0	0	0	0	3
17	0	0	0	0	2
18	0	0	0	0	1
19	0	0	0	1	1
20	0	0	0	1	3
Total	0	1	3	9	34
#/cm^2		7.81×10^2	2.34×10^3	7.03×10^3	2.65×10^4

0.20 uM diameter PSL beads

Scan Size: 80um x 80um
Sample/Line: 512

Scan #	Slide 1	Slide 2	Slide 3	Slide 4	Slide 5
1	0	0	0	1	3
2	0	0	0	1	2
3	0	0	0	0	4
4	0	0	2	0	1
5	0	0	0	2	2
6	0	0	0	0	3
7	0	0	0	0	1
8	0	0	1	0	1
9	0	0	0	1	0
10	0	0	1	1	2
11	0	0	0	0	1
12	0	0	0	0	3
13	0	0	0	0	2
14	0	1	0	1	1
15	0	0	0	0	1
16	0	0	0	2	1
17	0	0	1	0	4
18	0	0	1	3	2
19	0	0	0	0	4
20	0	0	0	1	2
Total	0	1	6	13	40
$\#/cm^2$		7.81×10^2	4.68×10^3	1.01×10^4	3.12×10^4

0.10 uM diameter PSL beads

Scan Size: 50um x 50um
Sample/Line: 512

Scan #	Slide 1	Slide 2	Slide 3	Slide 4	Slide 5
1	0	0	0	1	2
2	0	0	1	1	2
3	0	0	0	0	1
4	0	1	0	0	1
5	0	0	0	2	0
6	0	0	0	1	3
7	0	0	1	0	1
8	0	0	1	0	1
9	0	1	0	1	2
10	0	0	0	0	1
11	0	0	1	0	1
12	1	1	0	0	2
13	0	0	2	0	3
14	0	0	1	0	0
15	0	0	0	0	3
16	0	0	0	1	2
17	0	0	1	1	2
18	0	0	0	2	0
19	0	0	0	0	2
20	0	0	0	1	1
Total	1	3	7	11	30
#/cm^2	2.00×10^3	6.00×10^3	1.4×10^4	2.20×10^4	6.00×10^4

0.049 uM diameter PSL beads

Scan Size 25um x 25um
Sample/Line: 512

Scan #	Slide 1	Slide 2	Slide 3	Slide 4	Slide 5
1	0	0	1	0	2
2	0	0	1	0	1
3	0	0	0	2	3
4	0	0	0	1	0
5	1	0	0	1	1
6	0	0	2	0	2
7	0	1	0	1	0
8	0	0	0	0	1
9	0	0	0	0	2
10	0	0	1	1	1
11	1	1	1	0	2
12	0	0	0	0	0
13	0	0	0	2	0
14	0	1	0	1	3
15	0	0	1	1	0
16	0	0	0	0	2
17	0	0	0	1	1
18	0	0	0	0	1
19	0	0	0	0	2
20	0	0	0	0	0
Total	2	3	7	11	24
#/cm^2	1.60 x10^4	2.40 x10^4	6.40 x10^4	8.8 x 10^4	1.92 x10^5